2010

Volume phase transitions in surface-tethered, photo-cross-linked poly(N-isopropylacrylamide) networks

Ajay Kumar Vidyasagar
University of South Florida

Volume Phase Transitions in Surface-Tethered, Photo-Cross-Linked Poly(N-isopropylacrylamide) Networks

by

Ajay Kumar Vidyasagar

A dissertation submitted in partial fulfillment
of the requirements for the degree of
Doctor of Philosophy
Department of Chemical and Biomedical Engineering
College of Engineering
University of South Florida

Major Professor: Ryan G. Toomey, Ph.D.
Vinay Gupta, Ph.D.
Norma Alcantar, Ph.D.
John Wolan, Ph.D.
Martin Muschol, Ph.D.
Ashok Kumar, Ph.D.

Date of Approval:
June 30, 2010

Keywords: Poly(NIPAAm-co-MaBP), water, AIBN, free radical polymerization, hydrogels, hydrophilic, hydrophobic, pH, neutron reflection, FTIR, Hofmeister series, solid phase peptide synthesis, cloud point, demixing temperature

DEDICATION

I would like to dedicate this dissertation to Amma, Appa and my brother Vijay.

ACKNOWLEDGEMENTS

I would like to express my sincere gratitude to my major professor; Dr. Ryan Toomey for his invaluable inputs towards my training as a researcher. It was his constant encouragement and guidance that led to the fruition of this thesis.

I would like to thank all my committee members: Dr. Norma Alcantar, Dr. Vinay Gupta, Dr. John Wolan, Dr. Martin Muschol and Dr. Ashok Kumar for their advice and motivation. I am also grateful to my friends and colleagues: Leena Patra, Ophir Ortiz, Gulnur Efe, Maritza Muniz, Vinny, Sam DuPont, Carlos Bello and Ryan Cates. I would like to sincerely thank Dr. Norma Alcantar for letting me use her lab for most of my experiments and her students: Eva Williams, Jeffy Jimenez, Audrey Buttice and Dawn Fox who have become my very good friends. I would also like to express my gratitude to Dr. Jarek Majewski and Dr. Hillary Smith for their invaluable help with my neutron reflection experiments. Finally, I would like to thank Dr Venkat Bhethanabotla and the department of Chemical and Biomedical Engineering for their immense support throughout my education.

TABLE OF CONTENTS

LIST OF TABLES

LIST OF FIGURES

Volume Phase Transitions in Surface-Tethered, Photo-Cross-Linked Poly(N-isopropylacrylamide) Networks

Ajay Kumar Vidyasagar

ABSTRACT

The overall thrust of this dissertation is to gain a comprehensive understanding over the factors that govern the performance and behavior of ultra-thin, cross-linked polymer films. Poly(NIPAAm) was used as a model polymer to study volume phase transition in surface tethered networks.

Poly(NIPAAm) undergoes a reversible phase transition at approximately 32^{o}C between a swollen hydrophilic random coil to a collapsed hydrophobic globule state, thought to be caused by increased hydrophobic attractions between the isopropyl groups at elevated temperatures. We present a simple photochemical technique for fabricating structured polymer networks, enabling the construction of responsive surfaces with unique properties. The approach is based on the photo-cross-linking of copolymers synthesized from N-isopropylacrylamide and methacroyloxybenzophenone (MaBP). In order correlate layer swelling to the MaBP content, we have studied the swelling behavior of such layers in contact with aqueous solutions with neutron reflection.

The cross-linked networks provide a three-dimensional scaffold to host a variety of functionalities. These networks serve as a platform which can be used to amplify small local perturbations induced by various stimuli like temperature, pH, solvent, ionic strength and peptide modified hydrogels to bring about a macroscopic change. Neutron

reflection experiments have shown that the volume-phase transition of a surface-tethered, cross-linked poly(NIPAAm) network coincided with the two-phase region of uncross-linked poly(NIPAAm) in solution. Parallel measurements with ATR-FTIR investigating the effect of temperature, pH and salts suggest that the discontinuous transition is the result of cooperative dehydration of the isopropyl groups, with water remaining confined between amide groups in the collapsed state as weakly hydrogen bonded bridges. Hybrid polymers with specific peptide sequences have shown specific response to external cues such as pH and metal ions exhibiting unique phase behavior.

.

INTRODUCTION

Temperature-responsive polymers have gained significant importance for their ability to undergo drastic changes in their structure in response to external stimuli in aqueous media.[1-5] They have been studied extensively in applications such as drug delivery,[6-8] cell and bacterial attachment.[9-10] and separation processes.[11] One of the most studied temperature responsive polymer is poly(*N*-isopropylacrylamide) (poly(NIPAAm)). Poly(NIPAAm) undergoes a hydrophilic/hydrophobic transition at a lower critical solution temperature (LCST) of roughly 32^{o}C. At this temperature the polymer reversibly switches from a fully soluble, hydrophilic random coil at lower temperatures to an insoluble globule at higher temperatures.[12-14]

This transition has been attributed to changes in the hydrogen bonding tendency of water. Water molecules form ordered structures around both the hydrophilic amide moieties of NIPAAm and the hydrophobic isopropyl groups to maximize favorable hydrogen bonding associations. As temperature is increased, hydrogen bonding interactions grow weaker until the LCST is reached, wherein hydrophobic attractions between isopropyl groups dominate and collapse the polymer structure.[15-19] As the polymer goes through the hydrophilic/hydrophobic transition, Schild and co-workers showed that the intermolecular collapse of the polymer chains precedes intermolecular aggregation.[14] Moreover, the collapse of single polymer chains increases the scattering of light, which is known as the cloud point. The water that is removed and the phase separation of the collapsed polymeric molecules follow this cloud point. Chapter 1 and 2 discuss the general background and the polymer synthesis strategies and

characterizing techniques used to investigate swelling behavior and chemical interactions in responsive polymers in detail.

I have focused my attention on the effects of surface-attachment of poly(NIPAAm) networks to quartz and silica substrates. We are interested in surface attached networks of temperature polymers as a means to control surface properties in microfluidic devices. For instance, above the transition temperature, the networks can bind and hold proteins and cells. Below the transition, the networks repel proteins and cells. These networks thus offer potential as self-cleaning surfaces, as platforms for reversible diagnostics and as a means to separate biological material. That being said, confinement of a polymer alters its ability to swell compared to bulk polymers. However, there is limited understanding as to how surface attachment of a polymer chain can influence its volume transition behavior. Changes in the phase transition behavior in bulk polymers do not translate to those observed in surface attached networks which show swelling characteristics that are significantly different from unconstrained network as, shown by Harmon and coworkers.[20-21]

My hypothesis is that the nature of the volume-phase transition depends both on the chemical constituency as well as structural topology of the polymer. However, there have been few studies addressing these areas. We have designed poly(NIPAAm-MaBP) networks that will serve as model systems to probe relationships between surface confinement and intramolecular interactions with respect to volume-phase behavior. The volume phase transition of the polymers was characterized with neutron reflection and ellipsometry, allowing construction of volume-phase diagrams. The phase diagrams were interpreted with respect to a modified one dimensional swelling Flory-Rehner model.

Chapter 3 presents results using neutron reflection showing that the volume-phase transition of a surface-tethered, cross-linked poly(NIPAAm) network coincided with the two-phase region of uncross-linked poly(NIPAAm) in solution. This finding implies that cross-linking does not affect the miscibility gap of poly(NIPAAm). In uncross-linked systems, the extent of dilution can be arbitrarily controlled; and therefore, any part of the phase diagram can be accessed. Cross-linked systems, on the other hand, constrain the extent of dilution, and consequently a cross-linked system may or may not interfere with the two phase region of the phase diagram. For instance, if the cross-link density is sufficiently high, the network is prohibited from entering the miscibility gap, and therefore will move from a swollen to a less swollen state in a more or less continuous manner. Neutron reflection revealed that water is expelled discontinuously at low crosslink densities and continuously at high crosslink densities. The demarcation between the two behaviors occurred roughly at the critical point as measured by cloud point experiments.

Chapter 4 discusses neutron reflection experiments further revealing that the discontinuous concentration jump at low crosslink densities takes place in the presence of significant amounts of water and that water is not completely expelled in the process, with 2-3 water molecules remaining after the collapse of the network, independent of crosslink density. Parallel measurements with ATR-FTIR suggest that the discontinuous transition is the result of cooperative dehydration of the isopropyl groups, with water remaining confined between amide groups in the collapsed state as weakly hydrogen bonded bridges.[1, 2] Experiments involving D_2O-H_2O substitution on poly(NIPAAm-MaBP) networks have shown the existence of water trapped in hydrophobic domains in the collapsed networks which are able to diffuse in and out of the networks as indicated by D_2O substitution at temperatures as high as 102^{o}C.

The demixing behavior of poly(NIPAAm) is known to perturbed by the addition of co-solutes like Hofmeister series of salts.[3] The change in demixing temperature due to the salts is not purely concentration dependent. The change in magnitude of the demixing temperature is greatly affected by the nature of cosolute added and usually follows the Hofmeister series of salts.[3-5] It has been suggested that that salt, interacts with poly(NIPAAm) in 3 different mechanisms.[4-6] Firstly, the anions can polarize the water molecules that are hydrogen bonded to poly(NIPAAm). Secondly, the anions can interact with the hydrophobic hydration increasing the surface tension at the polymer/aqueous interface. Thirdly, the anions can directly bind with the amide groups of poly(NIPAAm).[4-6] We have shown that the primary interaction of salts with poly(NIPAAm) is through a direct interaction with the amide moieties which follows the Hofmeister series.

Chapter 5 focuses on using neutron reflection and ellipsometry to derive average water distribution and swelling characteristics of the surface confined poly(NIPAAm) coating. ATR-FTIR was used to study the molecular interactions between cosolute, poly(NIPAAm) and water. Previous results as discussed in chapter 3 have shown the presence of 2-3 water molecules per polymer segment corresponding to 30-35% of water that seems to be trapped even in the collapsed state.[1] The addition of a strong salting out salt like Na_2SO_4 seems to precipitate the polymer even at concentrations as low as 0.1M Na_2SO_4. The addition of salts forms a secondary driving force for the expulsion of water molecules from the collapsed polymer coatings resulting in only 15-20% of water left in the collapsed networks. Evidence of a direct interaction of salts with the amide moieties is presented. It is seen that the Hofmeister salts do not influence the hydrophobic hydration around the isopropyl groups as indicated by a linear increase in

surface tension due to the binding of anions to the amide moieties which follows the Hofmeister series.

Another interesting area of research is to combine synthetic polymers with peptides and other bio-molecules to form hybrid polymers. These polymers exhibit the functionality of peptides and also have the synthetic versatility and adaptability of synthetic polymers, effectively harnessing the best of both worlds. Recently, embedding specific peptide sequences have aided in better understanding in the nature of stimuli responsiveness in smart materials.[7] Peptides can undergo conformational changes due to changes in temperature, pH and specific binding behavior. Protein or peptide based hydrogels containing protein domains may self-assemble from block or graft copolymers containing biorecognition domains. Stimuli-responsive peptides can also be coupled with synthetic polymers to create stimuli-sensitive hybrid systems.[7-10] Our ultimate motivation was to engineer surface tethered poly(NIPAAm) coatings with peptide sequences that respond to specific environmental cues.

Chapter 6 discuses synthesis strategies to design peptide embedded poly(NIPAAm) based hydrogels using a modified Fmoc solid phase peptide synthesis method to create hybrid polymer architectures. We use NIPAAm copolymerized with *N-(*3-Aminopropyl*)*methacrylamide hydrochloride which has a pendent free amine group. This formed the starting resin to which target peptide sequences were engineered by adding one amino acid at a time. Though, short of our ultimate goal to create surface tethered peptide-polymer conjugates, I have demonstrated a simple and robust technique to embed peptide sequences in to poly(NIPAAm) hydrogels. Using this simple synthesis route, we have engineered a highly pH sensitive poly(NIPAAm) hydrogel with GEGVP a pentapeptide construct. We have also engineered poly(NIPAAm)-GGH constructs which

have an affinity to heavy metal ions like copper, nickel and zinc forming a very effective biosensor.

CHAPTER 1: BACKGROUND AND MOTIVATION

1.1 Hydrogels

Hydrogels are three dimensional polymeric structures that swell in aqueous solutions as shown in figure 1.1. They can swell several times their initial dry size depending strongly on the degree of cross-link density. Based on the method of cross-linking, hydrogels can be classified as physical and chemical cross-linked hydrogels.

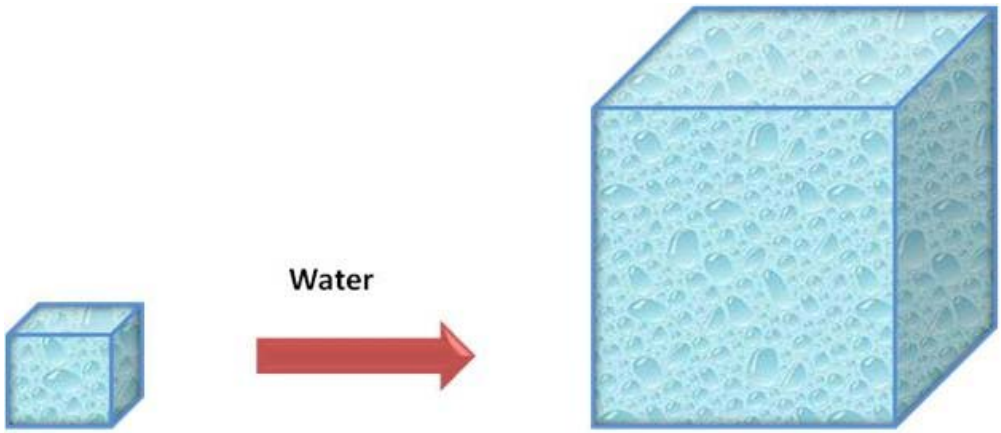

.Figure 1.1 Swelling of hydrogel in water

1.1.1 Physically Cross-Linked Hydrogels

Hydrogels are said to be physically cross-linked when the cross-linking is achieved by hydrogen bonds, coulombic forces or coordinate bonds with no chemical cross-linking agents. This type of polymer gelation is called sol-gel transition.

Being biodegradable, physical gels find applications mainly in drug delivery,[11, 12] and protein encapsulation [11, 12]. The lack of chemical cross-links help in the disintegration of the hydrogels and bringing about better release rates for the encapsulated drug. Alginate hydrogels are prime examples for protein encapsulation and delivery.[13] The physical cross-links do not require any harsh solvents that may inhibit protein activity. Moreover, anionic hydrogels formed with alginate and calcium chloride results in making the hydrogels reversible and aids in the rapid degradation of the hydrogels in the presence of chelating or monovalent ions.[13, 14] However, these Hydrogels lack mechanical strength and are not stable over long periods of time.[11, 12, 15]

1.1.2 Chemically Cross-Linked Hydrogels

Chemically cross-linked hydrogels are cross-linked covalently producing more stable and rigid cross-links. The formation of the polymer network involves the monomer, initiator and a cross-linker. Glutaraldehyde, ammonium persulphate (APS) with *N,N,N′N′*-tetramethylene-diamine (TEMED) and methylenebisacrylamide are common cross-linking agents employed. Glutaraldehyde has been used to cross-link hydrogels functionalized with amines, hydroxyl and hydrazide groups covalently.[16, 17]. Edman and co-workers[18] have synthesized polymers with dextran which can be used as a delivery vehicle for colon cancer therapy using APS with TEMED along with methylenebisacrylamide. Polyesters and polyamides have been synthesized by condensation reactions between hydroxyl groups or amines with carboxylic acids or their derivatives, the same methodology can be used to make hydrogels by cross-linking water soluble polymers forming amide linkages using *N,N*-(3-dimethylaminopropyl)-*N*-ethyl carbodiimide (EDC)as a cross-linker.[19, 20] Apart from these common cross-linkers, effective chemical cross-linking can also be brought about using enzymes. Recently, Sperinde and co-workers [21, 22] used transglutaminase which is a Ca^{2+}

dependent enzyme to catalyze the reaction between the γ-carboxamide group of the polyethylene glycol functionalized with glutaminyl groups(PEG-Q_a)and the ε-amine group of lysine to form a stable amide linkage.

1.2 Stimuli Responsive Polymers

Stimuli-responsive polymer gels are of significant interest due to their ability to undergo controlled and reversible shape changes in response to various stimuli like temperature, pH, ionic strength, electrical, magnetic, and light or their combinations.[23-32] The hydrogels respond to the stimuli with a change in volume, two or three-dimensional actuation or bending motion.

1.2.1 Temperature Responsive Polymers

Temperature or thermo responsive polymers are the most widely studied stimuli responsive polymer. In addition to the presence of hydrophilic groups, these polymers possess hydrophobic groups like methyl, ethyl and propyl groups.[31] Thermoresponsive polymers exhibit a lower critical solution temperature (LCST) which is the lowest temperature in the phase separation curve on concentration–temperature diagram. The polymers are hydrophilic below the LCST and swell when in contact with water molecules. Above the LCST, they expel water to form a more rigid and compact hydrophobic structure.

The most widely studied thermoresponsive polymer is poly(N-isopropylacrylamide) or poly(NIPAAm). Poly(NIPAAm) undergoes a reversible phase transition at approximately 32^{o}C in aqueous solutions wherein it changes from a fully extended hydrophilic coil structure to a more compact hydrophobic globule state.[33-37] Poly(N,N-diethylacrylamide) or poly(DEAAm) is another well studied thermoresponsive polymer

which has a LCST in the range of 25-35 ^{o}C. Figure 2 shows the chemical structure of some of the thermoresponsive polymers.

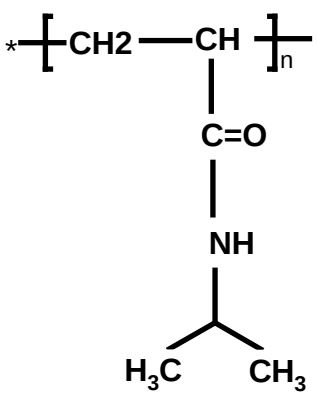

a. Poly (N-isopropylacrylamide)

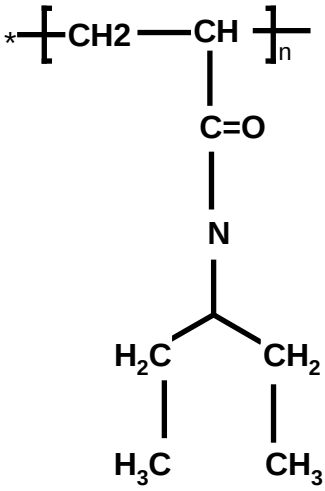

b. Poly (N,N-diethylacrylamide)

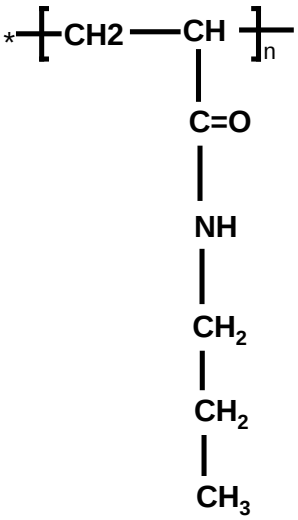

c. Poly(n- propylacrylamide)

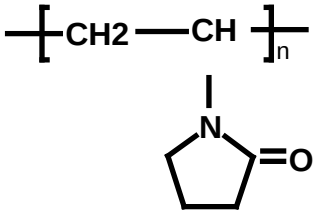

d. Poly(vinyl pyrrolidone)

Figure 1.2 Chemical structures of a. Poly(N-isopropylacrylamide), b. poly(N,N-diethylacrylamide), c. poly(N-propylacrylamide) and d. poly(vinyl pyrrolidone).

Control over LCST can be achieved by carefully adding hydrophilic or hydrophobic moieties to its molecular chains. In general, adding a small amount (1-10%) of a hydrophilic comonomer will increase the LCST whereas adding a small amount (1-10%) of a hydrophobic comonomer will reduce the LCST. For instance, addition of a hydrophilic monomer like acrylamide would make the LCST increase and depending on the amount added, even disappear.[38] However, on addition of a more hydrophobic monomer such as N-butylacrylamide would make the LCST to decrease.[38]

There are a few limitations using responsive polymers like poly(NIPAAm) including biocompatibility, mechanical strength and swelling-deswelling rates. These issues can be resolved to an extent by copolymerizing with comonomers like poly(methacrylic acid) (poly(PMAAc) and forming interpenetrating networks (IPN). [39]. The responsive polymers can be made more biodegradable by grafting them onto biopolymers like alginate, also exhibiting improved pH and thermal responses due to the presence of free and mobile graft chains.[40]

1.2.2 pH Responsive Polymers

pH responsive polymers contain ionizable pendants groups that can accept and donate protons in response to change in pH. The degree of ionization can be controlled by changing the environmental pH to a specific pH called pK_a. [41] Polymers with pendant groups that are weakly ionizable that form weak bases like pyridine or imidazole are strongly charged below their pK_a value. The polymers chains swell or uncoil as the resulting ionic interaction is much greater than the hydrophobic interactions between the alkyl side chains of the polymers. Conversely, as the pH is raised above the pK_a the number of charged inonizable groups reduces with a simultaneous increase in the hydrophobic interactions. This causes the polymer coils to collapse and eventually form

a rigid and compact globule structure. Conversely, polymers with weak negatively charged pendant groups like carboxylic acids and pendant alkyl side chains will be in an extended uncoiled state above their pK_a and will collapse forming a compact globular structure below their pK_a.[41]

Adjusting the pH to appropriate values to bring about phase transition is an important criterion. The pH range over which conformational changes are desired can be designed by incorporating an ionizable group with a pK_a matching the pH range in mind for the transition to take place or by changing the pH by adding hydrophobic moieties to the polymer backbone. Care should be taken in selecting the ionizable group for bring about the desired conformational change. For instance, poly(L-lysine) with a pKa ~10.5 is not a suitable candidate whereas poly(hystidine) with a pKa ~6.0 is a more suitable for biomedical applications requiring pH conditions close to the physiological pH of ~7.4.[42]

1.2.3 Ionic Strength Responsive Polymers

Ionic strength responsive polymers exhibit phase transitions due to the presence of different types of salts from different concentration of salts. It is seen that the ability of ions to influence phase transition follows a general trend called the Hofmeister series.[4, 5, 11] Hydrogels also respond to metal ions causing them to swell and collapse. Recently, it was shown that NIPAAm copolymerized with 1-vinylimidazole with affinity to bind copper(II) ions showed a salt concentration dependent thermal precipitation of the polymer.[43] The role of salts in the precipitation of poly(NIPAAm) is explained in more detail in section 1.13.3.

1.2.4 Electric and Magnetic Field Responsive Polymers

Electroactive polymers (EAP) which convert electrical energy into mechanical energy can be fabricated to respond to either an electric field or ions.[44, 45] Conducting polymers, polyelectrolyte gels and ionic polymer metal composites all fall under ionic EAPs.[44, 46-48] Though ionic EAPs can operate at low voltages (1-3V), they have a few limitations. Ionic EAPs need a protective layer to be operated in air and also show low electromechanical coupling efficiency, and have a slow response. On the other hand, electronic EAPs such as dielectrics, though require higher voltages (100-1000 V) to operate, they exhibit rapid response, have higher mechanical energy density and show greater strain.[24, 49]

Magnetic field responsive polymers can be made by incorporating colloidal magnetic particles within the gel network. In one such study,[50] magnetic particles of colloidal dimensions were incorporated into poly(NIPAAm) co-poly(vinyl alcohol) hydrogels. The magnetic beads aligned in a straight line when a uniform field was applied. They tended to form aggregates in non-uniform fields due to the magnetophoretic force directed to the highest field intensity. The ability of these gels to undergo rapid and controllable changes in shape can be used to mimic muscular contraction.[24, 50]

1.3 Applications

1.3.1 Responsive Polymers for Control of Cell Adhesion

Thermoresponsive polymers have been used successfully employed to regulate molecular recognition and control cell attachment and detachment without inhibiting any cellular functions. Poly(NIPAAm) with a LCST at around 32^{o}C in aqueous solutions expells water in the collapsed state above its LCST. Thermoresponsive surfaces provide an alternative to traditional cell removal processes involving mechanical dissociation and

enzymatic treatments that might hinder certain cellular functions.[51, 52] Okano and co-workers have extensively studied cell attachment and detachment using poly(NIPAAm) grafted to suitable substrates. They have shown that e-beam grafted poly(NIPAAm) on tissue cultured polystyrene dishes allowed cells to adhere and proliferate at temperatures above the LCST due to strong interaction between the hydrophobic poly(NIPAAm) surfaces and fibronectin, a extracellular matrix (ECM) protein. At temperatures below the LCST, the hydrophilic poly(NIPAAm) surfaces bring about the cell detachment.[53-56] Figure 1.3 shows cell detachment from a poly(NIPAAm) surface below its LCST.

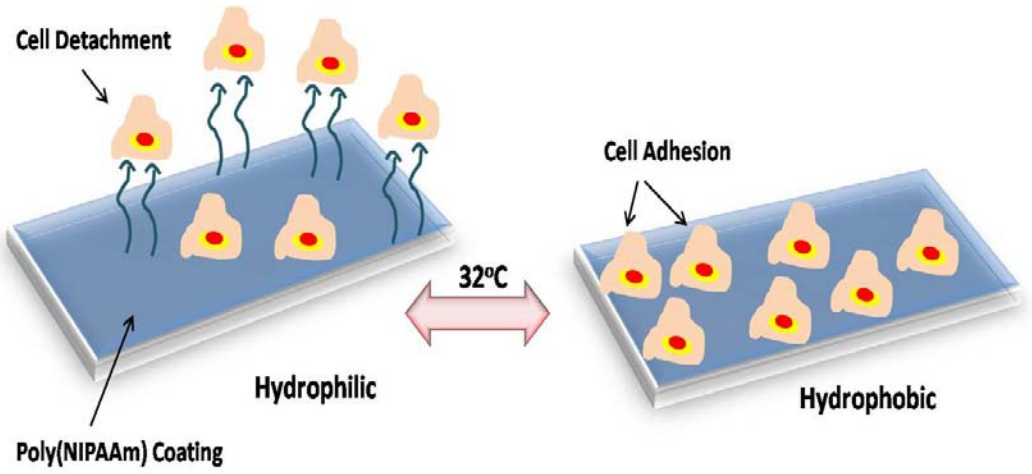

Figure 1.3 Cell detachment from a surface tethered poly(NIPAAm) coating.

1.3.2 Polymer Cushioned Model Lipid Layers for Cellular Membrane Behavior

Lipid layers supported by polymer cushions have been investigated for mainly lipid assembly and membrane structure and dynamics.[57-60] and finding applications in biosensors platforms.[61] However, supported lipid layers (SLBs) have an intrinsic problem of lack of space between the solid support and the bottom leaflet of the lipid

bilayer. There are strong van der Waals, electrostatic, hydrophobic and steric interactions between the lipid layer and the planer glass supports which trap a thin layer of water.[62, 63] This hydration layer is important in maintaining lateral mobility of the lipid in bilayer. [64-66] Recently, it was shown that a thermoresponsive polymer cushion provides an ideal surface for membrane deposition and help to facilitate deviations from planer geometry. This system provides an ideal platform to study protein-lipid interactions, trans-membrane ion transport and may have far reaching applications in membrane based biosensors.[67] Figure 1.4 shows the polymer cushioned lipid bilayer supported on a thermoresponsive polymer.

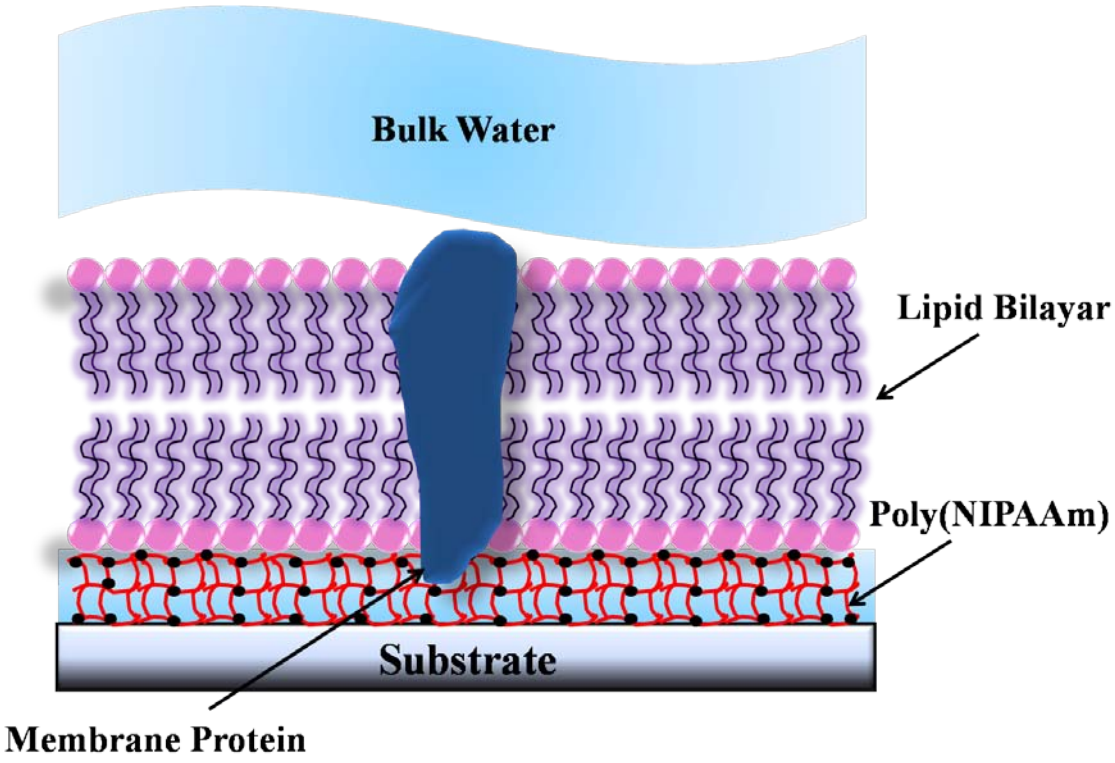

Figure 1.4 Polymer cushioned lipid bilayer supported on a thermoresponsive poly(NIPAAm) coating.

1.3.3 Microassembly

Microassembly is an active area of research where responsive polymers have been used in micropatterned surfaces with programmable chemistry having effective control over wettability and bio-fouling in these surfaces. Advances in microfrabrication coupled with wet chemistry have made it possible to create surfaces which host a number of different functional groups. Recently, using a microfabricated heated array, proteins and cells were selectively adhered to poly(NIPAAm) coating. When exposed to protein and cell samples, the patterned surfaces selectively adhered to the heating coil coated with poly(NIPAAm).[68] Figure 1.5 shows the schematics of the microfabricated heating array housing the adsorbed protein on top of a poly(NIPAAm) coating.[68]

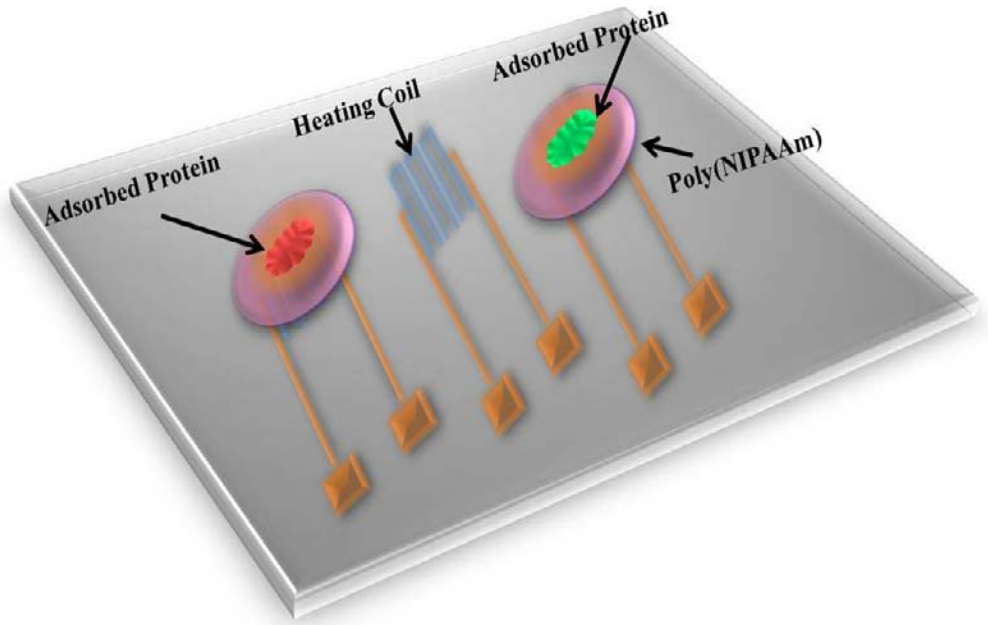

Figure 1.5 Microfabricated heating array with adsorbed protein on top of a poly(NIPAAm) coating.[68]

1.3.4 Drug Delivery

Many studies are currently underway looking into ways of delivering insulin through glucose responsive hydrogels. pH responsive hydrogels especially sensitive to glucose oxidase has been of particular interest as a suitable delivery vehicle for insulin.[69-71] Both glucose oxidase and catalase are immobilized in a polybasic pH responsive polymer. The glucose from the surrounding solution diffuses into the hydrogels triggering the catalysis of glucose by glucose oxidase to form gluconic acid which results in a pH drop within the hydrogels. The relative change in the osmotic pressure due to the diffusion of different solutes in and out of the hydrogels drives the swelling and collapse of the hydrogels.[72]

A new glucose sensitive hydrogel based on sulfonamide chemistry and covalently coupled glucose oxidase and catalase has been reported.[73]. The pH induced phase transition is seen between a pH range of 6.5-7.5 for hydrogels placed in an isotonic phosphate buffered solution at pH 7.4. The hydrogels showed a reversible swelling range between 12-8 water (g)/ polymer (g) for a glucose concentration of 0-300mg/dl at 37 ^{o}C.[73]

1.4 Volume Phase Transition in Responsive Polymers

Tanaka[74] demonstrated the unique properties of gels by investigating the volume phase transition of gels in a partially ionized acrylamide gel solvated in a water-acetone mixture for the very first time.

1.4.1 Fundamental Interactions for Volume Phase Transition in Gels

1.4.1.1 Van der Waals Interactions

It has been reported that for a partially hydrolyzed acrylamide gel swollen in a acetone-water mixture, the main polymer-polymer interaction is due to van der Waals forces. Acetone being a non-polar solvent helps in augmenting the attractive forces between the polymers chains in the network.[75, 76]

1.4.1.2 Hydrophobic Interaction

The hydrophobic polymer chains and the surrounding water molecules are strongly hydrogen bonded to form ordered ice-like structures called ice-bergs. This lowers enthalpy and entropy of mixing, giving rise to what is known as the hydrophobic interaction. Studies on the phase behavior of gels have shown that they swell at lower temperatures and collapse at higher temperatures. This is due to the hydrophobic interaction between the polymer network and water molecules and is opposite to that seen due to van der Waals interactions. The polymer network assumes a more compact and ordered structure as they shrink due to greater hydrophobic interactions at higher temperatures.[76-78]

1.4.1.3 Hydrogen Bonding

Hydrogen bonding seems to play a major role in the phase transition of responsive polymers. FTIR studies have revealed that there is significant intermolecular and intramolecular hydrogen bonding between polymer-water molecules and between polymer-polymer chains respectively. At the demixing temperature, there is a decrease in the intermolecular hydrogen bonding as water is expelled out of the network and a

corresponding increase in the intramolecular hydrogen bonding due to the close proximity of the polymer chains.[79, 80]

1.4.1.4 Electrostatic Interaction

Electrostatic interactions are long range interactions which become prominent in a hydrophobic environment. Strong repulsive interactions can be seen in polymers having with positively or negatively charged moieties. In order to maintain electro-neutrality, the counterions have to be localized near the polymer chains. This results in an increase in the osmotic pressure creating a Donnan potential inside and outside the polymer gels.[76] The different interactions are depicted as shown in figure 1.6(a-b) and 1.7(a-b)

a.

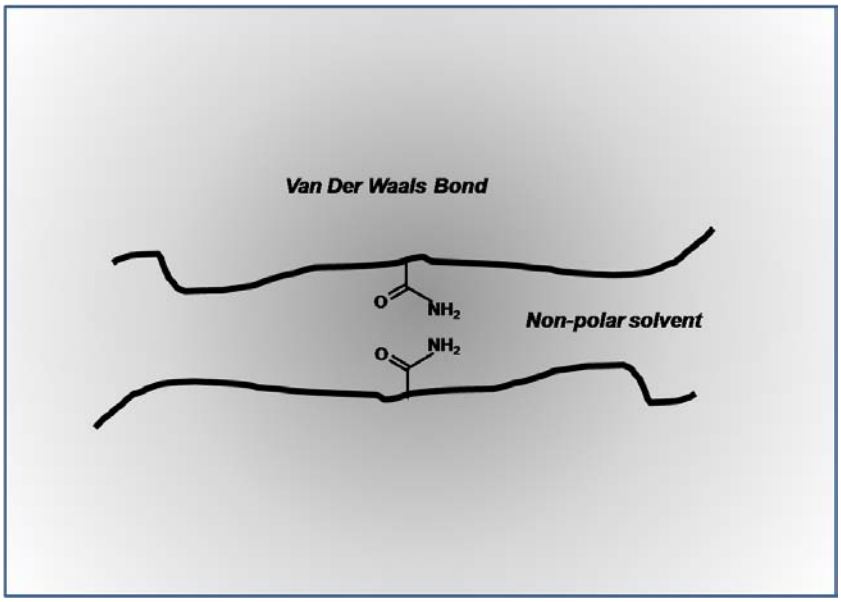

b.

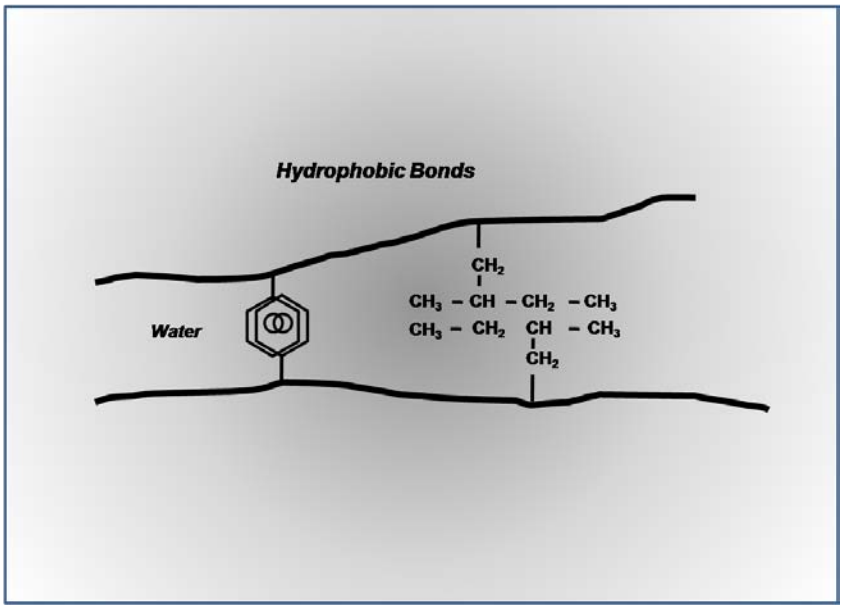

Figure 1.6(a-d) Fundamental interactions for volume phase transition in hydrogels.

Adapted from[76]

c.

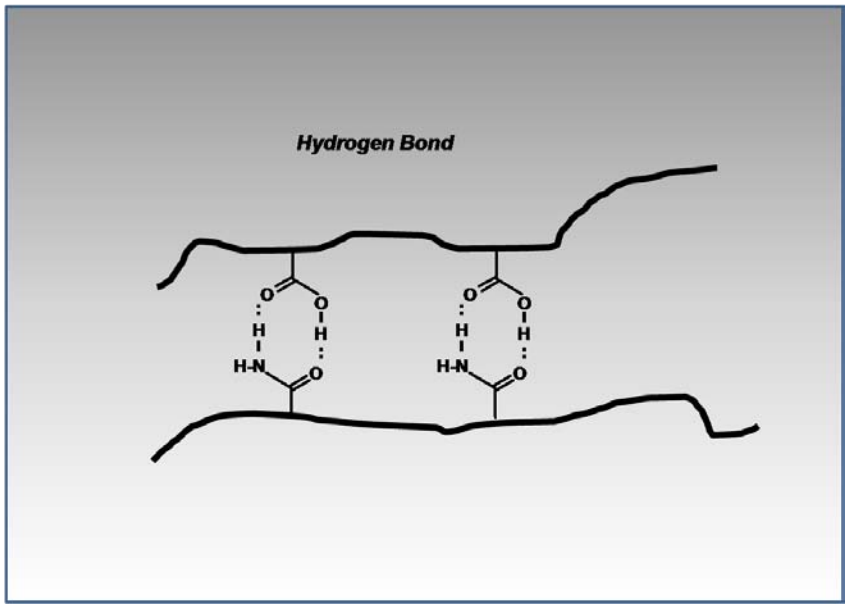

d.

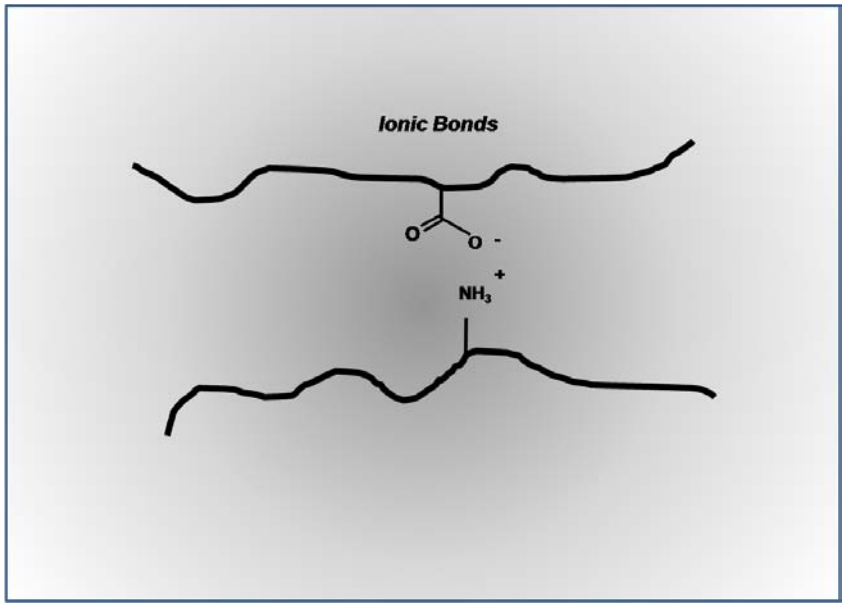

Figure 1.6(Continued)

1.5 Types of Volume Phase Transition in Thermoresponsive Polymers

Volume phase transitions can be classified into three categories based on their swelling behavior.

1.5.1 Thermoshrinking

Poly(NIPAAm) is a typical example of a gel exhibiting a thermoshrinking type of phase transition. An increase in temperature above its demixing temperature causes the gel to shrink in by one order of magnitude. Some of the thermoshrinking polymers are composed of monomers of N-methylacrylamide and N, N-dimethylacrylamide. The predominance of hydrophobic moieties in these polymers plays a crucial role in the shrinking of the gels.[75]

1.5.2 Thermoswelling

Thermoswelling polymer gels swell or expand in volume with increase in temperature. The hydrophilic comonomer like acrylic acid and methacrylic acid enable the gels to swell to exhibit a upper critical solution temperature (UCST).[75]

1.5.3 Convexo

Convexo type of phase transition is seen in polymers which can swell or shrink in response to specific stimuli. Cationic gels in acetone-water mixtures seem to be in the collapsed state at temperatures above 40^{o}C. As the temperature drops to 40^{o}C, the gel suddenly swells reaching its swollen state. It remains in this state till the temperature drops to 13^{o}C, where again it goes through a discrete phase change by collapsing to its shrunken state. [81]

1.6 Hydrophilic and Hydrophobic Hydration

Poly(NIPAAm), a thermoresponsive polymer has both hydrophilic (C=0, N-H) and hydrophobic (isopropyl) moieties. In the swollen state, water strongly hydrogen bonds with the hydrophilic amide (C=O, N-H) groups resulting in hydrophilic hydration. Water tends to form cage-like structures around the hydrophobic moieties when the polymer is below its LCST giving rise to hydrophobic hydration. As the temperature increases beyond the LCST, the water around the hydrophobic moieties is expelled bringing the hydrophobic moieties of the polymer chain close together known as the hydrophobic effect or hydrophobic interaction.[82-85]

It seems that the polymer precipitation from aqueous solutions or collapse of the gels is brought about due to the dominance of the hydrophobic moieties. Hydrogen bonds between water and polymer segments are first broken as the temperature is raised. Subsequently, hydrophobic groups dominate as polymer chains come closer resulting in the collapse of the gel or precipitation of the polymer from solution.

The swelling of polymer in water is strongly dependent on the molecular structure of the polymer. For example, it was found that NIPAAm and N-propylacrylamide (NNPAAm) had a discontinuous transition at 35^{o}C and 25^{o}C respectively whereas N-cyclopropylacrylamide (NCPAAm) had a continuous transition between 40-50 ^{o}C.[78]

In most cases, the degree of hydrophobic interactions is proportional to the number of water molecules that are available to form hydrophobic hydration around the alkyl groups and also increases with temperature. Therefore, gels with hydrophobic moieties larger surface area tend to have lower phase transition temperature.[76]

Specific interactions between polymer segments and water are necessary for driving the transition. At lower temperatures, a thin layer of water surrounds the hydrophilic amide moieties giving rise to negative values for both entropy and enthalpy to the solution process.

Water also surrounds the hydrophobic moieties forming ice-like structures at lower temperatures further increasing the entropy of the system. As the temperature increases, hydrogen bonds between water and the hydrophobic moieties break, which in turn leads to stronger interaction between polymer chains.[86, 87] This process is schematically shown in figure 1.7 for poly(NIPAAm).

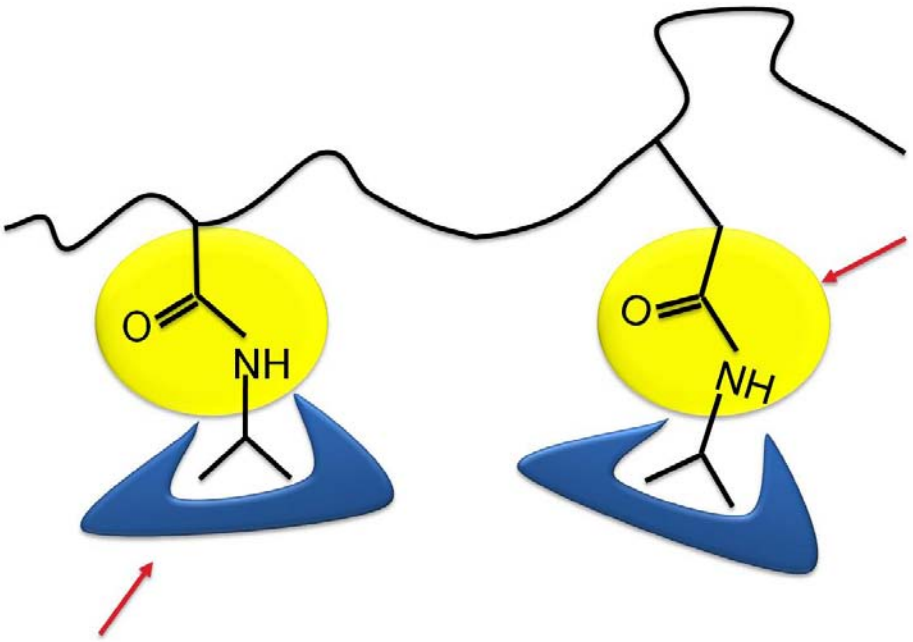

Release of ordered water cannot overcome entropy loss with collapse of network.

At higher temperatures hydrophobic forces dominate and drive collapse

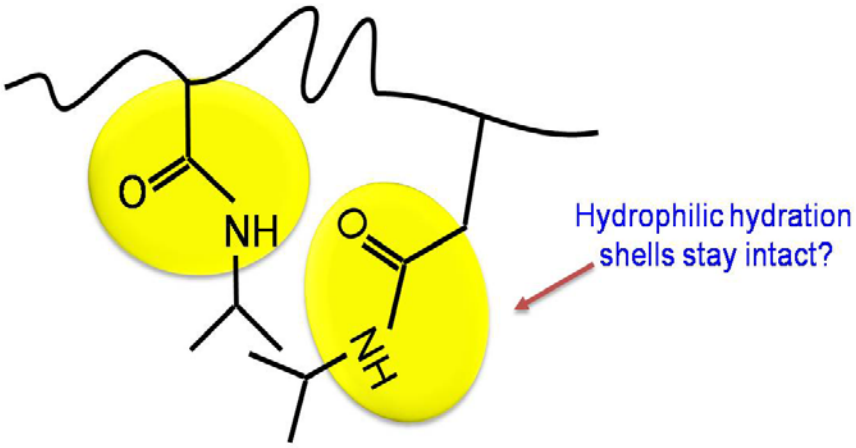

Release of ordered water from hydrophobic shells overcomes entropy loss with collapse of network

Figure 1.7 Schematic representation of hydrophilic and hydrophobic interaction in poly(NIPAAm).

1.7 The Flory- Huggins Model

The Flory–Huggins theory (Flory 1953) is a lattice mean-field approximation to macromolecular solutions where polymer segments and solvents molecules are distributed in a lattice with N_g elements.[31-34] It considers that there is an entropy-of-mixing and an interaction-energy contribution to the Gibbs free energy of mixing. The entropy of mixing contribution arises from the number of possible configurations of the solutes in solution. These are between polymer-polymer, solvent-solvent or polymer-solvent interaction. Larger the solute, the smaller its contribution to the entropy of-mixing. A typical lattice model for polymer-solvent system is shown on figure 1.8.

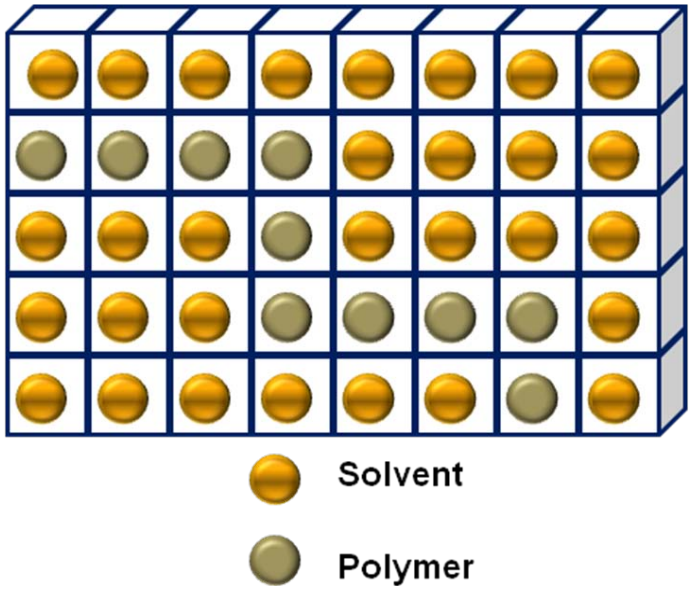

Figure 1.8 Lattice model of polymer segment and solvent molecules

The entropic contribution is given by,

$$\Delta S_m = -k(n_1 \ln \phi_1 + \ln \phi_2) \tag{1.1}$$

where k is the Boltzmann's constant, n_i is the number of moles and ϕ_i is the volume or molar fractions of 1 = solvent and 2 = polymer and are given by

$$\phi_1 = \frac{x_1 n_1}{x_1 n_1 + x_2 n_2} \tag{1.2}$$

$$\phi_2 = \frac{x_2 n_2}{x_1 n_1 + x_2 n_2} \tag{1.3}$$

where x_i are the number of segments in species (1 = solvent and 2 = polymer). For monomeric solvent, x_1= 1.

Upon dissolution solvent-solvent (1-1) and polymer-polymer (2-2) interactions are broken and solvent-polymer interactions are created. The exchange energy for one pair can be calculated

$$\Delta u = u_{12} - 1/2(u_1 + u_2) \tag{1.4}$$

The enthalpy of mixing for the number of the contacts N_{12} between solvent with volume fraction φ_1 and polymer with volume fraction φ_2 in the lattice with the coordination number z.

$$\Delta H_m = N_{12}\Delta u = N_g z \Delta u \phi_1 \phi_2 \tag{1.5}$$

Using thermal energy, the dimensionless Flory-Huggins interaction parameter χ can be obtained

$$\chi = z\Delta u / kT \tag{1.6}$$

where the interaction parameter $\chi \propto \frac{1}{T}$

This parameter depends on concentration and temperature

$$\chi = \chi_o + \chi_1\phi_2 + \chi_2\phi_2^{\,2} \tag{1.7}$$

$$\chi = \chi_S + \chi_H / T \tag{1.8}$$

with enthalpic and entropic components χ_H and χ_S respectively

$$\chi_H = \Delta h_1 / (RT\phi_2^{\,2}) \tag{1.9}$$

$$\chi_S = \Delta S_1 / (R\phi_2^{\,2}) \tag{1.10}$$

The total number of lattice sites N_g can be extended to Avogadro number N_A by

$$N_g = N_A n_1 / \phi_1 \tag{1.11}$$

Thus enthalpy of mixing ΔH_m can be rewritten as

$$\Delta H_m = kT\chi\phi_2 n_1 x_1 \tag{1.12}$$

The polymer-solvent interaction parameter accounts for free-energy changes caused by the mixing process. Values of χ are usually between 0 and 1, with an increased value of

χ indicating poorer solvents for the polymer and thus reduced degrees of polymer dissolution. It is important to recognize that χ is not a constant for a given system but is a function of temperature and concentration. If one combines the configuration and the interaction contributions, the Gibbs free energy of mixing can be expressed by

$$\Delta G_m = kT(n_1 \ln \phi_1 + n_2 \ln \phi_2 + \chi \phi_2 n_1) \tag{1.13}$$

1.7.1 Chemical Potential and Osmotic Pressure

The chemical potential μ of the solvent in the solution relative to its chemical potential μ^o in the pure liquid is obtained by differentiating the free energy of mixing, equation (2.22) with respect to the number n_1 of solvent molecules (Flory 1953). The result is multiplied by Avogadro's number N in order to obtain the chemical potential per mole and the equation is given by

$$\mu_1 - \mu_1^0 = RT\left[\ln(1-\phi_2) + (1-1/x_2)\phi_2 + \chi\phi_2^2\right] \tag{1.14}$$

where R is the gas constant.

For large values of x_2 and at high concentrations, equation (2.23) becomes,

$$\mu_1 - \mu_1^0 = RT\left[\ln(1-\phi_2) + \phi_2 + \chi\phi_2^2\right] \tag{1.15}$$

For the osmotic pressure,

$\pi V_1 = -(\mu_1 - \mu_1^o)$, here V_1 is the molar volume of the solvent. Hence, from equation (2.24), the osmotic pressure is given by,

$$\pi = -(RT / V_1)\left[\ln(1-\phi_2) + \phi_2 + \chi\phi_2^{\,2}\right] \tag{1.16}$$

1.7.2 Modified One-Dimensional Flory Rehner Model

The Flory-Rehner model has been the widely used to analyze swelling of networks.[88-91] It incorporates the osmotic pressure from solution behavior as shown in equation (2.25) and chain elasticity contributions. To develop a framework in which to understand the relationship between film composition and its structure in contact with aqueous solutions, we will map out the phase-volume behavior as a function of the relevant system parameters and interpret the phase windows with respect to the Flory-Rehner phenomenological model.[41]

$$\Pi = -K_B T\left[\phi + \ln(1-\phi) + \chi(\phi,T)\phi^2\right] + K_B T f\phi - K_B T\left(\frac{\phi_o}{N_c}\right)\left[\left[\frac{\phi}{\phi_o}\right]^{1-\frac{2}{d}} - \frac{\phi}{2\phi_o}\right] - 1 \tag{1.17}$$

The three terms preceded by K_BT describe the osmotic pressure due to mixing term from equation (2.25), the osmotic pressure due to counterions if present, and the osmotic pressure due to elastic deformation of the network. Equilibrium is defined when the osmotic pressure in the network is equal to the osmotic pressure outside the network. way. To improve agreement with experiment, empirical concentration dependence has been proposed [42]

$$\chi(T,\phi) = \chi_0 + \chi_1\phi + \chi_2\phi^2 + \ldots \tag{1.18}$$

where each term has a temperature dependence of the form.

$$\chi_K = \chi_{K,1} + \frac{\chi_{K,2}}{T} \tag{1.19}$$

1.8 Presence of Co-Existence Phase in Phase Transition

The existence of multiple phase during the discontinuous transition of NIPAAm has been reported.[92, 93] The temperature width for the co-existence in the case of neutral gels and ionic gels was found to be 0.05^{o}C and 0.1^{o}C respectively for cylindrical NIPAAm gels.[92] In gels with higher ionic content, the co-existence phase persisted over a temperature width of 4^{o}C. In such cases, the transition temperature is usually observed to be at the middle of the co-existence region. However, there is no theoretical explanation for such a premise.[92]

The presence of co-existence phase in NIPAAm is not explained by the Flory-Rehner theory as it assumes that at equilibrium, the gels are in a homogeneous state. Experimental results have shown that the phase co-existence is a stable or metastable equilibrium phenomenon.[92]

Hirotsu [92] showed the evolution of the phase co-existence in cylindrical NIPAAm gels. The cylindrical gels in their swollen state shrunk in size as the temperature increased. The transition from the swollen state to the shrunken state for an ionized NIPAAm gel with the formation of a bottleneck region as shown in figure 1.9. The co-existence phase starts at T_1 which demarcates changes from the completely swollen state with the formation of a nuclei and ends at T_2 demarcating the boundary after which the gels is in the shrunken state. On cooling, the nuclei are formed at both ends of the gel and moves towards the centre. This kind of phase co-existence where swollen gel, shrunken gel and solvent surround the gel exist is called triphasic equilibrium.[94]

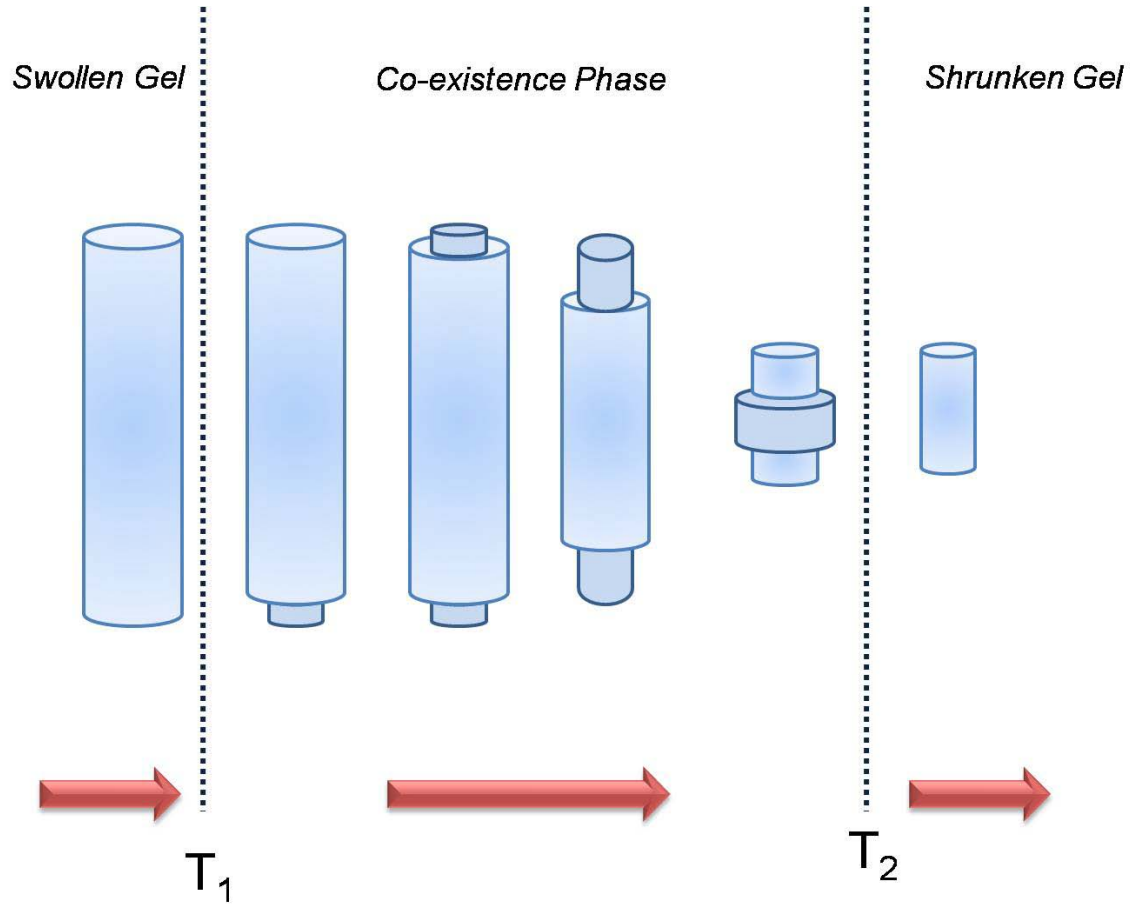

Figure 1.9 Schematic representation of NIPAAm gels exhibiting the presence of phase co-existence. Adapted from [92].

The apparent existence of the triphasic equilibrium over a wide temperature range is in violation of the Gibbs phase rule. According to the Gibbs phase rule, there should be only one temperature over which the triphasic transition should occur as a two component-three phase system should have only one degree of freedom.[92]

The gels are in a distinct thermodynamic state as the volume fraction of the co-existence phases is a monotonic function of temperature. This state is in a heterogeneous

condition due to the mixing of two phases. But the mixing ratio is not arbitrary, but has a definitive value which is a function a temperature. It is also seen that the formation of the bottleneck region is seen only in cylindrical gels suggesting that the distribution of domains is shape specific.[92]

It is seen that two completely different swelling curves can be obtained for the same gel by different methods. It has been reported that the discontinuous first order transition occurs on a local scale and the change in the total volume of the gels is more of a continuous phenomenon. Figure 1.10a depicts the swelling curve by measuring the diameter 'd' for the cylindrical gels and figure 1.10b depicts the swelling for by finding the weight 'W' of the gels. [92, 95]

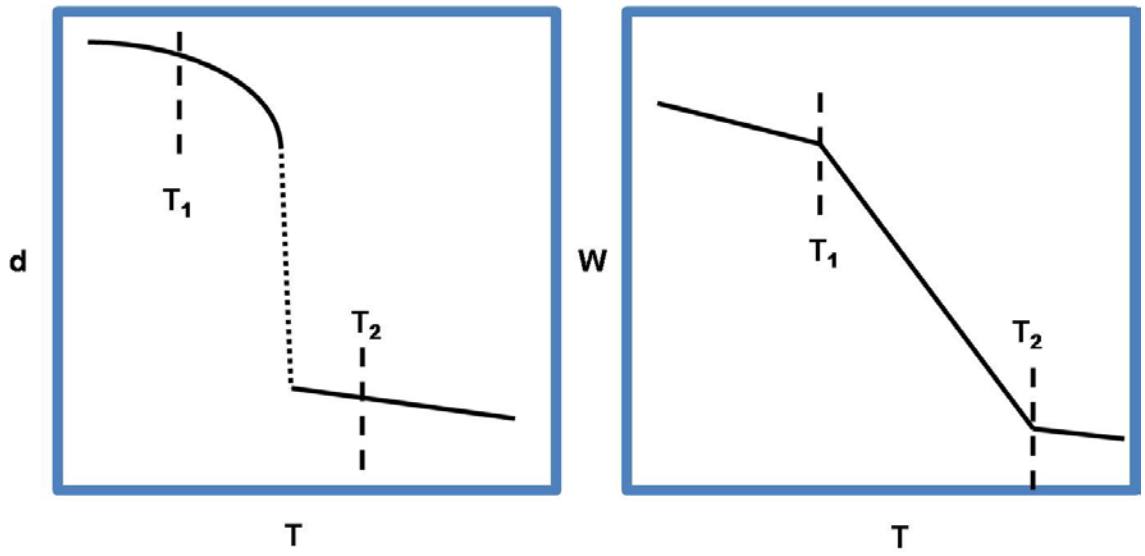

a. b.

Figure 1.10 (a-b) Schematic representation of different swelling curves for the same sample by measuring the diameter'd' and weight 'W' of the cylindrical gels as a function of temperature (T). Adapted from [92]

1.9 Water in Polymeric Systems

Water soluble polymers and polymer gels are associated with water and their role in hydrophobic and hydrophilic hydration is well documented. The interaction between water and polymer chains is of significant interest to the polymer community because of some unique properties that result due to their interaction. For instance, it is seen that water does not freeze even below its freezing point when associated with polymer chains.[96, 97]. This section will focus on the use of vibrational spectroscopy (Raman and FTIR) to elucidate the different molecular interactions of water with polymers and the different parameters that influence their association.

1.9.1 Effects of Degree of Cross-Linking of Gels on the Structure of Water

Water trapped in chemically cross-linked gels depends on the degree of cross-linking as the size of the spaces influences polymer-water interaction. The intensity of the collective band (C) given by $\int I_c(w)dw / \int I_{\parallel}(w)dw$ from Raman experiments where $I_{\parallel}$ is the intensity in the parallel position, have been shown to be affected by cross-link density.[98]

Maeda and coworkers have reported that the C value of a poly(acrylamide) or poly(PAAm) gels with a low degree of cross-linking to be nearly equal to aqueous solutions of PAAm.[99] Conversely, at higher cross-link density the C value was less compared to PAAm solutions. As the polymer concentration in gels and in solution was identical, the amount of hydration water is expected to be the same. Based on this, they proposed that water exists in three states inside the polymer gels; (1) hydration water, (2) water in spaces surrounded by polymer chains and (3) bulk water[98, 99] as shown in figure 1.11.

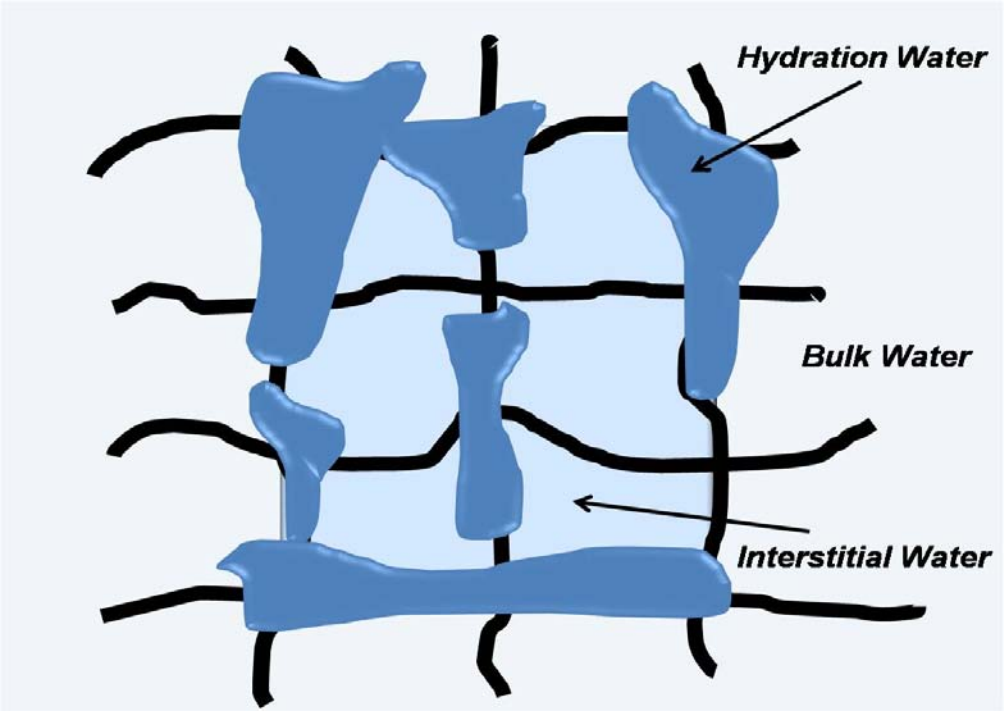

Figure 1.11 Formation of hydration and interstitial water with polymer gel. Adapted from [98]

1.9.2 Effects of Monomeric Structures on Surrounding Water

The role of monomeric structures on water can be explained by looking into the number of hydrogen bond defects that are introduced into the hydrogen bonded network structure of water per monomer unit of the polymer (N) defined as $N= P_d/f_x$ where p_d is the defect probability and f_x is the number of monomer unit per 0H oscillator.[92, 100] Maeda and co workers have determined the N values for some polymer systems at 25^{o}C as shown in table 1.[100]

Table 1.1. N values for different polymeric systems at 25 ^{o}C.[100]

Polymer	Molecular Weight	N
• Poly(acrylic acid)(PAA)	1000-5000	3.4
• Poly(acrylic acid sodium salt) (NaPAA)	5000	8.7
• Poly(ethylene glycol) (PEG)	2000-20000	1.0
• Dextran (DEX)	4000	2.3
• Poly(allylamine) hydrochloride (PAIA)	60000	7.6
• poly (vinylpyrrolidone) (PVP)	40000	1.0

The N values of polyelectrolytes like poly(acrylic acid) (PAA), poly(acrylic acid-sodium salt) (NaPAA), is greater than those of neutral polymers. This may be due to greater interaction between the ionizable groups and counterions of polyelectrolytes and water in their hydration shells.

In the case of the neutral polymers, the N values are greatly dependent on the volume ratios of their hydrophobic moieties to their hydrophilic moieties. [100] It follows the series PAAm > dextran > (poly(NIPAAm)> PEG = poly(N-vinylpyrrolidone) (PVP)).

The extra hydrophobic groups in poly(NIPAAm) might be responsible for a lower N value than PAAm. PVP with oxygen and nitrogen atoms buried inside a larger hydrophobic moiety makes is responsible for the lower N value compared to poly(NIPAAm).[100]. The N value depends on the whether there are ionizable groups or polar groups which tend to increase the N value due to their interaction with water. Conversely, the presence of hydrophobic groups might enhance hydrogen bonding resulting in lower N values.

1.9.3 Hydrogen Bonding Interactions

The miscibility of poly(NIPAAm) in water arises mainly due to the ability of the amide side groups to form hydrogen bonds with water molecules in addition to ordered water molecules around the hydrophobic isopropyl groups.[36, 101] FTIR has been used to delve into some of these mysteries. The high sensitivity of IR spectra not only towards conformational changes of a molecule but also to the local microenvironment of a molecule in addition to their ability to investigate interaction between molecules, especially the vibrations of an amide group makes it a very important tool in the investigation of polymer phase transition. The amide I and II are of particular interest based on their interaction with water molecules. The amide I mode comprises mainly due to the CO-stretching vibration) and the amide II mode mainly comprises of a combination of N-H-bending (60%) and C-N-stretching (40%) vibrations both sensitive to the strength of hydrogen bonding.[102]

Maeda and coworkers[102] investigated the coil-globule transition of poly(NIPAAm) in water and D_2O by (FTIR) spectroscopy. IR spectra of the polymer solutions measured as a function of temperature indicated that the intensities of the amide moieties and the isopropyl peaks greatly increased above the LCST. Heating the polymer solution resulted the amide II, C-H stretching and the C-H bending bands to shift to lower

wavenumbers (red shift) while the amide I band shifted to higher wavenumbers (blue shift). They found that the amide I band could be deconvoluted to one sub band centered at 1625cm^{-1} below the LCST whereas two components, one centered at 1625cm^{-1} and the other at 1650cm^{-1} were present at temperatures above the LCST. The sub band at 1625cm^{-1} was assigned to C-O group bound to water molecules through intermolecular hydrogen bonding and the sub band at 1650cm^{-1} was assigned to the C-O bound to the N-H group of the polymer through intramolecular hydrogen bonding.[102]

The dehydration of the isopropyl groups along with the polymer backbone indicated by a red shift in the symmetric and asymmetric C-H groups indicate the dominance of the hydrophobic moieties above the phase transition temperature.[102]

A recent dielectric relaxation study attributed the dehydration to characteristics resulting from the polymerization of the monomer, NIPAAm. [103] Water molecules found to be surrounding poly(NIPAAm) were found to be temperature independent. They concluded that the sharp transition seen in poly(NIPAAm) was induced by a cooperative dehydration of poly(NIPAAm).[103]

The effect of salts on the LCST of poly(NIPAAm) has been investigated Kesselman and coworkers using ATR-FTIR.[104] It was found that Na_2SO_4 and K_2SO_4, two strong salting out salts induced phase separation in aqueous poly(NIPAAm) solutions. It was seen that the addition of the sulphate ion not only depresses the transition temperature but also increases the importance of the hydrophobic interactions below the demixing temperature as evident from an increase in the relative area of the intramoledular sub band resulting from the deconvolution of the amide groups.[104]

1.9.4 Phase Transition Affected by Gel Dimension

The LCST seen in polymer solutions manifests as the volume phase transition temperature (VPTT) for gels. Large bulk hydrogels typically exhibit poor response time as their swelling/deswelling kinetics is usually governed by a diffusion limited transport process where the deswelling rate of hydrogels is inversely proportional to the square of its smallest dimension.[105, 106] Bulk hydrogels also show formation of bubbles and skin formation affecting deswelling kinetics.[107, 108]

Gels polymerized above the LCST exhibiting faster response time due to the presence of large pores have been reported. Microgels and nanogels often are in the size range of 1nm-1μm[109] exhibit similar VPTT as hydrogels. However, they exhibit improved response times and diffusivity and also have advantages in terms of size and volume and find applications in a number of fields like drug delivery,[110] as micro-actuators[111] and in sensor platforms.[112] The different gel dimensions are as shown in figure 1.12.

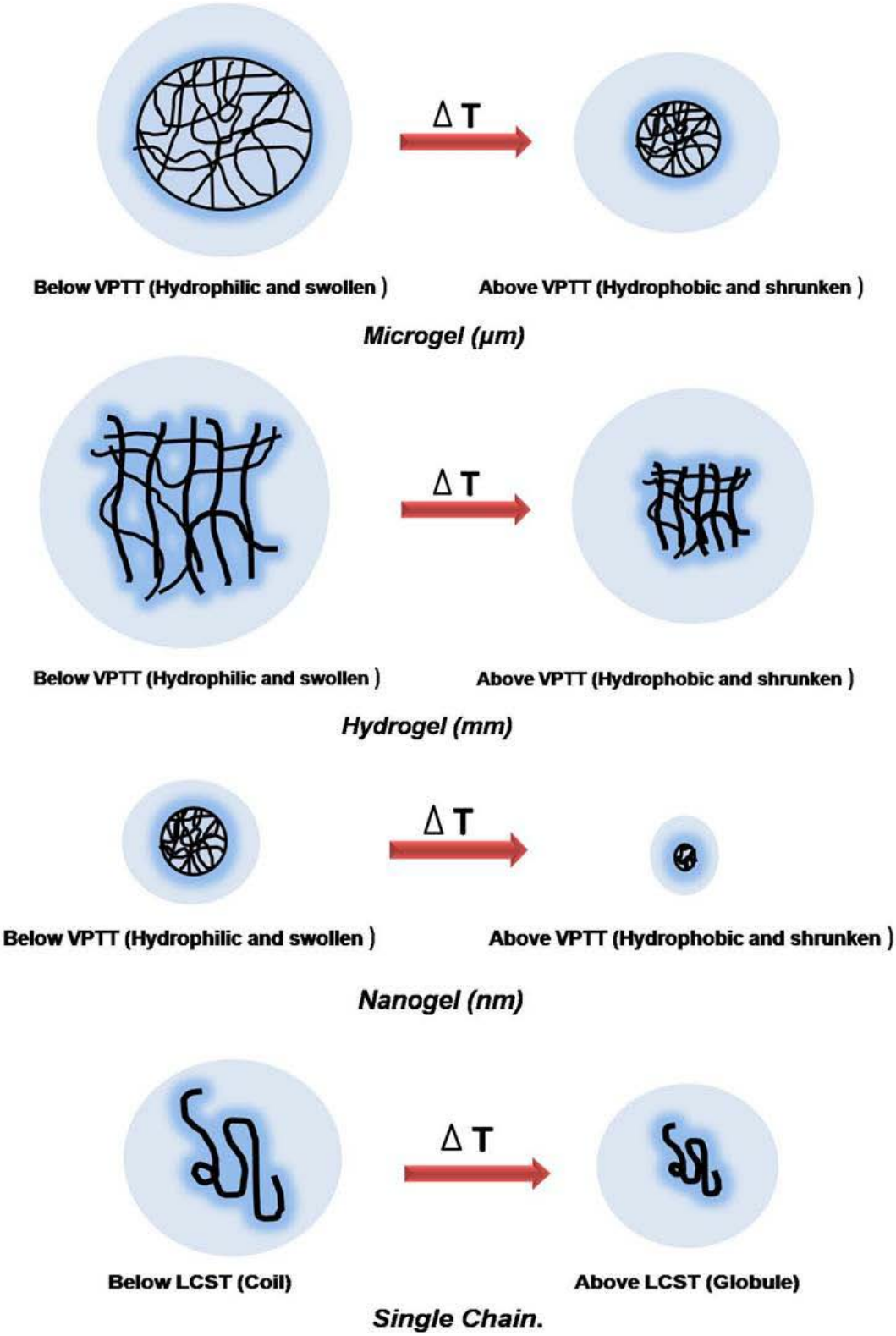

Figure 1.12 Schematic representation of gel dimensions of hydrogels, microgels, nanogels and single chain polymer segment. (Gel dimensions are not to scale).

1.10 Unconstrained and Surface Tethered Polymer Networks

Surface attached polymer networks provides an alternative to bulk hydrogels showing superior response times in swelling and deswelling kinetics compared to bulk gels where the collective diffusion step is the rate limiting step. Scaling down on the gel dimensions make them significantly enhances performance and has found applications in microfluidic platforms.[113] This makes it imperative that the characterization of surface tethered networks is pertinent. The swelling of unconstrained and surface-attached polymer gel is schematically shown in figure 1.13.

A critical issue in gaining insight in to surface tethered networks is characterizing the swelling behavior of these confined surfaces. Surface confinement allows the gels to swell only in one dimension, normal to the surface with no significant swelling parallel to the surface. This type of confinement will have an impact on the mechanical and structural properties in addition to permeability and dynamics of the network. It has been reported that surface tethered poly(NIPAAm) shows a VPTT that is higher than unconfined networks.[114, 115] It is also observed that the swelling ratio reduces drastically for surface tethered networks to about 15 fold compared to bulk gels which exhibit up to a 100 fold increase in swelling.[114]

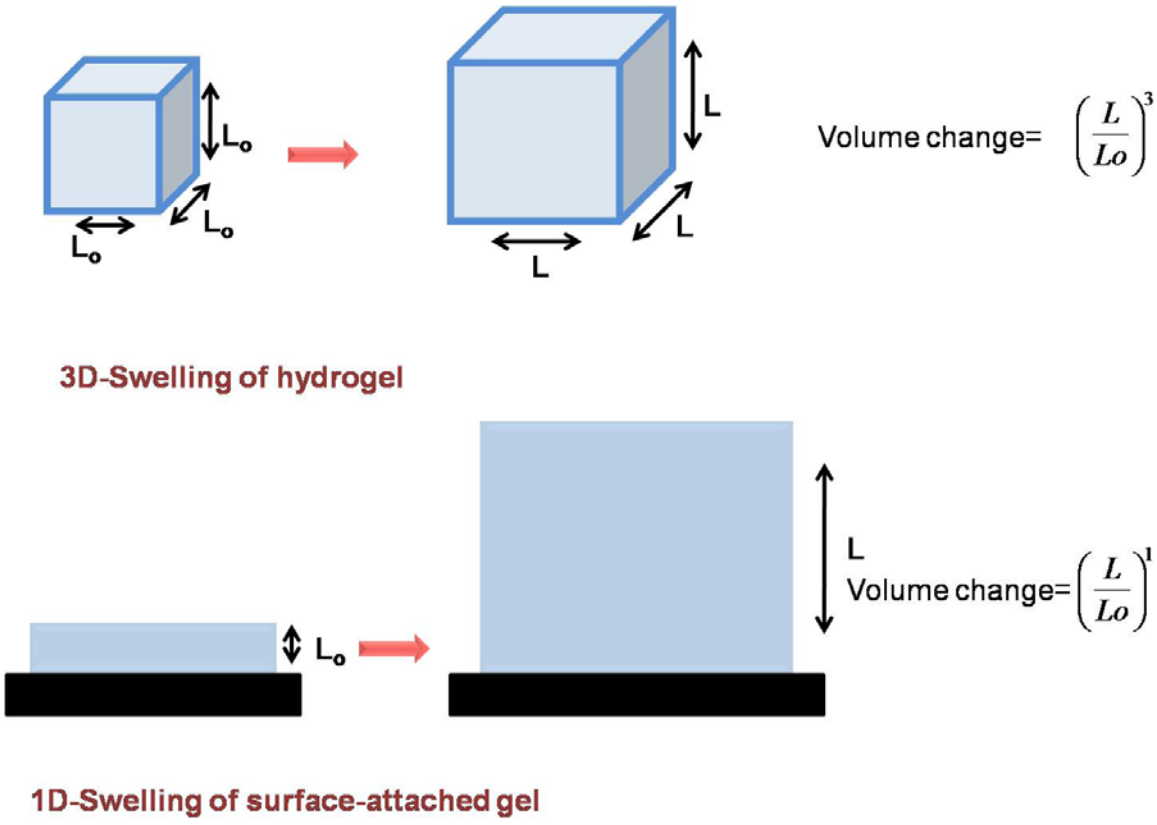

Figure 1.13 Swelling of unconstrained and surface-attached polymer gel.

For isotropic, neutral networks, the popular Flory-Rehner theo ry explains to an extent, the relationship between the cross-link density and the equilibrium swelling in a good solvent.[116, 117] For sufficiently low cross-link densities, the equilibrium swelling of a gel scales as the cross-link density to the $-^{3}/_{5}$ power as predicted by the Flory-Rehner model. As surface attachment restricts swelling to one dimension, a lower dependence on cross-link density is expected. [118]

A recent study by Toomey and co-workers[118] have shown that unconstrained networks swell to a much higher degree compared to surface-attached networks due to

higher degrees of freedom in unconstrained networks, while surface confinement physically or mechanically prevents the network to swell unconditionally.

The degree of swelling for a unconstrained gel is presumed to be equal.

$$\alpha_x = \alpha_y = \alpha_z \tag{1.20}$$

where α_i is the linear deformation L_e/L_o in the i direction. Considering simple geometric conditions, the degree of swelling for surface-attached networks will be the cube root of the unconstrained network.

For the nonattached gel, the degree of swelling in all three dimensions is presumed to be equal, where α_i is the linear deformation L_e/L_o in the i direction. Therefore, by constraining the network to the surface, from simple geometric considerations, it may be expected that the degree of swelling of the surface-attached network (sa) will be the cube root of the unconstrained network (uc), or $S_{sa} = S_{uc}^{1/3}$. [118]

It is seen that the linear swelling degree of surface-attached networks exceeds that of unconstrained networks. This observation can be better understood by the Flory-type expression for free energy.[119] The polymer network in a good solvent is subjected to two opposing forces: the thermodynamic force of mixing favoring swelling of the networks and the elastic retractile force which opposes swelling. The Gibbs free energy of the system can be written as

$$\Delta G = \Delta G_m + \Delta G_{elastic} \tag{1.21}$$

The mixing free energy is given as

$$\frac{\Delta Gm}{kT} = n_1 \ln(1-\phi) + \chi n 1 \phi \tag{1.22}$$

where *k* is the Boltzmann constant,

T is the absolute temperature,

n_1 is the number of solvent molecules,

φ is the polymer fraction in the swollen gel, and

χ is the Flory polymer−solvent interaction parameter.

The expression for the elastic free energy is

$$\frac{\Delta G_{elastic}}{kT} = v\left(\frac{d}{2}\right)\left[\alpha^2 - 1 - \ln\alpha\right] \tag{1.23}$$

where v is the number of cross-links in the network and *d* is the number of dimensions in which the network can swell. The polymer volume fraction φ in the swollen network is related to its linear deformation α is given as

$$\phi = \frac{\phi_o}{\alpha^d} \tag{1.24}$$

After minimization of free energy Δ*G* of the swollen network, we get the following relationship for the equilibrium linear deformation α and the degrees of freedom by which the network is capable of swelling.[118]

$$\alpha \approx \left[\frac{1}{\left(\frac{1}{2} - \chi \right) \phi_o N_c} \right]^{-1/(d+2)} \tag{1.25}$$

We see that α shows a stronger dependence on the cross-link density $1/N_c$, where N_c is the number of segments between cross-links as swelling is confined to fewer dimensions. As the volumetric swelling degree $S = \alpha^d$, the dependencies of both S and α can be determined for three-dimensional and one-dimensional swelling in a good solvent and are given as[118]

$$\alpha_{uc} \approx \left(\frac{1}{\phi_o N_c} \right)^{-1/5} \qquad S_{uc} \approx \left(\frac{1}{\phi_o N_c} \right)^{-3/5} \tag{1.26}$$

,

$$\alpha_{sa} \approx \left(\frac{1}{\phi_o N_c} \right)^{-1/3} \qquad S_{sa} \approx \left(\frac{1}{\phi_o N_c} \right)^{-1/3} \tag{1.27}$$

,

Toomey and co-workers[118] further showed that the surface-attached networks show greater linear deformation than the equivalent unconstrained networks which can be at least quantitatively explained by the above model. They concluded that the surface-attached network experiences a higher mixing osmotic pressure, which is partially relieved by further extension in its swelling direction. This leads to higher linear swelling ratio in surface-attached networks than in unconstrained networks. [118]

It is seen that confinement affects lateral swelling for networks with higher cross-link density and for those containing a high concentration of ionizable groups. [32, 114, 115, 120, 121] In particular, the volume phase transition temperature started decreasing above a critical film thickness and the presence of a substrate prevented the network from collapsing completely even above the phase transition temperature.[120, 122] The swelling in the lateral direction due to osmotic force induces a biaxial compressive stress. Such mechanical stresses can be large enough to suppress adhesion forces bringing about delamination of the film from the substrate. [122, 123]

1.11 Synthesis Strategies for Fabricating Polymer Thin Films

Surface-attached polymer thin films can be fabricated by

1. Crosslinking copolymerization (adding multifunctional comonomers),
2. Crosslinking (co)polymers with reactive groups, and
3. Crosslinking with high-energy irradiation.

Crossing polymers by adding multifunctional comonomers usually involves a reaction mixture containing monomers, a cross-linking agent, and a free-radical initiator is can be either spin coated on to a substrate or alternatively confined between two planar substrates aided by spacers and polymerized in situ.[114, 122] Among the free radical polymerization techniques, UV-initiated polymerization is a popular method allowing patterning of polymer thin films on different substrates.[124] The photo-initiator is added directly to the reaction mixture or can be immobilized to the substrate. Chemical immobilization of the photo-initiator provides us with a reactive surface from which the growth of a polymer film can be initiated. This method also allows us to have control over thickness of the film by varying the exposure times and also the gives the opportunity to work with substrates with complex geometries.[115, 120, 125]

A schematic representation of UV photo-polymerization of NIPAAm using *N*,*N*′-methylenebisacrylamide (BisAAm) as the cross-linking agent and benzoin ethyl ether (BEE) as the photo-sensitizer is shown in figure 1.15 The UV light irradiates BEE to generate a stable triplet state.[126] BEE in the triplet state can abstract any hydrogen atom to create an active site for the surface-graft polymerization. Grafted poly(NIPAAm) gels are then formed on the surface of the substrate due to free radical interaction with either the monomer or the cross-linking agent. [125]

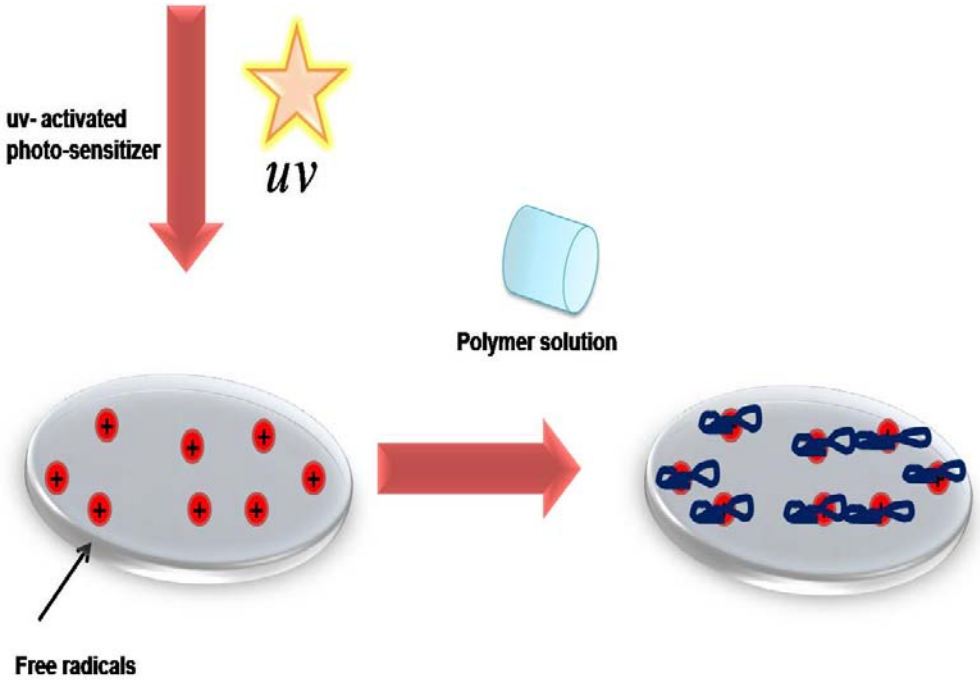

Figure 1.14 Schematic representation of grafted poly(NIPAAm) by photo-cross-linking. Adapted from [125]

Electrochemically-induced polymerization technique is another example of free-radical polymerization. The method involves the decomposition of an electro-active initiator like KPS which could be at a positive or at a negative potential (as shown in figure 1.15).

Free radical polymerization begins with the decomposition of the initiator at the electrode surface giving rise to a polymer coating. Polymer metal interaction is due to strong adhesion forces based on physisorption. For instance, poly(NIPAAm) thin film was grown by electron transfer from a conducting surface to a redox-active initiator like potassium persulphate (KPS) .[127] The film thickness was controlled by varying the electrolysis time.

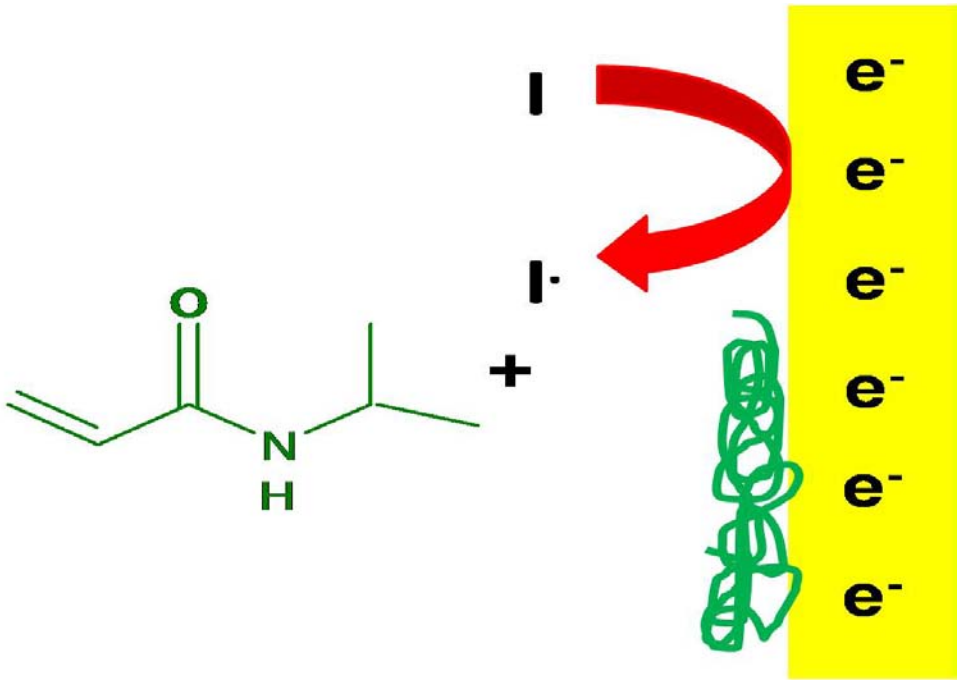

Figure 1.15 Schematic representation of an electrochemically induced polymerization process.

Plasma polymerization is a single -step, solvent-free process used for producing highly cross-linked hydrogel thin films without the need of cross-linking agents as cross-linking is brought about through the bombardment of ions/electrons during the vapor phase deposition process. In addition, substrate temperature and ion bombardment flux and

energy to the growing polymer film can be easily modified and controlled due to the reactor configuration used, providing very uniform cross-link density distribution.[128-130] However, delamination of polymer films remain an issue and require an adhesion mediator to effectively attach films to solid substrates. For instance, NIPAAm films have been known to delaminate from silicon substrates in aqueous environments. The use of adhesion promoters like γ-methacryloxypropyl trimethoxysilane, 3-aminopropyl triethoxysilane, vinyl triethoxysilane and (N,N′-diethylamino) dithiocarbamoyl propyl-(triethoxy) silane have been used with good results.[114, 131-134]

The cross-linking of copolymers containing photo-reactive pendent groups or monomers like benzophenone or 4-cinnamoylphenyl methacrylate with UV irradiation is another technique which offers another route to fabricate robust thin films with controllable film thickness and cross-link density. [121, 135-138] We have used this strategy to photo-cross-link poly(NIPAAm) thin films using benzophenone modified pendent groups. This particular technique is explained in more detail in the next section.

Polymerization using high-energy irradiation (e.g., electron beam, g-rays, UV-light) is another widely used method to produce thin films. The irradiation leads to random chain scission and recombination of the free radicals that are formed in the process to give rise stable cross-linked networks. Polymer films of a lateral resolution of 100nm have been produced by this process. The film thickness is controlled by varying the irradiation dosage.[139-141]

Another popular technique is fabricating thin films using the multiple layer-by-layer (LbL) method shown in figure 1.16, producing polymer thin films with tailored functionalities. [142] This technique is based on sequential steps involving chemical reactions between

copolymers containing amino or carboxylic groups.[143] For instance, thermoresponsive hydrogels was prepared from a sequential chemical reaction between poly(vinylamine-co-N-vinylisobutyramide) [poly(VAm-co-NVIBA)] and poly(acrylic acid). The carboxyl group of polyAAc was activated by 1-ethyl-3-(3-(dimethylamino)propyl)-carbodiimide hydrochloride (EDC) for the reaction with the amino group of poly(VAm-co-NVIBA) to yield the amide linkage.[143] By using similar sequential steps, any number of thin films can be assembled on top of each other with different functionalities.

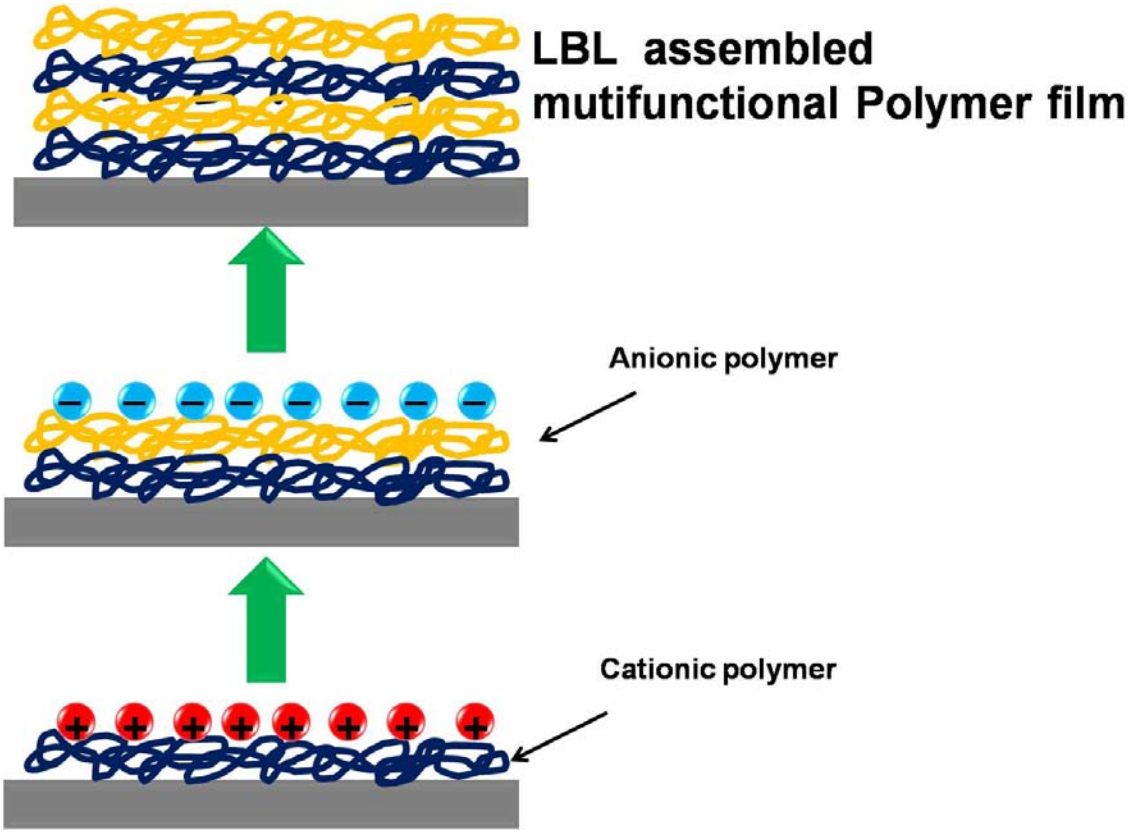

Figure 1.16 Layer by layer (LBL) assembly of multifunctional polymer film.

1.12 Formation of Surface-Attached Networks from Benzophenone Based Chemistry

The use of photo-cross-linkers is a popular way to cross-link polymers or attach a biomolecules to polymeric surfaces. The use of benzophenone and benzophenone like photo systems provides robust cross-linking across different platforms.

The use of benzophenone (BP) photoprobes can be attributed to three advantages. [144]

1. BPs is chemically more stable than diazo esters, aryl azides, and diazirines.
2. BPs can be manipulated in ambient light and can be activated at 350-360 nm, avoiding polymer and protein-damaging wavelengths.
3. BPs can react preferentially with any unreacted C-H bonds, even in the presence of solvent water and bulk nucleophiles. These three properties together provides for an efficient way to covalently cross-link polymer surfaces with remarkable site specificity. [144, 145]

1.12.1 Mechanism of BP Cross-Linking

Crossing of the benzophenone photophore takes place at 350-360nm which results in the promotion of a photon from a nonbonding n orbital to an antibonding π* orbital of the carbonyl group as shown in figure 1.17. This leads to the formation of a biradicaloid triplet state, the electron- deficient oxygen n-orbital abstracts hydrogen atoms from neighboring weak C-H bonds combining with the half-filled n-orbital.[144] When amines or other similar heteroatoms are close to the excited carbonyl group, a electron transfer step takes place resulting in the abstraction of protons from adjacent alkyl groups and a radical 1, 2 shift. Stable C-C bonds are then formed when ketyl and alkyl radicals

combine forming benzpinacol-type compounds. The biradicaloid species is known to only to attack C-H bonds which are in close geometric proximity. The reactant and substrate must be close enough for sometime at the interactive distance, furnishing the primary source of the site specificity. The lifetime of the excited state containing two unpaired electrons which is much longer than that of the single state. The triplet state usually lasts for 80-120 ps in the absence of an abstractable proton, but the lifetime might be 100 times shorter in the presence of a suitably oriented C-H bond.[144, 145]

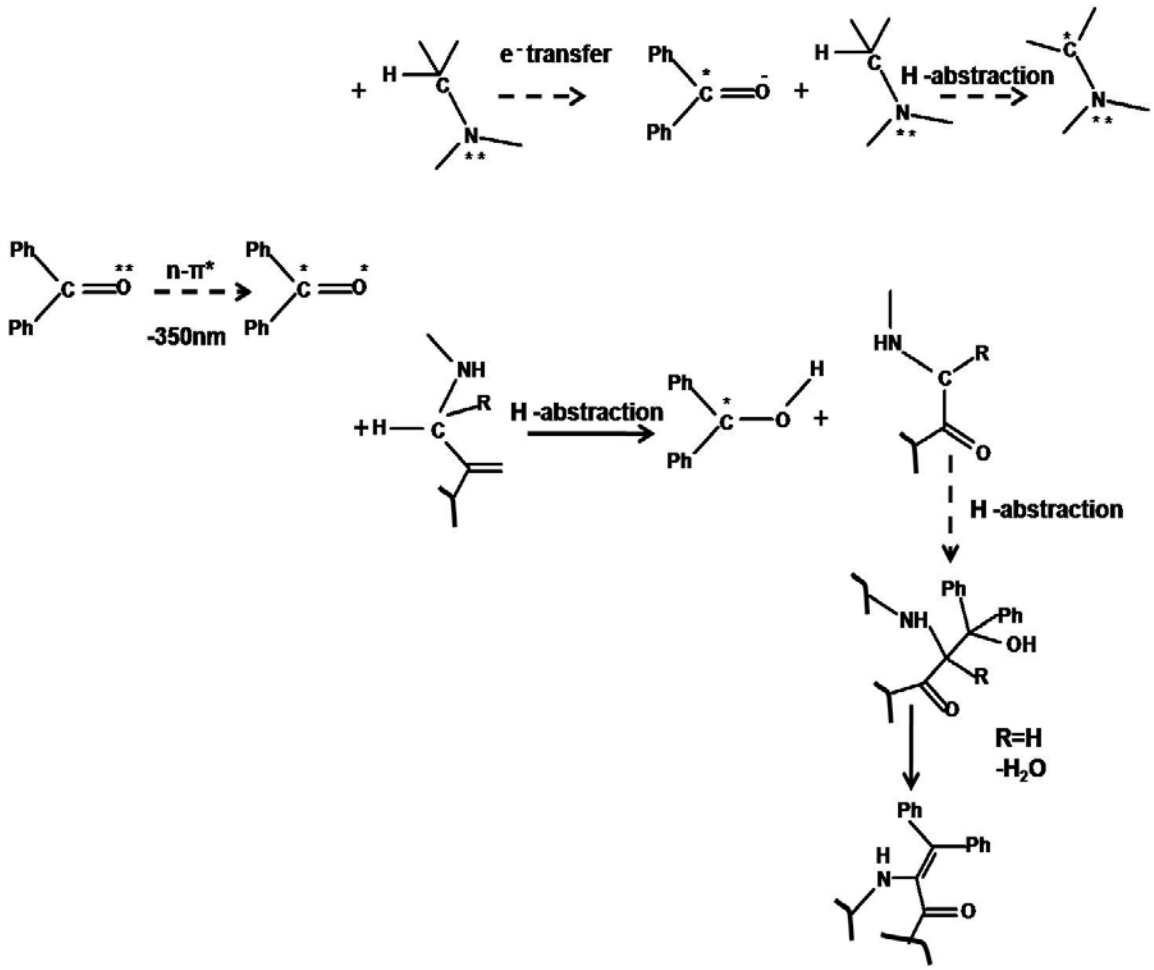

Figure 1.17 Schematic representation for the formation of C-C bonds by benzophenone chemistry. Adapted from [144]

1.13 Effect of Additives on the Phase Transition Behavior of Responsive Polymers

1.13.1 Effect of Solvent on Phase Transition of Poly(NIPAAm)

Poly(NIPAAm) is soluble in water and most organic solvents like terahydrofuran (THF),acetone, dimethyl sulfoxide (DMSO). Chloroform, dioxane (DO), methylethylketone (MEK) and low molecular weight alcohols.[146-151] The addition of organic solvents seem to depress LCST first and then subsequently increase it.

For instance, in a methanol-water system, [146, 148, 150] methanol at a mole fraction χ_M lower than 0.05,the transition temperature T_t is unperturbed; for 0.05 < χ_M < 0.35, the T_t decreases from 32°C to reach a minimum value of -7.5°C. As χ_M > 0.35, T_t increases sharply; and above χ_M 0.46, the polymer does not precipitate even in boiling solution. However, aqueous solutions containing appropriate amounts of methanol can be used to precipitate poly(NIPAAm) at room temperatures. The intra and interchain hydrogen bonding of poly(NIPAAm) and the intermolecular hydrogen bonding interactions between poly(NIPAAm) and solvent molecules by using FTIR reveal that in the C–H stretching region, both the N-isopropyl group and the polymer backbone undergo drastic conformational change upon the solvent composition. It was found that the amide I was mainly involved in intermolecular hydrogen bonding with water molecules, with the polymer chains being both flexible and disordered in a mixed solvent system when the volume fraction of the added methanol was below 15%. When the volume fraction was between 15-65%, the intermolecular hydrogen bonding was gradually replaced by interchain and intrachain hydrogen bonding between the polymer and causes the polymer to aggregate. When the volume fraction is higher that 65%, the

interchain hydrogen bonding became predominant due to the higher concentration of methanol and results in PNIPA system becoming homogeneous solution again.[152]

Another example of cononsolvency is Poly(NIPAAm) in water-dimethylformaide (DMF) where the transition was found to be continuous and dependent on both temperature and cross-link density. [151]. PNIPA gels solvated in acetonitrile (AcN)–water, THF-water, and DO-water mixtures showed a “reentrant-convex” type of swelling. Herein, the gels reswelled after reentrant phase transition for a low mole fraction χ_M of AcN, THF, and DO. At intermediate χ_M the poly(NIPAAm) gels showed a maximum swelling and shrank again gradually in the high χ_M regime.[146] The biphasic response of phase transition of polymer in mixed solvents is important not only in interpreting the role of hydrophobic and hydrogen bonding effects on phase transition but also find relevance in biological processes like protein aggregation.[146]

The mechanism of cononsolvency can be explained in terms of breakage of hydrogen bonds between water molecules arranged in a tetrahedral lattice about the alcohol in a water-alcohol mixture. This phenomenon is called clathrate-hydrate formation.[153] In pure aqueous systems, water molecules assumes a’ icelike’ structured arrangement around hydrophobic isopropyl groups and forms hydrogen bonds with the amide residues of the poly(NIPAAm) segments.

The addition of alcohol would result in the formation of clathrate hydrates by removing water molecules solvating poly(NIPAAm). This process not only breaks hydrogen bonds but also favors greater hydrophobic interactions between the isopropyl moieties resulting in the shrinkage of the polymer network. At higher volume fractions of the alcohol, water

forming clathrate structure diminish enabling direct interaction of alcohol with poly(NIPAAm).This process increases polymer-solvent interactions and subsequently results in the swelling of poly(NIPAAm). [146]

1.13.2 Role of Surfactants on Phase Transition of Poly(NIPAAm)

Surfactants like sodium dodecyl sulphate (SDS) used to alter the phase transition temperature of poly(NIPAAm). Eliassaf and co-workers[154] reported that 1% SDS increases the viscosity of poly(NIPAAm) solution thus inhibiting the precipitation of the polymer even at boiling temperatures.

The general consensus is that the phase transition temperature T_t of poly(NIPAAm) increases with an increase in SDS concentration C in the solution. This Change in phase transition seems to fall into three regimes.[146]

1. When C < 10 μM: the no-interaction regime T_t remains unchanged.
2. At 10 μM > C < 0.79 mM: the abnormal regime at SDS concentration above T_t remains unchanged, but the polymer does not precipitate above T_t.
3. C > 0.79 mM: T_t increases with SDS concentration.

At a concentration below 10 μM, the SDS concentration is too low to induce any changes to T_t. As the SDS concentration increases, there is greater interaction between the polymer segments and SDS enhancing solubility without actually changing T_t. The polymer segments remain unimolecularly dispersed even above T_t. This process has been described as intermolecular solubilization.[146]

A variety of techniques including small-angle neutron scattering, [155] static and dynamic light scattering,[156] and conductometric measurements,[157] have been employed to investigate the conformational details of poly(NIPAAm) with different SDS concentration at temperatures. In all these studies, the transition temperature in the presence of SDS was found to be relatively independent of polymer concentration, polydispersity, and molecular weight of the sample. This suggests that the transition is governed more by local short range interactions.[146]

The role of other surfactants has also been investigated. Schild and co-workers[158] and Sakai and co-workers [159]carried out experiments on sodium *n*-alkylsulfonates ranging from methyl to *n*-hexadecyl. They have most cases found identical results with respect to the role of different surfactants on T_t. Sakai and co-workers reported that surfactants with chain length up to $n = 8$, and even at a concentration as high as 100 mM, have practically no effect on the T_t. On further increase in chain length, T_t increased with increase in surface concentration.

Schild, [160] in his PhD work investigated the role of different cationic and nonionic head groups, with $C_{12}H_{25}$ tail as the hydrophobic part. It was seen that for poly(NIPAAm) and dodecyltrimethylammonium bromide (DTAB), the surfactant binding takes place near the CMC. However, in the case of nonionic Triton X-100, interaction appears to exist above critical micelle concentration (CMC) and for the Zwittergent 3-12, micellization was unaffected by poly(NIPAAm). Wu and Zhou[161] compared the effect of cationic dodecylpyridine bromide (DPB). They concluded that the attraction between DPB and the amide group reduces hydrophilicity of the gel network and hence shifts the transition to a lower temperature compared to SDS.[146]

It can be concluded that the effect of surfactants on T_t increases in the order nonionic < cationic < anionic which forms a general order for the adsorption of surfactants on polymers. For linear alkyl sulfonates, the T_t increases with increase in alkyl chain length. However, for identical chain lengths, the variation in T_t depends on the chemical nature of the head group. Though this behavior is attributed to differential adsorption on to poly(NIPAAm), the reasons governing such adsorptions still remain unclear.[146]

1.13.3 Effect of Salts on the Phase Transition of Poly(NIPAAm)

The general observation is that neutral salts can considerably alter the solution properties of macromolecules such as solubility, precipitation temperature and viscosity. The nature of individual ions determines to what extent these changes are manifested. [162, 163]It is believed that the effect of different ions on the stability and solution properties generally believed to follow the Hofmeister series, which ranks the various salts on their ability to salt out, in other words to precipitate proteins from aqueous solutions.[164, 165]The effect of the Hofmeister series of salts is more pronounced for anions than cations and is quite general. The typical order for the anion series is as follows: [6, 146]

$$CO_3^{2-} > SO_4^{2-} > S_2O_3^{2-} > H_2PO^-_4 > F^- > Cl^- > Br^- \sim NO_3^- > I^- > ClO_4^- > SCN^-$$

Ions on the left of the series are called kosmotropes, which tend to precipitate proteins out of the solution and prevent protein unfolding and is called the salting out effect whereas ions on the right are chaotropes, generally increase solubility and promote the denaturation of proteins and is called the salting in effect. Chloride is usually considered the dividing line between these two types of behavior and more or less exhibits both behaviors.[6]

Poly(NIPAAm) hydrogels exhibit a decrease in gel volume with an increase in salt concentration. The poly(NIPAAm) completely collapse at high salt concentrations with the transition being discontinuous or continuous depending on the type of salt employed. Linear poly(NIPAAm) solutions show a similar trend with an decrease in T_t with a corresponding increase in salt concentration.[146]

The following conclusions can be drawn:[146]

1. Generally almost all inorganic salts lower the T_t. This decrease shows a linear dependence with concentration.
2. The salts can be ranked based on a reduction in their transition temperature can be ranked according to the Hofmeister series which list salts on their ability to precipitate proteins out of solution. The order is as follows: NaI < KI < LiCl < NaBr ~ KBr < $MgCl_2$ < NaCl ~ KCl ~ CsCl < RbCl < $CaCl_2$ < $SrCl_2$ < $BaCl_2$ < NaOH ~ KOH < NaF ~ KF < $LiSO_4$ < $MgSO_4$ < K_2SO_4 < K_2CO_3 ~ $NaCO_3$ < $Na_2P_2O_7$ ~ Na_3PO_4 ~ Na_2SO_4.
3. The efficiency of cations to lower transition temperature is not as pronounced as anions. [6] For anions, the efficiency of lowering T_t follows the ranking I^- < Br^- < Cl^- < F^-, while the remaining are almost independent of the cation except Li^+.[166] However, T_t shows a small dependence for certain divalent cations Mg^{2+} < Ca^{2+} < Sr^{2+} < Ba^{2+}, which is in the reverse order of their ionic radius.[166]
4. It is seen that all salts do not lower the T_t in the same manner. Salts of Cl^- and Br^-, bring about a discontinuous change in the gel volume, whereas salts of I^- and F^- induce a more continuous volume change.

5. Tetraalkylammonium ions are unique in that they do not follow any particular trend. The tetraalkylammonium bromide salts follow the order $(C_3H_7)_4NBr$ < $(C_2H_9)_4NBr$ < $(C_4H_9)_4NBr$ < $(CH_3)_4NBr$ < H_4NBr < $(C_5H_{11})_4NBr$.[167, 168]
6. Salts of organic acids also do not stick to any particular trend and the sodium salts follow the order as follows C_6H_5COONa < HCOONa < CH_3COONa.[166]

Specific interactions polymer-polymer, polymer-water, polymer-ion, and water-ion interactions should be considered to investigate the role of salts on transition temperature. Poly(NIPAAm), an isomer of poly(isoleucine), consists of a hydrocarbon backbone with a pendant amide group. Above its LCST, it rapidly precipitates or collapses to form compact globule structures.[33, 34, 36, 102]

The influence of Hofmeister anions on the polymer and the hydration water can be explained by three different interactions. First, the anions can polarize adjacent water molecules involved in hydrogen bonding with the amide moieties. Second, these species can interfere with the hydrophobic hydration of the polymer by increasing the surface tension of the surrounding areas near the polymer backbone and the isopropyl side chains. Third, the anions may bind directly to the amide moieties. The first and second interactions seem to bring about salting out effect in the polymer and the third interactions causes the salting in effect in the polymer.[4-6, 46]

Figure 1.18 represents a schematic representation of the interaction of salts with poly(NIPAAm) The hydrophobic collapse of poly(NIPAAm) can be explained on the basis of a direct interaction of the anions with the polymer and its first hydration.[4, 5]

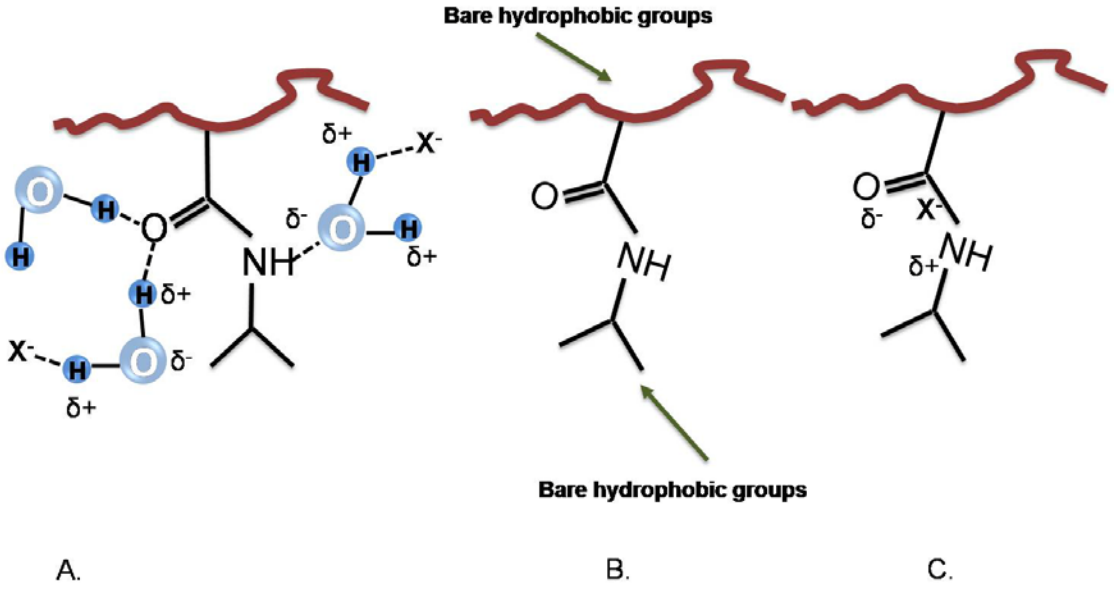

Figure 1.18 Schematic representation of the interaction of Hofmeister anions with poly(NIPAAm). Adapted from [4]

1.13.4 Effect of Salts on the Hydrophobic Groups

Anions can interact with the hydrophobic hydration of poly(NIPAAm) by increasing the surface tension at the hydrophobic-aqueous interface.[6] It is seen that with an increase in the salt concentration, the surface tension also increases at the polymer-aqueous interface. [169, 170] A two step transition is also seen in the case of poly(NIPAAm) solvated in Na_2SO_4 wherein, the first step of the two-step phase transition in the presence of salting out salts results from the perturbation of water molecules hydrogen-bonded to the amide moieties, whereas the second step involves the dehydration of the hydrophobic portion of poly(NIPAAm).[4, 5] Though concentrated salt solutions can destabilize the hydrophobic groups, it has also been seen that this fact alone might not be sufficient enough to explain their role in altering the transition temperature. For instance, the effect of salts on the activity coefficients of trimethyl amine, having

somewhat similar structure as the pendent isopropyl group in poly(NIPAAm) , in aqueous solution follows the following order:[171]

$LiCl < NaI < KI < SrCl_2 < NaBr < KBr < NaCl < KCl < Na_2SO_4 < K_2SO_4$

This order is very similar to the effect of salts on poly(NIPAAm). However, the fact that the activity co-efficient's are very sensitive to the non-polar groups due to the nature of cations, while the effect of cations on poly(NIPAAm) seem insignificant. Moreover, the abrupt changes in the gel volume at the transition temperature due to an increase in the salt concentration cannot be fully explained by the salting out of the non-polar groups in poly(NIPAAm) because the activity coefficients change linearly with the salt concentration in almost all cases. [146]

1.13.5 Interaction of Salts with Water Structure

Hofmeister anions can polarize a water molecule that is directly involved in hydrogen bonding with the amide the moieties as shown in figure 1 19. The hydration entropy ΔS_{hyd} is a quantitative measure of the ability of an anion to polarize the first hydration shell of water around the polymer.[6]

Cremer and co-workers[4] have studied specific effects of different ions on poly(NIPAAm) using vibrational sum frequency spectroscopy (VSFS). They have shown weak OH peaks in the absence of salts. The addition of chaotropic anions seems to make the OH peaks more prominent. SCN^-, the most chaotropic anion, induced the greatest water-peak intensity, whereas SO_4^{2-}, the most kosmotropic species seem to have no influence on the nature of the water peaks. They concluded that the water

structure was ion dependent and the intensities of the OH peaks which usually occurs in the region 3200cm^{-1}-3400cm^{-1} followed the following Hofmeister series.

$SCN^- > ClO_4^- > I^- > NO_3^- \approx Br^- > Cl^- >$ pure water $\approx F^- \approx SO_4^{2-}$

A simple model proposed by Frank and co-workers[172] suggesting that small and polyvalent ion will be a structure maker whereas large monovalent ion should be structure breaker was adapted by Saito and co-workers[167] who studied the viscosity B coefficient (VBC) of salts. It was suggested that structure makers will have a positive (VBC)[173, 174] value and would increase hydrophobic interaction which would subsequently bring about a decrease T_t of Poy(NIPAAm).[167, 168, 175] On the other hand, structure breakers could increase the T_t by increasing the hydrophobic hydration. The unitary partial molar entropy, which takes into account both the characteristics of the species and its interaction with the salt solution, is another interesting route to understand water structure. [146, 176]

Both VBC and unitary partial molar entropy of the solution of a salt show differences for cations Na^+, K^+, and Cs^+ which are atleast quantitatively as large as those in the anionic series Cl^-, Br^- and I^-. Hence, it's possible to conclude that both cations and anions should have similar effects on T_t. However, it is seen that the ability of cations to influence the T_t is quite small. Among alkali metal cations, Li^+ is the smallest and Cs^+ the largest. Another discrepancy would be that though Li^+ an alkali cation smallest in size should be a structure-maker series and the most efficient in lowering T_t, and Cs^+, the largest cation should have minimal role in T_t. However, Li^+ has the least ability to lower T_t, whereas Cs^+ is similar to K^+ and Na^+.[146, 172]

1.13.6 Direct Interaction of Salts with Amide Groups

Cremer and co-workers have shown strongly and weakly hydrated anions affect the LCST of poly(NIPAAm) by different mechanisms.[4, 5] The surface tension causing the hydrophobic collapse and also brings about a decrease in the transition temperature for chaotropes. For kosmotropic ions, both the polarization of hydration shell of water molecules and surface-tension are both play a role. Specifically, the first step of the two-step phase transition process in the presence of kosmotropes is due to the perturbation of solvation waters that are hydrogen-bonded to the amide moieties, whereas the second step involves the dehydration of the hydrophobic portion of PNIPAM. The direct ion binding is a saturation process leading to salting-in of poly(NIPAAm). But Cl^- and other kosmotropes do not show any binding to the polymer. It was seen that changes in the molecular weight of poly(NIPAAm) had some influence on its interaction with salts, however the general trend of the overall process was very similar for different molecular weights. [5] [146]

Von Hippel and co-workers [177] investigated the nature of binding of different salts with amide moieties and non-polar groups using the technique of recycling chromatography with poly(acrylamide) (PAAm) and poly(styrene) (PS) columns. They showed that neutral salts bind to PAAm with similar effect to their ranking in the Hofmeister series. It was seen that none of the salts bind to the PS matrix alluded to the fact that the main binding site on PAAm is the amide moieties. It is also seen that cage-like water structures around the hydrophobic groups were found to non-rigid and permitted ion movement ruling out the possibility of selective ion screening by the hydration layer.[177] It has also been shown that a methyl group attached to amide carbon has fractionally larger contribution toward ion-binding specificity than a methyl group attached to the amide nitrogen.[178] We can thus arrive at the conclusion that ions should bind to the

amide moieties of poly(NIPAAm) with the same specificity as in PAAm. The relative binding of the salts to PAAm gel follows the following order:[146, 177]

$NaF < Na_2SO_4 < KCl < NaCl, RbCl < CsCl, LiCl < NaBr < NaNO_3 < MgCl_2 < CaCl_2, BaCl_2, NaSCN < NaI$

However, this ranking of ion binding to amide group do not match up with respect to their effectiveness in perturbing the T_t.[146]

1.14 Peptide Modified Responsive Surfaces

Surfaces that change properties in response to local environmental stimuli are increasingly being studied for biomedical applications. Recently, embedding specific peptide sequences have aided in better understanding in the nature of stimuli responsiveness in smart materials.[7] Peptides can undergo conformational changes due to changes in temperature, pH and specific binding behavior. Protein or peptide based hydrogels containing protein domains may self-assemble from block or graft copolymers containing biorecognition domains. Stimuli-responsive peptides can also be coupled with synthetic polymers to create stimuli-sensitive hybrid systems.[7-10]

One of the most popular stimuli responsive peptides is a peptameric sequence VPGVG belonging to the elastin-like polypeptide (ELP) family. The fourth residue of this pentamer is a guest residue which can be substituted with any amino acid except proline to alter the physicochemical properties of the ELP.[179] The pentamer exhibits a sharp reversible hydrophilic-hydrophobic transition know as the transition temperature T_t which can be triggered by temperature, pH or ionic strength. Similar to responsive polymers like poly(NIPAAm), ELP's exists in an extended conformation at temperatures

below T_t being completely soluble in water, while at temperatures above T_t, it collapses into a ordered β-spiral that aggregates and subsequently precipitates out of solution.[180-184] This particular property of ELP's has been applied to develop various routes for purification of biomolecules.

It has been shown that fusing ELP's to protein followed by a temperature-induced precipitation process, termed as inverse transition cycling, was used to purify numerous recombinantly expressed proteins. [179, 185-188] ELP's fused to protein have also been used in the remediation of toxic metals[189] and targeted drug delivery by selective aggregation of drugs or alternately through thermal activation of drug-bearing cell penetrating peptides in hyperthermic tumors.[190-193]

Wang and coworkers[9] have engineered a hybrid hydrogel by synthesizing a copolymer of N-(2-hydroxypropyl)-methacrylamide (HPMA)13, and a metal-chelating monomer N-(N',N'-dicarboxymethylaminopropyl)methacrylamide (DAMA), by radical copolymerization. This was then coupled to two His-tagged coiled coils were used to assemble hybrid hydrogels. Hydrogels with these features offers the possibility of exhibiting unique biological properties by tailoring the coiled coils, for instance coiled coils with different T_t values could be used to assemble hybrid hydrogels that would display accordingly different gel structural transition temperatures. Another example would be to use two or more coiled coils can be used together to achieve stepwise transition which would be hard in the case of synthetic polymers.

1.14.1 Solid Phase Peptide Synthesis

The Merrifield solid phase peptide synthesis is a popular route to engineer peptide sequences anchored to a solid support.[194] This technique involves the addition of the first amino acid of the targeted peptide chain to a solid support via covalent bonding. Subsequent addition of amino acids is then brought about in a stepwise manner until the desired peptide sequence is achieved. A critical advantage with this method is use of solvents to wash away impurities rather than using recrystallization methods which are both time consuming and tedious. This greatly simplifies the synthesis scheme and shortens the reaction time required for the synthesis of the peptides. [194]

1.14.2 Fmoc -Solid Phase Peptide Synthesis

Fmoc based solid phase peptide synthesis is based on using an orthogonal protecting group using the base labile N-9-fluorenylmethoxycarbonyl (Fmoc) for protecting the α-amino group and acid labile / tert-butyl (tBu) for protecting the side chain groups. This method is slightly different from the Merrifield approach which uses acidolysis to remove both temporary and permanent groups protecting the peptides.[194] Fmoc chemistry allows removal of both temporary and permanent protecting groups through different chemical mechanisms employing milder chemicals compared to Merrifield approach. Both tBu and trityl based side chain protection can be easily removed using trifluoroacetic acid (TFA). TFA is an excellent solvent for peptides which is readily removed by evaporation.

The reaction scheme for peptide conjugation is as shown in figure 1.19. Fmoc protected amino acids are attached to the resin/polymer gel in DMF or N-methylpyrrolidone (NMP) either with preformed esters or using activation reagents that generate benzotriazolyl esters in situ. The side chain functionalities are protected by TFA labile protecting

groups. Deprotection of the Fmoc head groups after successful coupling of the amino acids is brought about using 20% Piperidine. While deprotection with Piperidine is effective in most cases, sometimes it becomes necessary to use 1,8-diazabicyclo(5.4.0)undec-7-ene (DBU) which causes rapid deprotection and less enantiomerization, when Piperidine is found to be ineffective in bringing about complete deprotection.

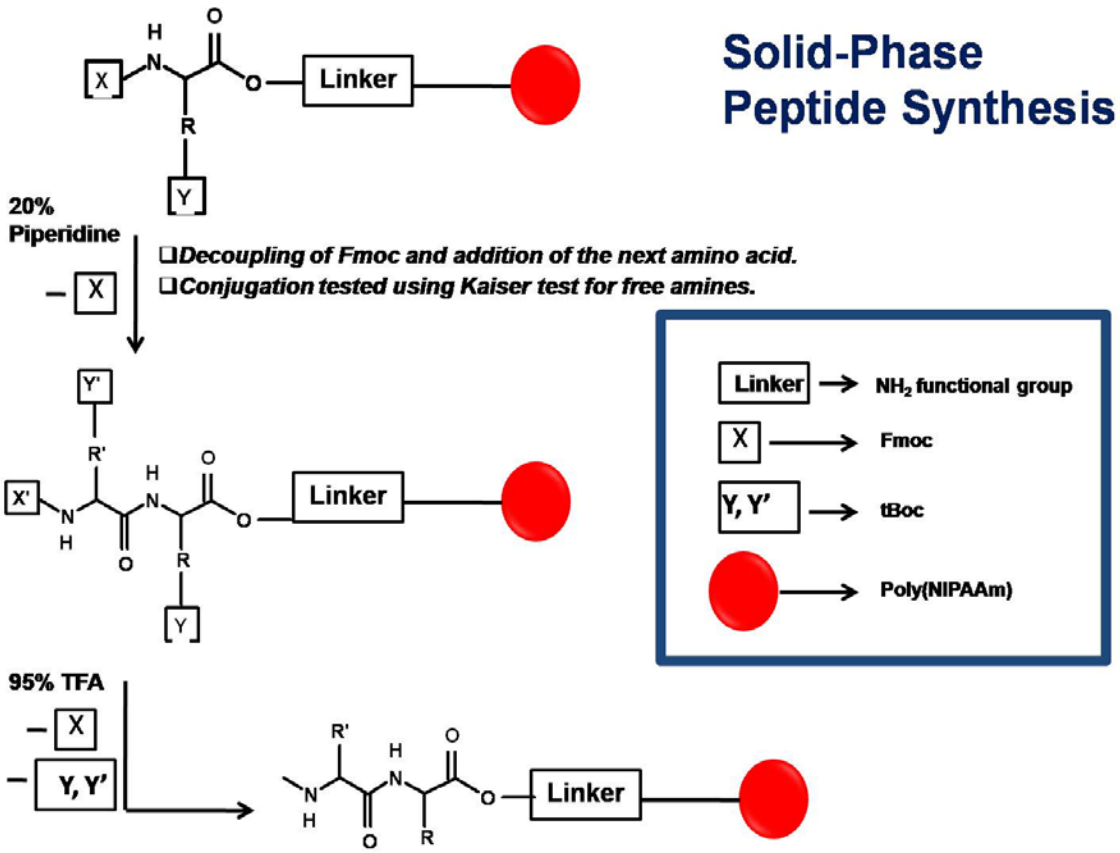

Figure 1.19 Schematic representation of peptide conjugation to poly(NIPAAm) gels by Fmoc solid phase peptide synthesis.

1.14.3 Fmoc Deprotection Mechanism

Fmoc deprotection is usually achieved by adding 20-50% v/v piperidine in DMF to the reacting mixture. The mechanism of the deprotection process is shown in figure 1.20. The most important step in the deprotection process is the deprotonation of the flurene ring in order to generate aromatic cyclopentadiene type intermediate. This quickly eliminates to form dibenzofulvene which is in turn scavenged by piperidine. While piperidine is effective in most cases, longer peptide sequences are not completely deprotected even in the presence of high Piperidine concentrations. In such cases, the use of a stronger base like 1,8-diazabicyclo[5.4.0]undec-7-ene (DBU) can be employed for better results.[195] DBU provides rapid deprotection and reduces enantiomerization of the resin bound C-terminal Cys(Trt). In batch synthesis, DBU along with 2% Piperidine results in better scavenging of the dibenzofulvene which is generated during the Fmoc removal process and thus prevents any subsequent alkylation of the resin amino groups.[196, 197]

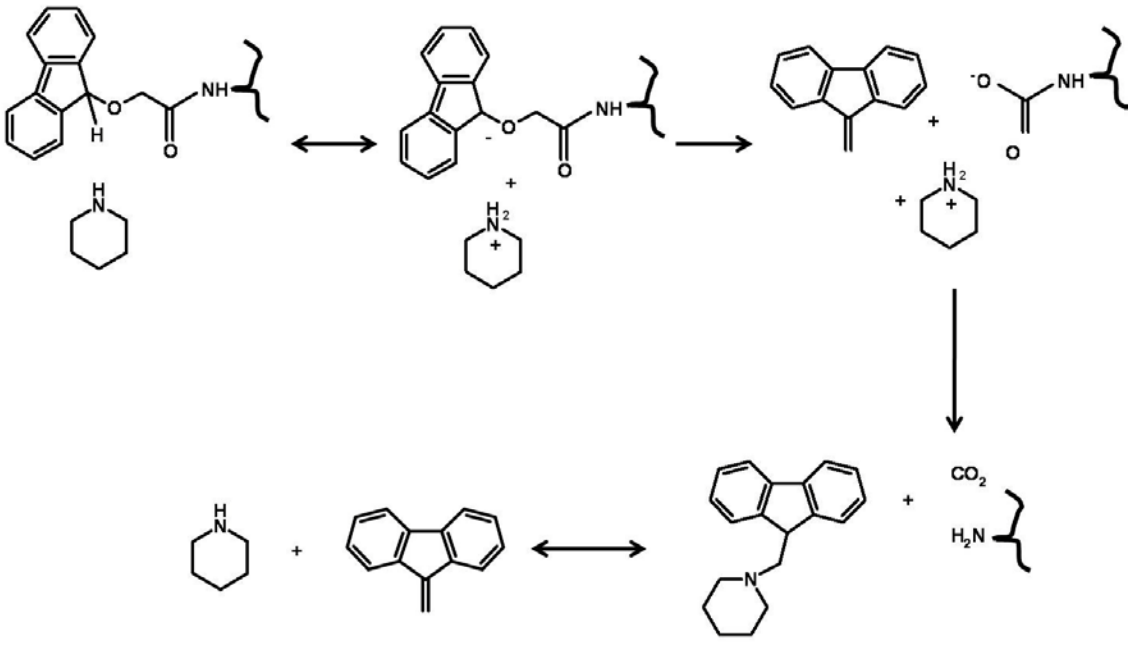

Figure 1.20 Reaction scheme for Fmoc deprotection.

1.14.4 Limitations of Fmoc Chemistry

Fmoc peptide synthesis process involves many complex chemical reactions that can affect the success of the growing chain assembly of peptides. Aggregation during chain assembly in a common occurrence for peptide sequences of more than 50 residues. As chain length increases, the separation of the peptide from the byproducts becomes increasingly difficult. To overcome these difficulties, methods involving chemoselective ligation, wherein smaller peptides are coupled together in aqueous solutions can be employed. Another popular alternative is to use chemoselective purification techniques which enable chemical tagging of the peptides helping in their separation. [197]

CHAPTER 2: EXPERIMENTAL PROCEDURES

2.1 Materials

N-isopropylacrylamide (NIPAAm), Diethylacrylamide (DEA), 4-hydroxybenzophenone, methacroyl chloride, triethylamine, acetone, D_2O (99.9 atom %), azobisisobutyronitrile (AIBN), hexanes, diethylether and 3-aminopropyl triethoxysilane were purchased from Sigma. Acetone was distilled from calcium hydride before use and NIPAAm was recrystallized from hexanes. All other chemicals were used as received.

2.2 Synthesis of Methacryloxybenzophenone (MaBP)

Methacroylbenzophenone (MaBP) was synthesized from 4-hydroxybenzophenone and methacroyl chloride in dry acetone at 0 °C. Triethylamine (TEA) was used as the acid scavenger. A 1:1:2 mole ratio of 4-hydroxybenzophenone, methacroyl chloride was added to dry acetone and TEA. The reaction was run for 5 hours and the product was purified by running it through a column using benzene as the solvent and silica gel as the stationary phase. The monomer was subsequently dried under vacuum. The monomer yield was around 85% MaBP. The reaction scheme is as shown in figure 2.1.

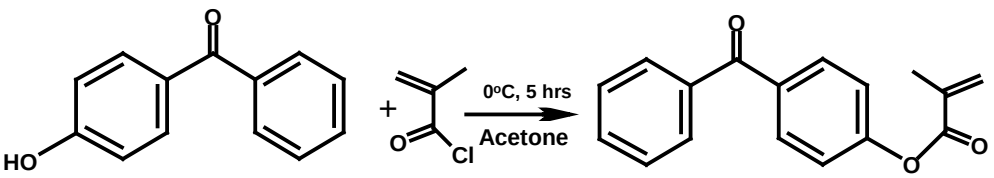

4-Hydroxybenzophenone Methacroyl chloride Methacroyloxybenzophenone

Figure 2.1 Synthesis of methacroyloxybenzophenone (MaBP)

2.3 Characterization of Methacryloxybenzophenone (MaBP)

MaBP characterized with an INOVA 400 NMR spectrometer. The spectrum had typical aromatic peaks (multiplet) at 7.2-8.0 with 9 protons associated with the aromatic benzophenone ring and a singlet at 2.1 representing the methyl group characteristic of MaBP.

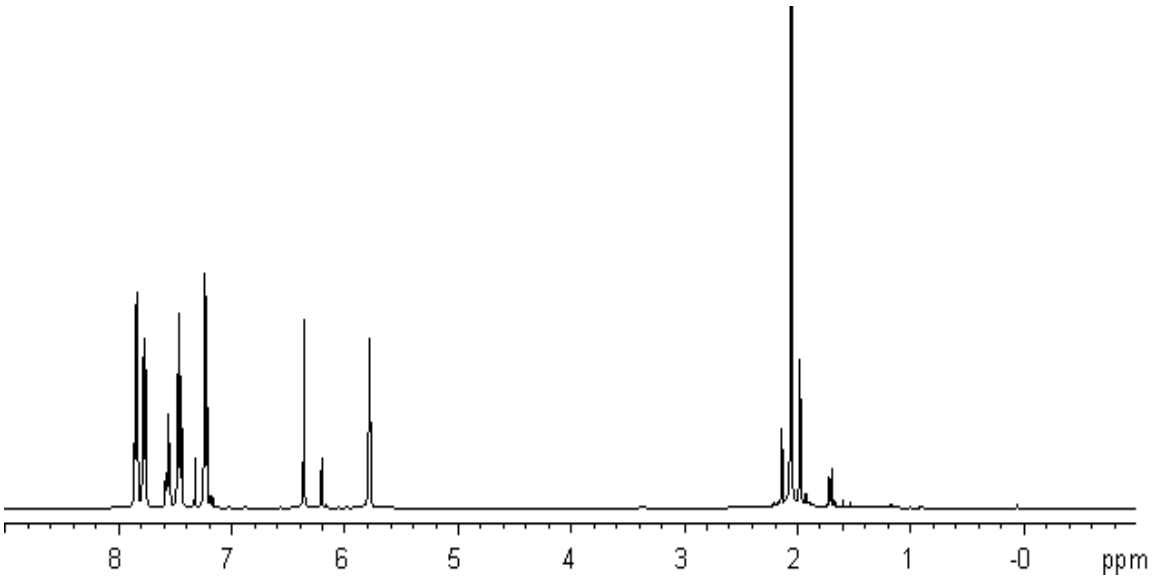

Figure 2.2 ^{1}H NMR spectrum of MaBP in $CdCl_3$.

2.4 Synthesis of N-(benzophenone)methacrylamide (NBPMA)

N-(benzophenone) methacrylamide (BPMA) was synthesized from 4-aminobenzophenone and methacroyl chloride in dry acetone at 0 °C. Triethylamine (TEA) was used as the acid scavenger. Both acetone and TEA were distilled before use. A 1:1:2 ratio of 4- aminobenzophenone, methaacryol chloride and TEA was used for the synthesis dissolved in acetone.

The reacted product was run through a column using benzene as the solvent and silica gel as the stationary phase. The monomer was subsequently dried under vacuum. The monomer yield was around 85% MaBP. The reaction scheme is as shown in figure 2.3.

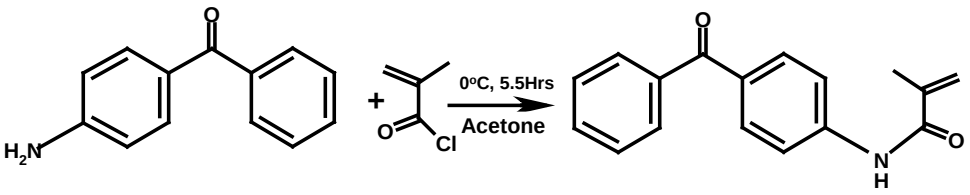

4-aminobenzophenone Methacroyl chloride (NBPMA)

Figure 2.3 Synthesis of N-benzophenone(methacrylamide) (NBPMA).

2.5 Characterization of N-benzophenone(methacrylamide) (NBPMA)

NBPMA was characterized with an INOVA 400 NMR spectrometer. The spectrum had typical aromatic peaks (multiplet) at 7.2-8.0 with 9 protons associated with the aromatic benzophenone ring and a singlet at 2.1 representing the methyl group characteristic of NBPMA shown in figure 2.4.

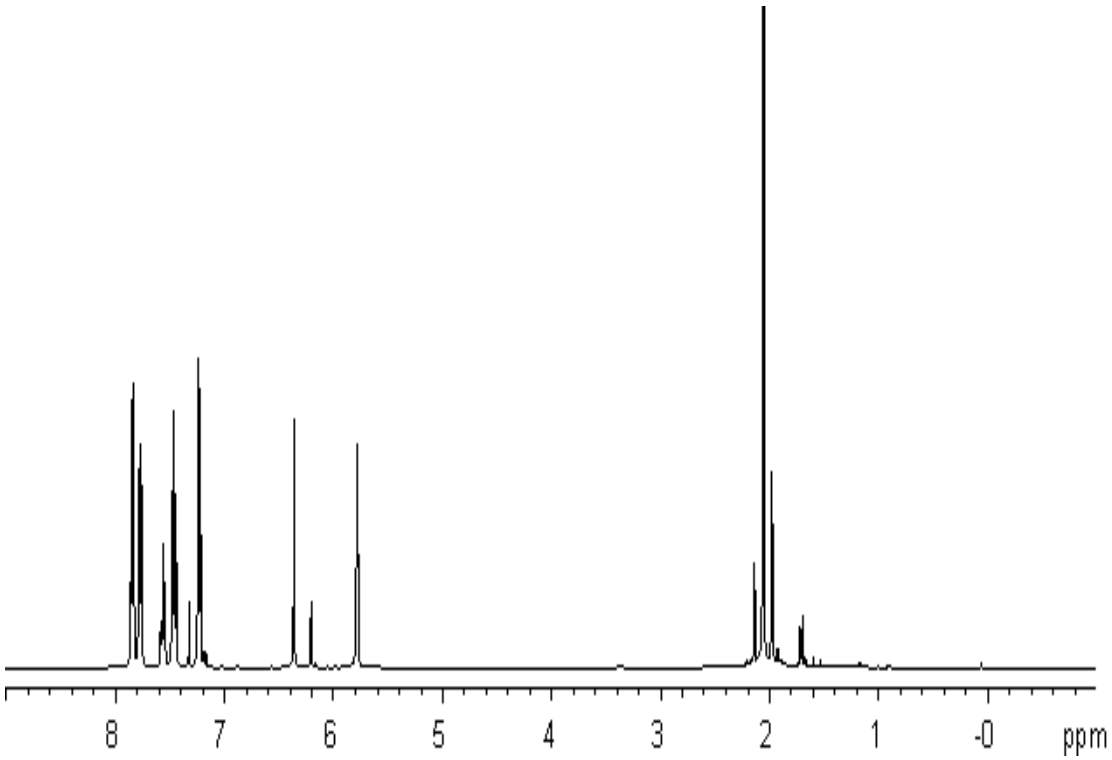

Figure 2.4 ^{1}H NMR spectrum of NBPMA in $CdCl_3$.

2.6 Polymer Synthesis and Characterization

2.6.1 Synthesis of Poly(NIPAAm-co-MaBP) Polymers

Poly(NIPAAm-co-MaBP) was copolymerized with x mol% MaBP (x=1%, 3%, 5% and 10%) using 0.1% AIBN as the initiator. The reaction was carried out for 18 hours at 65^{o}C in dioxane under nitrogen. The sample was degassed with nitrogen by freeze and thaw cycles prior to the reaction. After completion, the polymer was precipitated in diethyl ether. The polymer yield was around 88%.The reaction scheme is shown in figure 2.5.

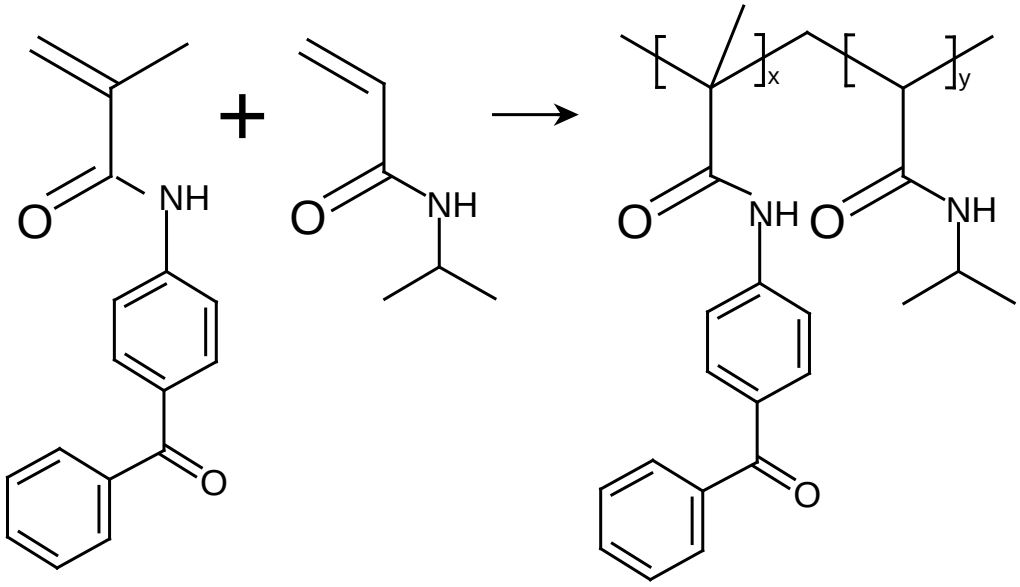

Figure 2.5 Synthesis of poly(NIPAAm-co-MaBP(x)) with varying mole % of amounts of MaBP.(x= 1%, 3%, 5%, and 10%)

2.6.2 Characterization of Poly(NIPAAm-MaBP)

The ^{1}H NMR ($CDCl_3$, δ: 1.0 (s CH_3) ppm; 4.0 (s NH); 7.2-8.0 (m 9H of aromatic group) ppm spectrum for poly(NIPAAm-MaBP(3%) is shown in Figure 2.6. The NH peak at 4.0(s) ppm and methyl group at 1.0 ppm are characteristic of NIPAAm. The peaks in the inset between 7.2-8.0(m) ppm show the aromatic groups of MaBP. The NMR spectrum showed complete incorporation of the MaBP groups. NMR analysis were similarly conducted on all samples with MaBP varying from 1%-10% to confirm incorporation of MaBP into the polymer. The aromatic peaks between 7.2-8.0 ppm increase in intensity as the MaBP content increases to 10%. The actual percentage of MaBP was calculated from the integration of the CH peaks of the aromatic group and the integration CH peaks of the isopropyl group of NIPAAm in the NMR spectrum with an error estimate of 5%.

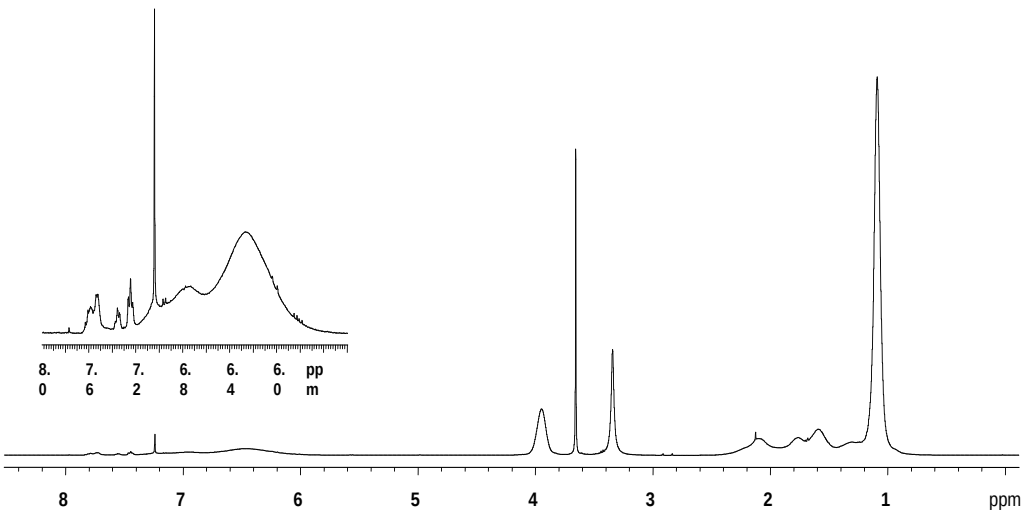

Figure 2.6 ^{1}H NMR spectrum of poly(NIPAAm-co-MaBP(3%)) in $CdCl_3$.

2.6.3 Molecular Weight Determination

The number average molecular weight and polydispersity index is shown in table 1. GPC on all samples were performed by Viscotek ^{TM} using RI, VIS, RALS, and LALS with good signal-to-noise from all detectors. Molecular weights were determined by the triple detection method. Table 2 lists the molecular weight distribution and polydispersity index for poly(NIPAAm-MaBP).

Table 2.1. Physical characteristics of poly(NIPAAm-co-MaBP)

Feed (MaBP)	Actual (MaBP)	Mn	Mw/Mn
1.0 mol%	1.0 mol%	36,683 g/mol	3.94
3.0 mol%	3.0 mol%	42,830 g/mol	4.70
5.0 mol%	4.9 mol%	75,374 g/mole	2.55
10.0 mol%	9.8 mol%	96,241 g/mole	2.43

2.6.4 Synthesis of Poly(diethylacrylamide-co-MaBP) (Poly(DEA-co-MaBP)) Polymers

Poly(DEA-co-MaBP) was copolymerized with 3 mol% MaBP using 0.1% AIBN as the initiator. The reaction was carried out for 18 hours at 65^{o}C in dioxane under nitrogen. The sample was degassed with nitrogen by freeze and thaw cycles prior to the reaction. After completion, the polymer was precipitated in diethyl ether. The polymer yield was around 86%. The reaction scheme is as shown in figure 2.7.

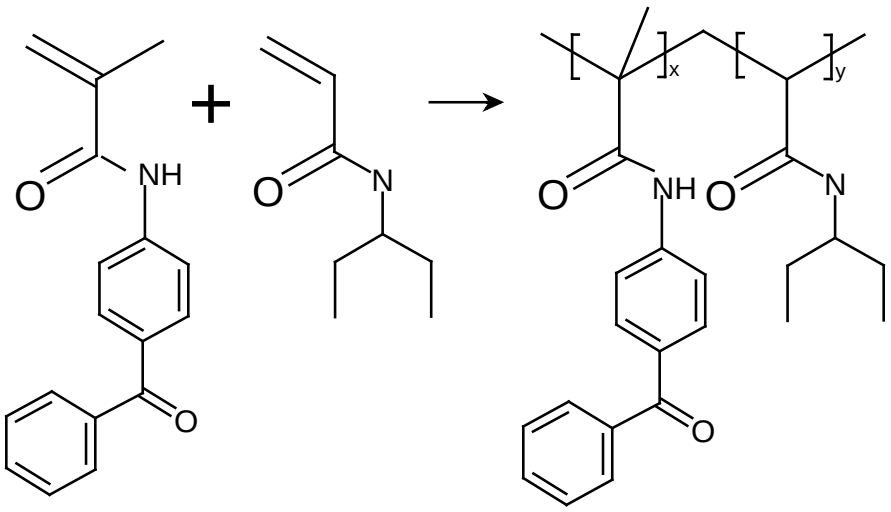

Figure 2.7 Synthesis of poly(DEA-co-MaBP)

2.6.5 Characterization of Poly(DEA-co-MaBP)

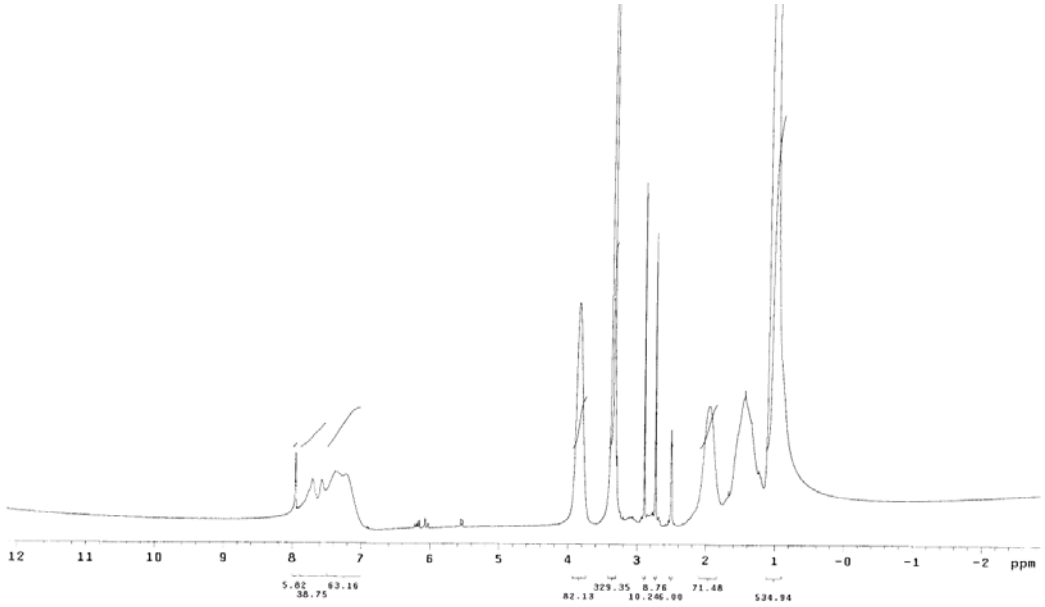

Figure 2.8 ^{1}H NMR spectrum of poly(DEA-co-MaBP(3%)) in $CdCl_3$.

2.6.6 Synthesis of Poly(NIPAAm-co-3-aminopropylmethacrylamide-co-NBPMA)

Poly(NIPAAm-co-3-APMA-co-MaBP) Polymers

Poly(NIPAAm-co-3-APMA-co-MaBP) was copolymerized with 2 mol% 3-APMA and 3 mol % MaBP using 0.1% AIBN as the initiator. The reaction was carried out for 18 hours at 70^{o}C in DMF under nitrogen. The sample was degassed with nitrogen by freeze and thaw cycles prior to the reaction. After completion, the polymer was precipitated in diethyl ether. The polymer yield was around 78%. The reaction scheme is as shown in figure 2.9.

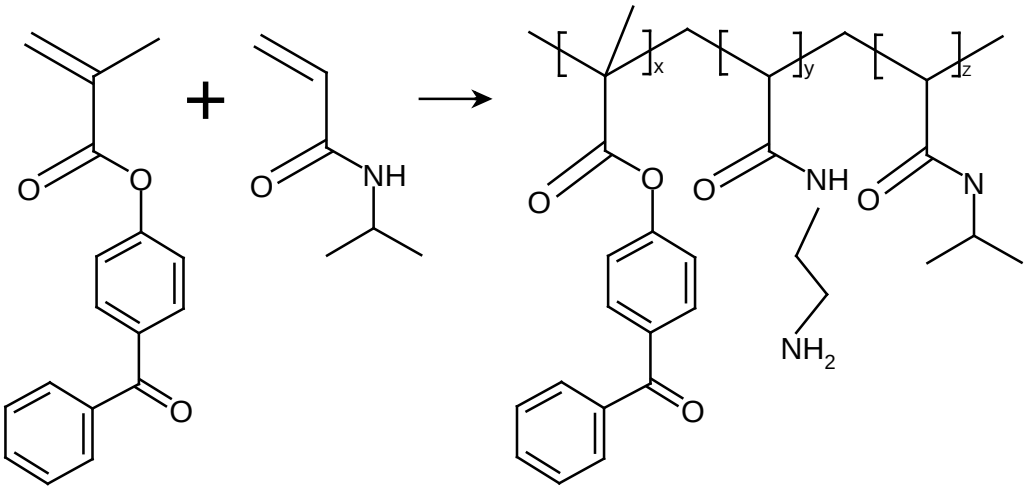

Figure 2.9 Synthesis of poly(NIPAAm-co-3-APMA-co-MaBP).

2.6.7 Characterization of Poly(NIPAAm-co-3-APMA-co-MaBP)

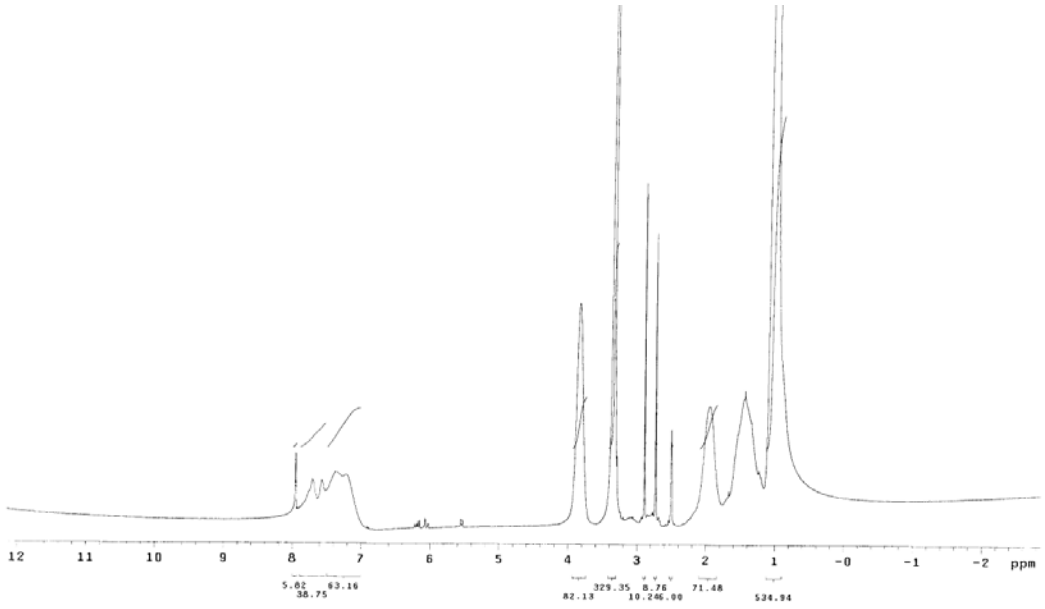

Figure 2.10 ^{1}H NMR spectrum of poly(NIPAAm-co-3-APMA(2%)-co-MaBP(3%)) in $CdCl_3$.

2.7 Determination of Demixing Temperature

The sample was placed in a temperature-controlled solution cell. The temperature was ramped at 0.2°C/min in the temperature range between 15 to 60°C. The turbidity of the samples was followed during heating by monitoring the scattered light intensity at an angle of approximately 45°. The demixing temperature was taken at the point where the scattered intensity increased by 10%. In all cases, the temperature range over which the scattered intensity changed was approximately 1^{o}C.

2.8 Preparation of Surface Tethered Poly(NIPAAm) Photo-Cross-Linked Networks by Spin-Coating

Substrates (either quartz or silicon) were cleaned with ozone to remove any organic impurities followed by deposition in a 1% solution of 3-aminopropyltriethoxysilane in acetone. The substrates were heated to 100^{o}C to drive condensation of the silane groups to the substrate surface. A solution of poly(NIPAAm-co-MaBP) in cyclohexanone was spin cast on the freshly prepared substrate. Cross-linking was accomplished by exposing the film to UV light (365 nm) for 30 minutes. Figure 2.11 shows a schematic representation of the spin casting process of depositing the benzophenone modified poly(NIPAAm-co-MaBP) polymers onto quartz or silica substrates. Figure 2.12 shows reaction scheme for the photochemical cross-linking of poly(NIPAAm).

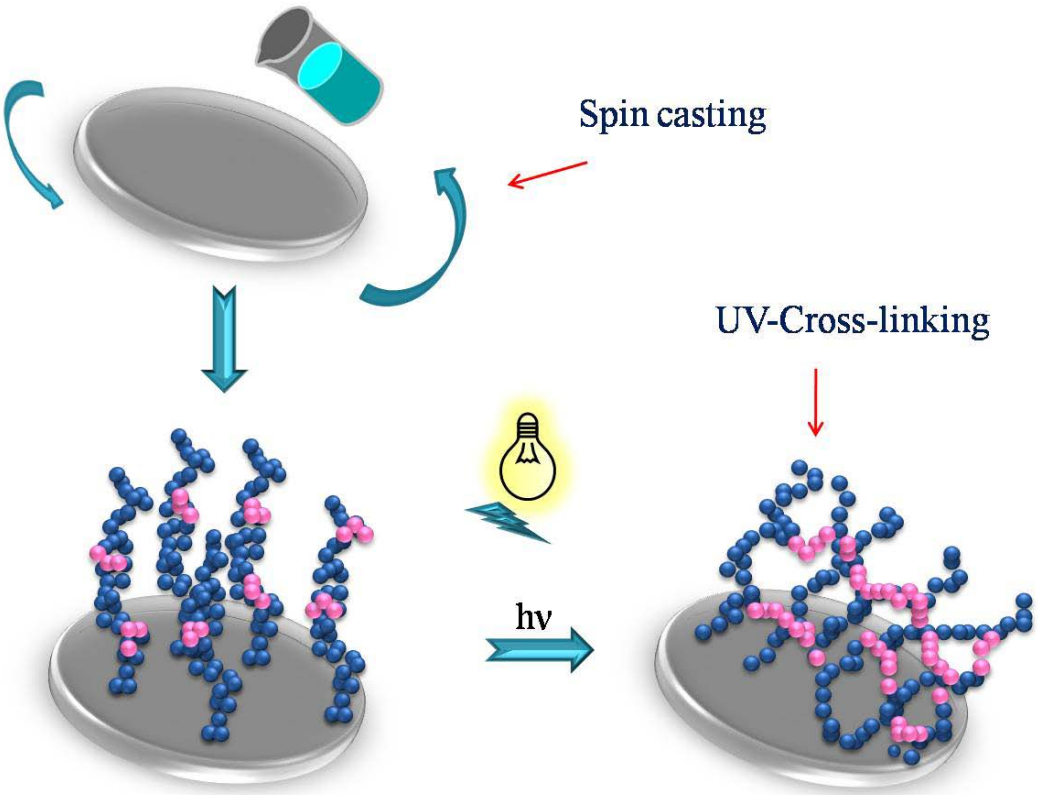

Figure 2.11 Schematic representation of the spin casting process of photochemically modified poly(NIPAAm-co-MaBP) networks to quartz or silica substrates.

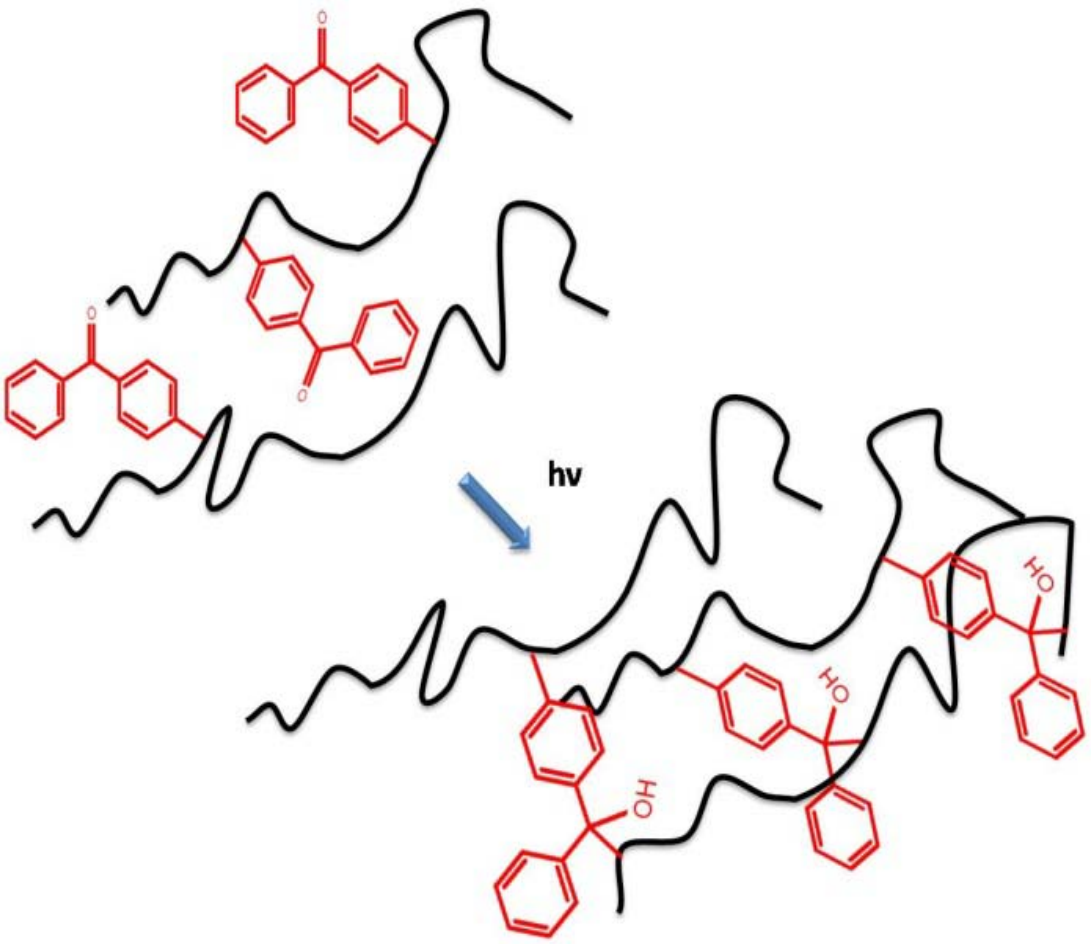

Figure 2.12 Photochemical cross-linking of poly(NIPAAm-co-MaBP).

2.9 General Procedure of Peptide Conjugation to Poly(NIPAAm) Hydrogels

1. Poly(NIPAAm) hydrogels was synthesized by adding 200mg of NIPAAm monomer, 3 mole% of NBPMA and appropriate amount of 3-APMA(2 and 10 mole%) to 1ml of DMF and photo-cross-link using UV irradiation.
2. Poly(NIPAAm) gels were then cut into small pieces and transferred to a peptide reaction vessel and washed thoroughly with DMF to remove unreacted monomers.

3. Prepare the appropriate Fmoc protected amino acid by adding excess (4 times the mole % of 3-APMA) of the amino acid to the reaction mixture containing the sample hydrogels.

2.10 Kaiser Test or Ninhydrin Test

The Kaiser test was done to monitor the presence or absence of free amine groups in the sample hydrogel. The addition of amino acids was also subsequently tested using the Kaiser test for the presence or absence of a free amine group.

The Kaiser test kit consists of phenol (80% in ethanol), KCN in water/pyridine and ninhydrin (6% in ethanol).

The test procedure is as follows:

1. Remove a few gels from the reaction vessel prewashed with DMF.
2. Transfer the gels into a small glass test tube and add 3 drops of phenol, KCN and ninhydrin to each test tube containing the sample gels.
3. Mix well and heat the test-tube at 120°C for 5 minutes.
4. Blue/violet color indicates the presence of a free amine group in the hydrogel whereas a yellow/orange color indicates the absence of a free amine group in the sample hydrogel.

2.11 Synthesis of Poly(NIPAAm-co-NBPMA-co-3-APMA)- GEGVP Conjugates

Poly(NIPAAm-co-NBPMA-co-3-APMA) hydrogels were cut into small pieces and transferred to a peptide reaction vessel. Glycine (G) Glutamic acid (E),Valine (V) and Proline (P) are added in the ratio of 4:1 with respect to 3-APMA and subsequently conjugated to the hydrogels using Fmoc based peptide synthesis. The addition of each amino acid and the subsequent removal of the Fmoc group was verified by the Kaiser

test which tests positive for the presence of a free amine group by turning the gel and the reaction mixture blue and tests negative in the absence of a free amine group by remaining colorless or pale yellow.

2.12 Synthesis of Poly(NIPAAm-co-NBPMA-co3-APMA)-GGH Conjugates

Poly(NIPAAm-co-NBPMA-co-3-APMA) hydrogels were cut into small pieces and transferred to a peptide reaction vessel. Glycine (G) and Histidine (H) are added in the ratio of 4:1 with respect to 3-APMA and subsequently conjugated to the hydrogels using Fmoc based peptide synthesis to get the desired peptide sequence. The Kaiser test was then performed as mentioned in section 2.7 to verify the coupling of the amino acids to the NIPAAm hydrogels.

2.13 Instrumentation

2.13.1 Neutron Reflection

Neutron reflection was used to characterize and study the swelling behavior of the poly(NIPAAm-co-MaBP) films.[198, 199] Neutron reflectometry is a powerful experimental technique used to investigate the structure of thin films. A neutron beam can be elastically scattered of a flat sample interface giving us vital information about the thickness, roughness, coverage, and material composition details of a sample layer perpendicular to the reflecting surface. Each neutron can be seen as a wave with a wavelength corresponding to its momentum. This relationship is defined by the de Broglie formula given as:

$$\lambda = h/p \qquad (2.1)$$

where p is the neutron's momentum, λ is the neutron's wavelength, and h is the Planck's constant.

Constructive interference between neutron waves occurs there is a difference in the refractive index of the materials and can be calculated using Bragg's law.

$$n\lambda = 2d \sin(\theta) \qquad (2.2)$$

where λ is the neutron's wavelength, θ is the neutron's incident angle, and *d* is the distance between layers in the sample.

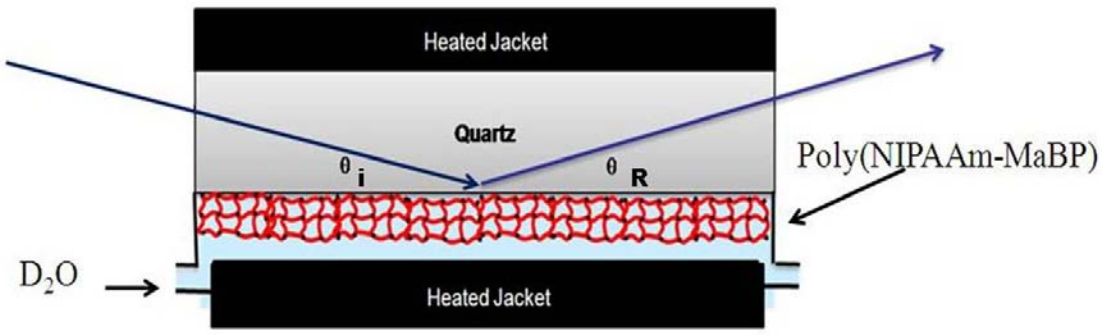

Figure 2.13 Schematic representation of neutron reflectivity.

The neutron reflectivity measurements were carried out on the Surface Profile Analysis Reflectometer (SPEAR, Manuel Lujan, Jr. Neutron Scattering Center, Los Alamos National Laboratory). SPEAR is a time-of-flight (TOF) reflectometer employing a polychromatic, pulsed neutron source. The basic principle of neutron reflectometry

involves directing a collimated neutron beam towards a flat interface at a low incidence angle, θ, and measuring the ratio of reflected intensity to incident intensity, R, as a function of momentum transfer vector $q_z = 4\pi\sin\theta/\lambda$, where λ is the neutron wavelength. The schematic representation of a typical neutron reflection setup is as shown in figure 2.13. The range of neutron wavelengths used in the experiments was 1–16 Å, determined by the TOF technique. We used two experimental configurations: (i) for measurements in the dry state and against vapors the neutrons were entering quartz or Si substrates from the air (or vapor) side, and (ii) an "inverted" geometry with D_2O (solvent) on the bottom and quartz (or silicon) substrate above the solid-liquid interface. The lower medium has a higher scattering length density than the upper one. Under these conditions, the reflectivity R =1 for q_z below a critical value $q_c = 4\pi\ (\Delta SLD)^{1/2}$, where ΔSLD is the scattering length density difference between the upper and lower media. Neutron reflectivity data collection typically lasted typically 3.5–4.5 hours. The reflectivity data were reduced using the incident neutron intensity spectrum. Based on measured data, a "model" reflectivity profile was generated using Parratt's recursion formalism[200] and compared to the measured reflectivity profile. The model was then adjusted to obtain the best least-squares fit to the data using genetic optimization followed by Levenberg-Marquardt nonlinear least-squares method.

2.13.2 Attenuated Total Reflection / Fourier Transform Infrared (ATR/FTIR) Spectroscopy

IR spectroscopy is an extremely useful technique for investigating structural changes in a majority of proteins that cannot be studied by X-ray crystallography and NMR.[201] In particular, attenuated total reflection Fourier transform infrared spectroscopy (ATR-FTIR) is one of the most powerful methods for recording IR spectra for both biological and

polymeric materials. It offers a fast and reliable signal even for very low sample concentrations. The samples of interest can be studied as a function of temperature, pressure, and pH, as well as in the presence of specific ligands.[201]

In the present study, we have investigated the phase behavior of poly(NIPAAm) copolymers in water and D_2O in order to reveal changes in the hydration states of NIPAAm during the phase transitions. Figure 2.14 shows a typical ATR-FTIR setup with a coating of poly(NIPAAm). By carefully controlling film thickness to be near the penetration depth of the IR beam, we can effectively block out any solvent peaks from the IR spectrum.

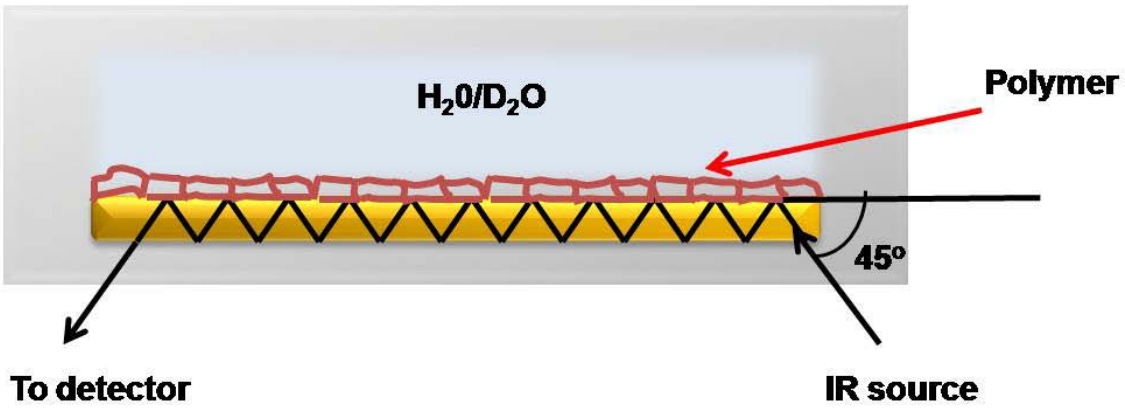

Figure 2.14 Schematic representation of ATR-FTIR

ATR-FTIR measurements on poly(NIPAAm-co-MaBP) were performed using a Nicolet 6700 FTIR spectrometer equipped with a temperature controlled multibounce ATR ZnSe plate. The polymers dissolved in acetone were cast on to the ZnSe plate and heated to 60°C for 2 hours to remove residual acetone. An FTIR spectrum was then performed to

determine that there was no residual acetone left in the polymer cast on the ZnSe plate. All FTIR measurements were done in the temperature range of 24°C-102°C in absorbance mode with 100 scans and a resolution of 4 cm^{-1}. The spectral ranges for all scans were in the region between 4000-650 cm^{-1}. The crystal background was subtracted from the samples for each run.

The ATR correction can be used as follows. A FTIR spectrum collected in the ATR mode is related to a spectrum collected by transmission mode by the following equation:

$$S_{ATR}=k_1*S_{CORR}*D_P \tag{2.3}$$

where S_{ATR} is the ATR spectrum

k_1 is an arbitrary constant

S_{CORR} is the corrected spectrum

D_p is the ATR penetration depth

The penetration depth is given as

$$D_p = \frac{\lambda}{2\pi n_c \sqrt{\left(\sin^2\phi - \left(\frac{n_s}{n_c}\right)^2\right)^2}} \tag{2.4}$$

where φ = effective angle of incidence.

n_c = Refractive index of crystal.

n_s = Refractive angle of sample.

λ = Wavelength.

For any given experiment,

$$D_P = 1/(k_2 * v) \tag{2.5}$$

where v is the wavenumber and k_2 is a constant related to the angle of incidence and refractive index of the sample and ATR crystal.

In order to calculate the corrected spectrum, we have to calculate

$$S_{CORR} = S_{ATR}/(D_P * k_1) \tag{2.6}$$

Also,

$$S_{CORR} = S_{ATR} * v/k \tag{2.7}$$

where k is an arbitrary constant.

2.13.3 Ellipsometry

Ellipsometry is a technique that measures the change in polarization state of a beam of light upon reflection from the sample of interest.The nature of this polarization state depends on a number of factors like sample thickness and refractive index. The raw experimental data are usually expressed as two parameters Ψ and Δ. The polarization state of the light incident upon the sample may be decomposed into an s (out of plane) and a p (in plane) component. The intensity of the s and p component, after reflection, are denoted by R_s and R_p. The fundamental equation of ellipsometry giving the change

in the polarization ellipse upon reflection is fully characterized by the ratio ρ, which is expressed as the ellipsometry angles ψ and Δ and is given as:

$$\rho = r_p / r_s = \tan\psi \exp(i\,\Delta) \qquad (2.8)$$

We use a rotating compensator ellipsometer with an attenuated total reflection (ATR) configuration, in which a sample is placed on the backside of a prism (LaSFN9) with a refractive index of 1.845, with the incident beam probing the interface from the prism side. The light-source is a He-Ne laser with a wavelength of λ = 633 nm. The technique is quite similar to surface-plasmon resonance (SPR), however, we do not need a gold layer, thus simplifying the experimental set-up. The temperature of the flow cell is controlled by a peltier heating device with a precision of 0.1 ^{o}C.

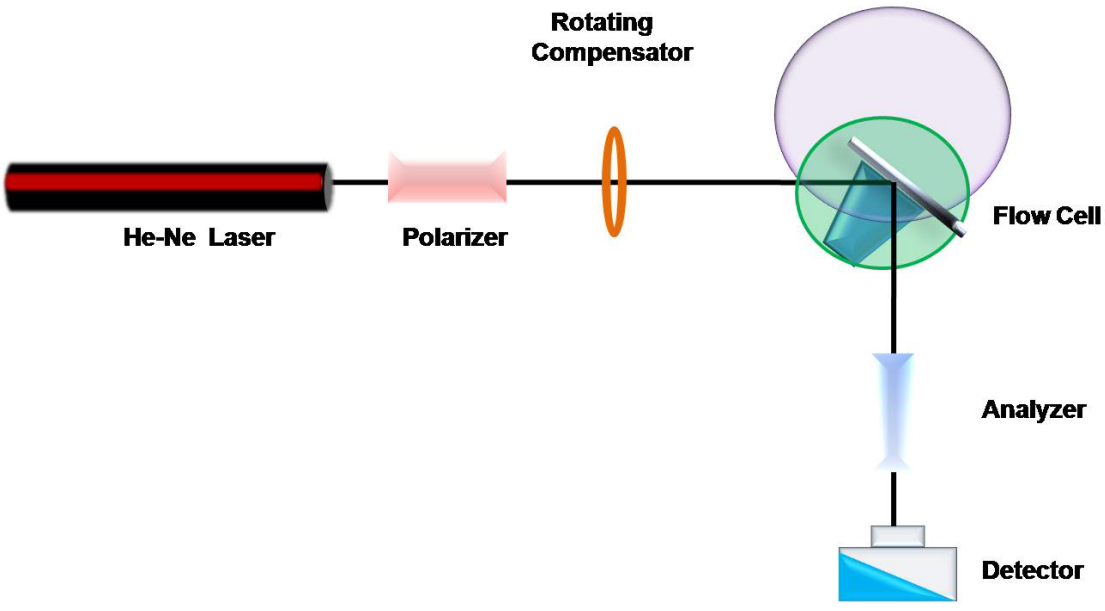

Figure 2.15 Schematic representation of rotating compensator ellipsometer with an ATR configuration.

The thickness of all films was in the optical range, giving rise to sufficient features in the recorded spectra to infer the refractive index profile. To analyze the data, model refractive index profiles were generated, and the ellipsometric parameters were numerically calculated using the matrix optical formulation.[202] The parameters of the model were adjusted to minimize the differences between the simulation and experimental data. A typical ellipsometry setup is as shown in figure 2.15

2.13.4 UV-Vis Spectroscopy

Aqueous solutions of Poly(NIPAAm) and poly (NIPAAm) gels exhibit strong scattering, turbidity changes upon heating which can be studied using UV-Vis spectrophotometry. The data can be collected in both as transmittance or absorbance. There would be a decrease in transmittance and an increase in absorbance signals when the temperature is increased. Both measurements can be determined as a function of temperature or pH.

The UV-Vis spectroscopy was connected to a water bath for temperature in order to investigate phase transition behavior of poly(NIPAAm) and peptide conjugated poly(NIPAAm) gels. The 0.5 cm long sample cell was completely filled with poly(NIPAAm) gels and the sample was equilibrated before taking measurements. All polymer gels were heated from 22°C to 45°C.

CHAPTER 3: DEMIXING BEHAVIOR OF LINEAR AND SURFACE TETHERED POLY(NIPAAm) NETWORKS

3.1 Introduction

Lower critical solution temperature (LCST) polymers experience a sharp volume-phase transition when subjected to small perturbations in external stimuli.[82] For example, it is well known that poly(N-isopropylacrylamide) (poly(NIPAAm)) undergoes a hydrophilic/hydrophobic transition at roughly 32°C.[33, 36, 37] This transition has been attributed to changes in the hydrogen bonding tendency of water. [35, 203-206] In poly(NIPAAm), it is thought that water molecules form ordered structures around both the hydrophilic amide moieties and the hydrophobic isopropyl groups to maximize favorable hydrogen bonding associations. As temperature is increased, hydrogen bonding interactions grow weaker until the LCST is reached, wherein hydrophobic attractions between isopropyl groups dominate and collapse the polymer structure.

With respect to the nature of the hydrophilic/hydrophobic transition, aqueous solutions of linear poly(NIPAAm) exhibit a concentration dependent demixing temperature. In particular, Afroze et al determined that the critical point of poly(NIPAAm) occurs at a temperature of 29.5°C and a volume fraction, ϕ, of 0.43.[207] As the polymer concentration is reduced towards zero, the demixing temperature approaches 34°C. To explain this phenomenon, the effective Flory interaction parameter χ can be expanded in powers of φ with a minimum of three terms, wherein each term is a function of temperature.[94, 208, 209]

An important question concerns the use of a concentration dependent χ parameter derived from solution phase diagrams to describe the behavior of constrained systems, including end-tethered or cross-linked polymers. Baulin and co-workers showed that a self-consistent field theory formulated in terms of a composition dependent χ parameter could lead to vertical phase separation in poly(NIPAam) brushes.[210] An explicit form of χ was not considered in the study; however, if $\chi(T,\varphi)$ could be indeed expanded in powers of φ up to the third-order term, bilyar type profiles should be seen in poly(NIPAAm) brushes. Yim and co-workers showed direct experimental evidence of bilayer structures that result from vertical phase separation in poly(NIPAAm) brushes with NR.[211] Mendez and coworkers used the explicit concentration and temperature dependent χ parameter of Afroze et al. to predict compositional profiles of poly(NIPAAm) brushes as a function of temperature.[212] The approach produced results that, at least in qualitatively, capture whether or not a brush undergoes a broad or a sharp transition as a function of molecular weight and surface coverage. [213-215]

Our results on the swelling behavior of surface-tethered poly(NIPAAm) networks as characterized by neutron reflectivity permit a simpler comparison between constrained and unconstrained LCST polymers. Harmon and co-workers showed that cross-linked poly(NIPAAm) thin films can undergo significant temperature-induced structural changes with surface plasmon resonance.[114, 115] Significantly, the transition temperature appeared to be lower than the cloud temperature observed in linear poly(NIPAAm) solutions.

We prepared surface-tethered networks from photo-cross-linkable poly(NIPAAm) copolymers with benzophenone-pendant monomers.[118] Ultraviolet radiation (λ = 350 nm) triggers the n,π* transition in the benzophenone moieties leading to a biradicaloid

triplet state that abstracts a hydrogen from a neighboring aliphatic C-H group, forming a stable C-C bond.[216] Neutron reflection reveals that the discontinuity in the volume transition of the surface-tethered networks coincides with the miscibility gap of non-cross-linked linear poly(NIPAAm). This result signifies that the concentration dependent χ interaction parameter is unaffected by cross-linking and can be used to model volume phase transitions in constrained systems.

3.2 Results and Discussion

We investigated cross-linked poly(NIPAAm-co-MaBP) coatings on solid quartz substrates by neutron reflection. All polymers were spin-cast from cyclohexanone followed by heating at 90 ^{o}C for 10 minutes to remove any excess solvent that may be present. It is of utmost importance to accurately determine the neutron scattering length density (SLD) of the spin cast film in order to properly constrain the fits neutron reflection data. The SLD depends on the sum of the bound coherent neutron scattering lengths b_i of the constituent atoms and the molar volume of the polymer layer, defined as the density ρ divided by the molar mass M [198, 199]

$$SLD = \rho \sum_{i=1}^{n} b_i \Big/ M \tag{3.1}$$

The density of the layer was determined to be 1.2 g/cm^2 as independently measured by x-ray reflection. Hence, the neutron SLD of the spin-cast film was estimated to be 0.96 x10^{-6} Å^{-2}

Figure 3.1 shows the neutron reflection profile from a 320 Å thick film measured under a dry environment and D_2O vapor at 23 ^oC. The Kiessig fringes persisted over 6 orders of magnitude loss in the reflectivity in both cases. The reflection profile had a scattering length density 0.64 x 10^{-6} $Å^{-2}$ fitted in the dry environment. This is 33% lower than the expected value of 0.96 x10^{-6} $Å^{-2}$. This discrepancy can be accounted for if bound water is associated with the poly(NIPAAm) segments. In a two-component system comprising species *i* and *j*, the measured SLD_{layer} is related to sample composition via

$$SLD_{layer} = \phi_i SLD_i + \phi_j SLD_j \tag{3.2}$$

Where $SLD_{i,j}$ is the SLD of each species in the unmixed state, respectively and $\phi_{i,j}$ is the volume fraction of each species. This relationship assumes that mixing does not affect the molar volumes of either species. Assuming an SLD of 0.96 x10^{-6} $Å^{-2}$ for dry poly(NIPAAm-co-MaBP), the estimated volume fraction of H_2O in the spin-cast layer is 20%. Exposure of the layer to D_2O vapor during the measurement resulted in an increase of the scattering length density to 2.4 x 10^{-6} $Å^{-2}$, however, the layer thickness increased only 6% to 340 Å. In other words, it was seen that D_2O replaces H_2O, which enhances contrast but does not significantly alter the film thickness. The volume fraction of D_2O in the layer is 25%, close to 20% in the case of H_2O. Based alone on the contrast variation between H_2O and D_2O, the scattering length density of dry poly(NIPAAm-co-MaBP) (without bound water) is estimated to be approximately 0.9 x 10^{-6} $Å^{-2}$, which is in agreement with the value calculated using the densities obtained from X-ray reflection.

It needs to be noted that rinsing the layer in water for the first time after cross-linking generally resulted in a 5-10% reduction in thickness but no apparent change in the

scattering length density. Subsequent rinses did produce a further loss in material. We were able to reproduce measurements from a single sample over a 2 month period, which were both reproducible and consistent from run to run, giving us confidence that the films are stable even after repeated solution/dissolution cycles.

After each neutron reflectivity experiment of the polymer against bulk liquid, the dry layer was measured and all thicknesses were within 5% of each other. Immediately after a run in D_2O, the SLD of the polymer layer (measured in air) was between approximately 1.0 and 1.5 x 10^{-6} $Å^{-2}$, reflecting bound D_2O remaining in the layer. In subsequent measurements, the SLD slowly decayed to 0.6 x 10^{-6} $Å^{-2}$ as H_2O vapor from the air replaced D_2O.

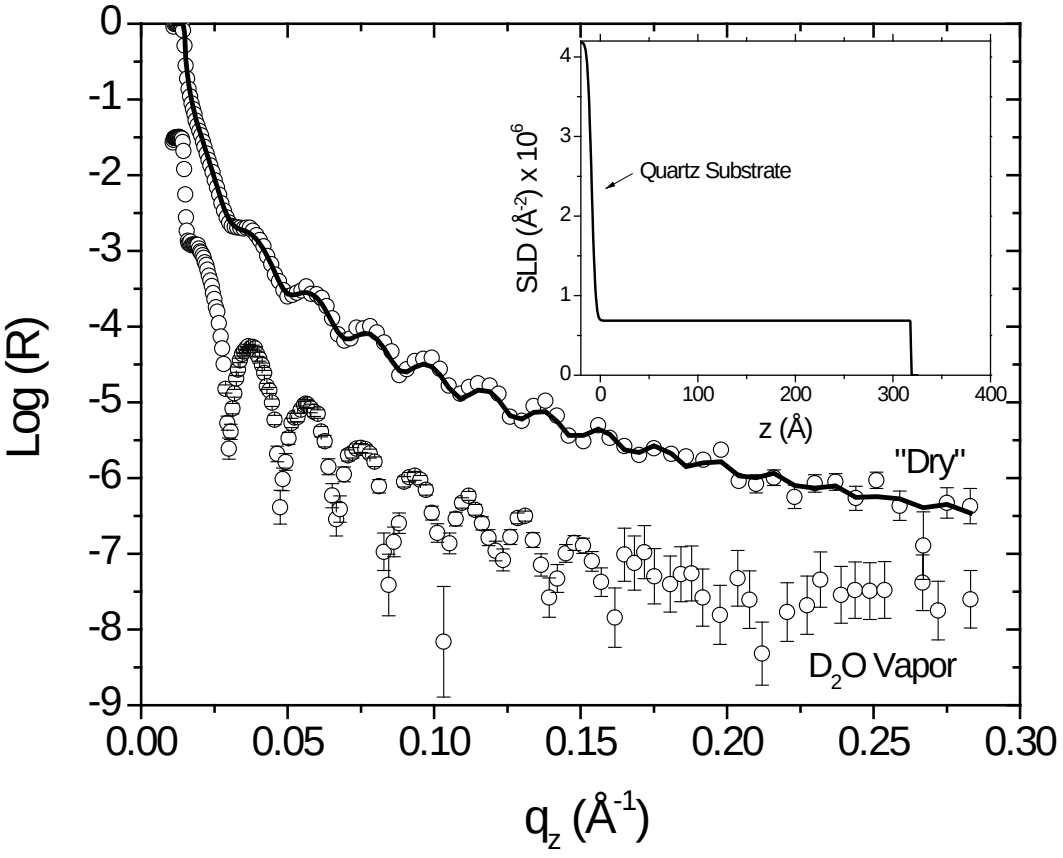

Figure 3.1 Neutron reflectivity data for surface-tethered poly(NIPAAm-co-MaBP) layer in a humidity free "dry" and a D_2O vapor environment at 23°C. The solid curve drawn through the "dry" data points corresponds to the best fit, which is shown in the inset. The data have been offset vertically for clarity. Error bars for the reflectivity data represent statistical errors in these measurements.

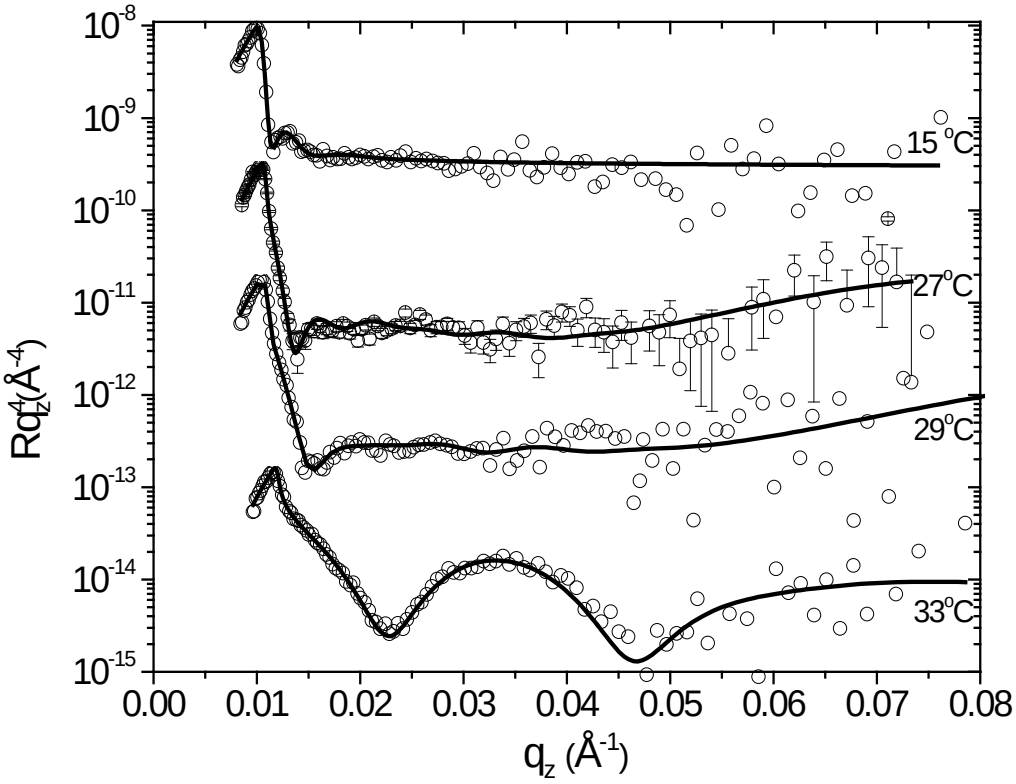

Figure 3.2 Four examples of the neutron reflectivity data for surface-tethered poly(NIPAAm-co-MaBP) layer exposed to bulk D_2O as a function of temperature. The data and fits (solid lines) have been offset vertically for clarity. The curves through the data correspond to best fits. Error bars for the reflectivity data represent statistical errors in these measurements. The resulting polymer volume fractions, ϕ, at different temperatures are show in Figure. 3.4.

Figure 3.2 shows the examples of the neutron reflection profiles and the corresponding best fits of the poly(NIPAAm-co-MABP) layer exposed to bulk D_2O over a temperature range of 15-33°C. The data are presented as reflectivity Rq_z^4 to compensate for the q_z^{-4} decay that results from Fresnel law. The data are shifted on the y axis for clarity.

Between a temperature range of 15°C and 29°C, the reflection profile shows a gradual broadening of the first Kiesseg fringe, corresponding to a reduction in the overall thickness of the layer. At temperatures between 29 and 33°C, the spacing between fringes abruptly changes and giving rise to higher order fringes in the reflectivity profile. Above 33°C the spacing between fringes remain relatively constant with two to three well defined fringes.

The reflectivity profiles at each temperature were initially modeled using a single slab of constant SLD, with a smeared interface between the layer and solvent. The best fit profiles at low temperatures, however, were inadequate using this model as shown in Figure 3.3. A functional form consisting of three slabs, each of constant SLD, with smeared interfaces between the slabs by error functions was chosen. Though this approach was sufficient to generate reasonable fits at all temperatures (Figure 3.2), there are possibilities of better capturing intricate detains in diffuse interfaces using more complicated models, providing better fits.[217, 218] For instance, there is fine-structural detail that is not captured completely in the three-slab simulations (such as the 27°C run, Figure 3.2). However, our attempts to use more sophisticated models, including cubic splines, showed that the fits, while quite sensitive to small changes in interfacial details, did not produce statistical differences in the overall thickness.

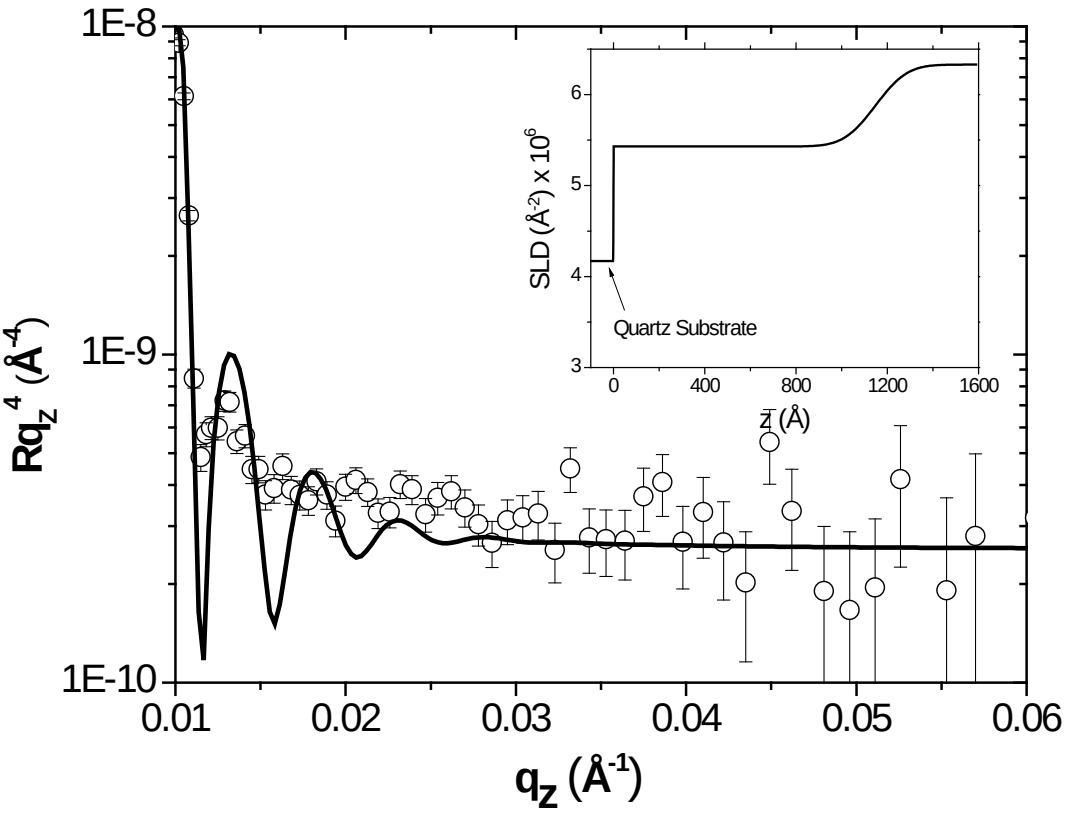

Figure 3.3 Neutron reflectivity data for surface-tethered poly(NIPAAm-co-MaBP) in D_2O environment at 15°C. The solid line though the data corresponds to the best fit using a single slab SLD profile. The inset shows the SLD distribution obtained from the best fit.

The polymer segment profiles that correspond to the best fits in Figure 3.3 are presented in Figure 3.4. Each polymer volume fraction profile, $\varphi(z)$, was estimated from its scattering length density profile $SLD(z)$ according to equation 3.2. For every temperature, the integral of the volume fraction profile over the extension of the layer was within 5-10% of each other. In other words, although the polymer expands and contracts, its total mass remains constant. The polymer volume fraction profiles show a gradual reduction as temperature is raised from 15 to 29°C. In this temperature regime,

the average thickness decreased from 1100 to 750 Å. The average thickness <z> is defined as $2\int z\phi(z)dz \Big/ \int \phi(z)dz$. Moreover, in every case, a relatively diffuse interface was observed at the D_2O boundary, which was most likely the result of dangling ends that effectively behave as a brush. Between 29 and 31°C, the average thickness abruptly changes from 714 (+/- 35) Å to 339 (+/- 34) Å. Above 31°C, the layer thickness continues to contract, but is only very weakly dependent on temperature. No discernable difference in layer thickness was observed between 42°C and 49°C.

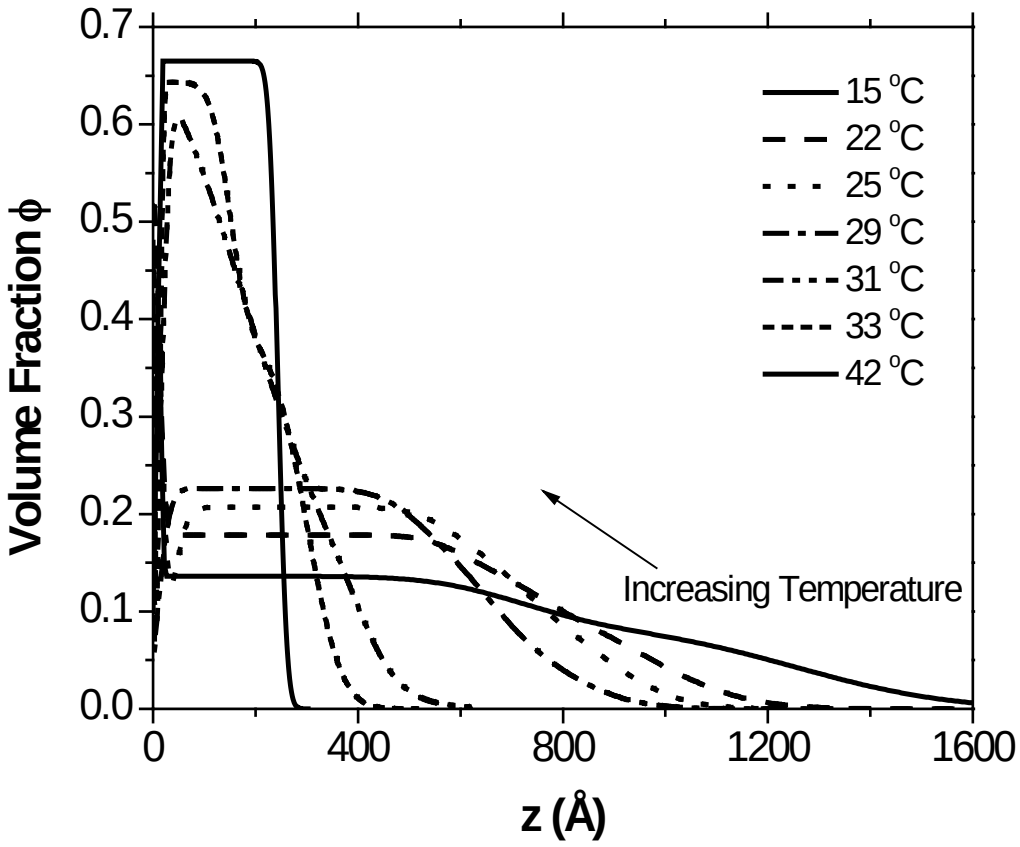

Figure 3.4 Volume fractions of the poly(NIPAAm-co-MaBP) in bulk D_2O as a function of the distance from the substrate and temperature. The data is the outcome of the best fit profiles obtained from fitting neutron reflectivities. The examples of such fits are shown in Fig. 3.2.

In the high temperature regime, the volume fraction profiles are nearly uniform with a roughness of approximately 10 Å. Interestingly, there was also a 20-50 Å thick D_2O rich layer next to the substrate, which could be the result of D_2O that cannot escape as the layer collapses. While the nature of this trapped D_2O was not fully investigated in the experiments, repeated temperature cycles showed that the width of the D_2O layer was not consistent from run to run and may be related to the rate of temperature change. The width of the D_2O rich layer, however, did not affect the SLD of the collapsed portion of the poly(NIPAAm-co-MaBP) network.

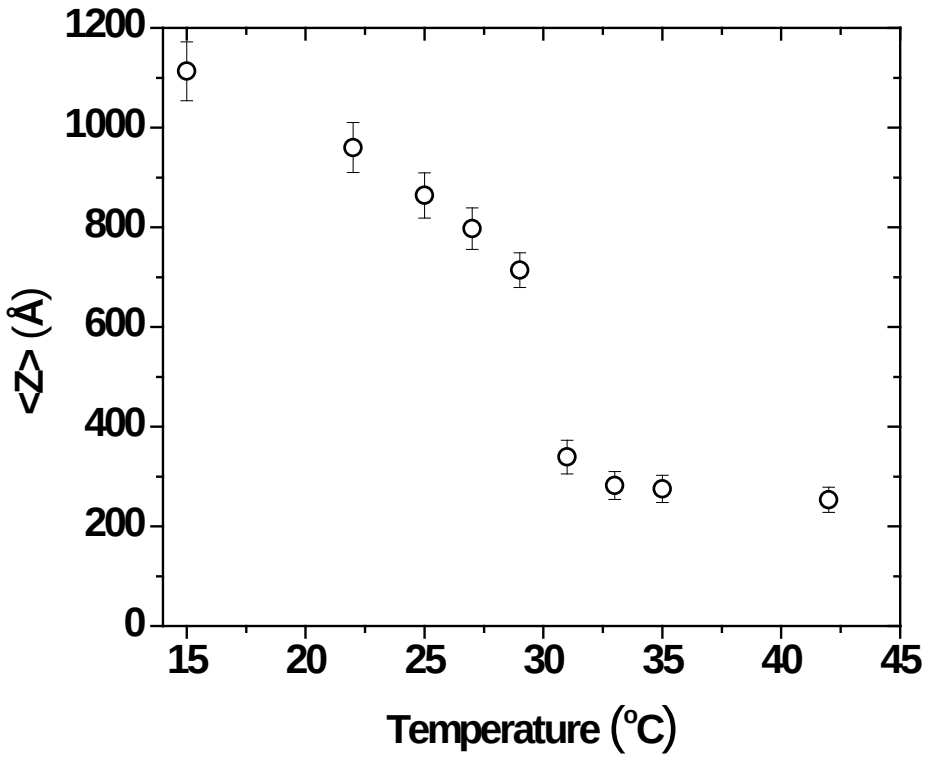

Figure 3.5 Variation of average thickness <z> of the surface-tethered poly(NIPAAm-co-MaBP) network as a function of temperature.

Figure 3.5 shows the change in the average thickness as a function of temperature. Above 15°C, the thickness appears to decrease approximately linearly with temperature.

At approximately 30 °C, the layer collapses to nearly its thickness as measured in the dry state. It is seen that there is still about 30-35% water, which corresponds to 2-3 D_2O molecules per polymer segment. It is tempting to explain the nature of the collapse based on the experimentally determined phase diagram for linear poly(NIPAAm) solutions. As the demixing temperature of linear poly(NIPAAm) is a strong function of concentration with almost no effect on molecular weight, it is expected that cross-linking will have minimal effect on the phase behavior.[219-221] Afroze and coworkers fit experimental phase diagrams of linear poly(NIPAAm) with a quadratic form of a compositional dependent χ parameter[207]

$$\chi_{eff}(T,\phi) = \chi_0(T) + \chi_1(T)\phi + \chi_2(T)\phi^2 \tag{3.3}$$

Where the coefficients depend on temperature via

$$\chi_i(T) = A_i + B_i T \tag{3.4}$$

The A_i and B_i parameters are given in Table 2.1. Using these parameters, the phase diagram is drawn in Figure 3.5 showing the binodal boundaries. The binodal curve envelopes the two-phase region or the miscibility gap of poly(NIPAAm). Superimposed on the binodal are the experimentally determined demixing temperatures for poly(NIPAAm-co-MaBP), as determined by turbidity measurements. The degree of agreement between the demixing behavior of poly(NIPAAm-co-MaBP) and the data of Afroze et al. is not surprising for two reasons: 1. The demixing temperature of poly(NIPAAm) has been shown to be relatively independent of molecular weight; and 2.

The 3% mole content of MaBP in poly(NIPAAm-co-MABP) is not significant enough to perturb phase behavior.

Table 3.1 Parameters in Equations 3.2 and 3.3 for the χ parameter of linear poly(NIPAAm) solutions obtained by Afroze et al.[207]

i	A_i	B_i (K^{-1})
	-	
0	12.947	0.04496
1	17.92	-0.0569
2	14.814	-0.0514

The extent of dilution in linear polymer systems can be arbitrarily controlled, and therefore, any part of the phase diagram can be accessed. Cross-linked systems, on the other hand, limit the extent of dilution, and consequently a cross-linked system may or may not interfere with the two phase region of the phase diagram depending upon the extent of cross-link density. If the cross-link density is sufficiently high, the network is prohibited from entering the miscibility gap, and therefore will move from a swollen to a less swollen state in a more or less continuous manner. The open circles on the phase diagram represent the polymer volume fraction of the surface-tethered poly(NIPAAm-co-MABP) network as a function of temperature. The polymer volume fractions were determined from the flat regions of segmental profiles given in Figure 3.4, where edge effects do not play a role. In the temperature regime of 15-29°C, the network lay entirely in the single phase region of the phase diagram for linear poly(NIPAAm). At approximately 30°C, the network enters the two-phase region of the phase diagram and

jumps to the coexistence point on the polymer-rich binodal. Above 30°C, the network follows the coexistence curve of the phase diagram.

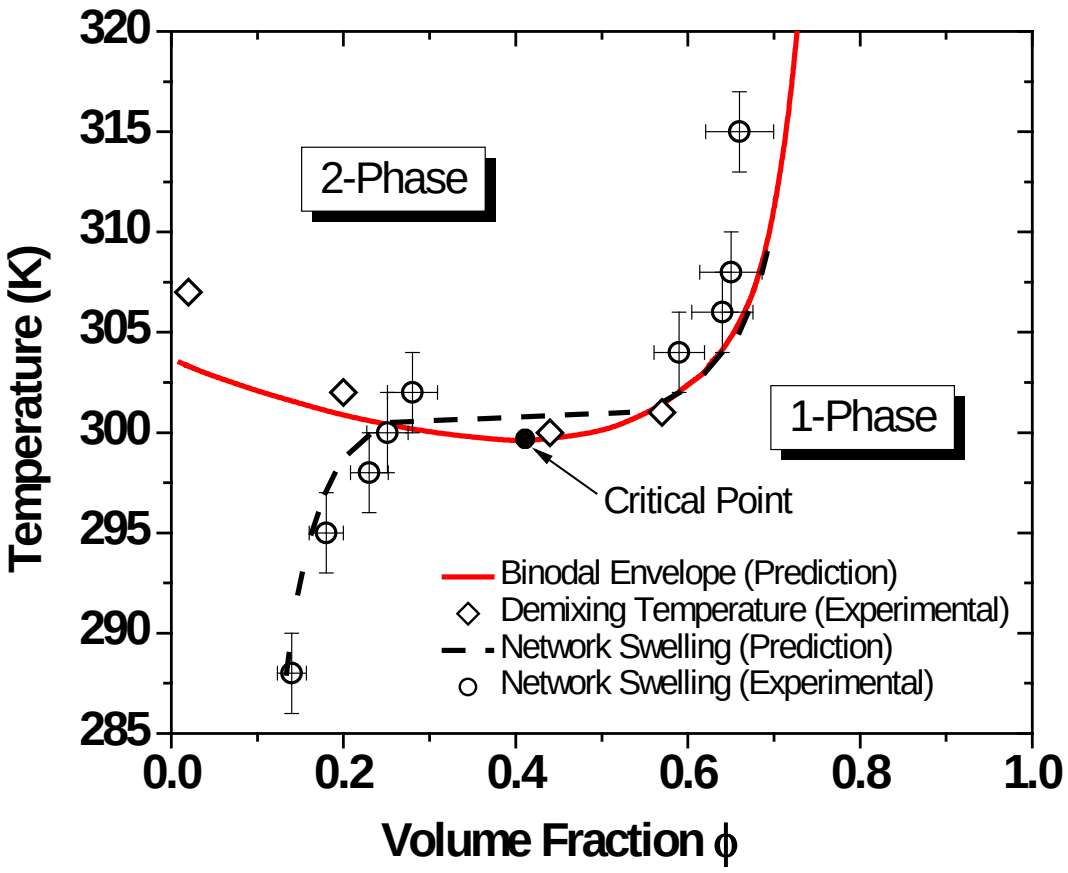

Figure 3.6 Experimental demixing temperature (◇) of uncross-linked poly(NIPAAm-co-MABP) and experimental swelling curve (○) of the surface-tethered poly(NIPAAm-co-MABP) network. Also shown are the predicted binodal for linear poly(NIPAAm) at infinite molecular weight and the predicted swelling curve for the surface-tethered network derived from Equation 3.7.

Using the χ_{eff} parameter from Equations 3.3-3.4, we can attempt to model the equilibrium swelling of the network within the Flory-Rehner framework.[116, 117] The free energy

density $\Delta G_{network}$ of a perfect phantom network prepared with N_{eff} effective mesh chains per unit volume is

$$\frac{\Delta G_{network}}{kT} = (1-\phi)\ln(1-\phi) + \phi(1-\phi)\chi_{eff}(\phi,T) + \frac{1}{2}\nu_e\left[\alpha_x^2 + \alpha_y^2 + \alpha_z^2 - 3 + \ln(\alpha_x\alpha_y\alpha_z)\right] \quad (3.5)$$

k is the Boltzmann constant and α_i is the linear deformation of network in the *i* direction. The first two terms account for the mixing of polymer and solvent and the last term accounts for elastic deformation of the network. For one-dimensional swelling[118, 222], $\alpha_x = \alpha_y = 1$ and $\alpha_z = \varphi_o/\varphi$ which equals the swollen ratio of the network relative to its preparation state and φ_0 is the polymer volume fraction in the relaxed state at the time of cross-linking.

The equilibrium swelling state is found by setting the chemical potential of the solvent μ_s in the network equal to its bulk value (which in a pure solvent is zero):

$$\frac{\mu_s}{kT} = \frac{\partial(\Delta G_{network}/\phi)}{\partial(1/\phi)} \quad (3.6)$$

$$\frac{\mu_s}{kT} = 0 = \ln(1-\phi_e) + \phi_e + \left[\chi_{eff} + \frac{\partial\chi_{eff}}{\partial\phi}\phi_e\right]\phi_e^2 + \frac{\phi_0}{N_{eff}}\left[\left(\frac{\phi_e}{\phi_0}\right)^{-1} - \frac{\phi_e}{2\phi_0}\right] \quad (3.7)$$

where N_{eff} is the effective degree of polymerization between cross-links. N_{eff} is the only adjustable parameter in the model, which when set to 100, produces good agreement

between the model and the experimental data. The model is represented by the dashed black line on the phase diagram in Fig. 3.6. While the agreement between model and experiment is encouraging, there are still a few caveats. Application of Equations 3.3-3.4 at temperatures and compositions beyond the range of experimental data used to fit the parameters A_i and B_i may not be appropriate. Second, the deformation term in Equation 3.5 assumes that the network is prepared from equilibrium Gaussian coils, which may not be an appropriate assumption in thin, spin-cast films. Finally, the value of N_{eff} is not explicitly known, but is a fit parameter.

Nonetheless, despite these shortcomings, the swelling discontinuity in the surface-attached network coincides with the two-phase region of uncross-linked poly(NIPAAm), which suggests that cross-linking does not affect the miscibility gap. Consequently, the two-phase region serves as a potential guide for anticipating volume-phase transitions in networks. For instance, a lower cross-link density is expected to result a slightly higher demixing temperature and larger discontinuity in swelling (on account that the network would enter a wider region of the two-phase region). On the other hand, if the network is constrained to the region below the critical condition, the network is expected to show a smooth volume transition. The next chapter presents data illustrating the adequacy of using the χ_{eff} parameter in Equations 3.3-3.4 for different states of cross-linking.

3.3 Conclusions

Surface-tethered poly(NIPAAm-co-MaBP) networks in D_2O were characterized with neutron reflection and compared to the demixing behavior of linear poly(NIPAAm) in solution. The change in thickness of the surface-tethered network as the temperature was increased from 15 to 49 °C was considerable, permitting comparison of the network

to the phase behavior of uncross-linked poly(NIPAAm). Interestingly, both the swelling of the network and the demixing behavior of the linear poly(NIPAAm) could be explained with the same concentration-dependent Flory χ parameter. While these experiments do not shed light on the molecular interpretation of the composition dependence, they do point to the idea that constraints on linear chains do not alter this dependence. Consequently, the binodal envelope for two-phase region in solutions of linear poly(NIPAAm) serves as a potential guide for understanding volume-phase transitions in networks and other confined geometries.

CHAPTER 4: CONTINUOUS AND DISCONTINUOUS PHASE TRANSITION IN SURFACE TETHERED POLY(NIPAAm) NETWORKS

4.1 Introduction

Though LCST polymers in confined geometries have found success in technologies that benefit from reversible modulation of surface properties, Still, the relationship between cloud points of LCST solutions and volume-phase transitions in confined systems remain unclear. For instance, if the demixing of a swollen polymer network traverses a cloud point, a concentration jump must occur at the temperature of interference. On the other hand, if the path of demixing avoids all cloud points, the deswelling will be continuous.[1]

Herein, the swelling of surface-tethered, crosslinked networks of poly(N-isopropylacrylamide) copolymerized with *x* mol% of methacroyloxybenzophenone (MaBP) (*x*=1, 3, 5, 10 %) were compared to the miscibility gap of poly(NIPAAm-co-MaBP) in aqueous solution. Poly(NIPAAm) is a well-studied system that has a two-phase envelope more or less resembling miscibility square. The lower critical solution point lies at approximately 27 ^{o}C and a volume concentration of ~0.40, which has been reported to be mostly independent of molecular weight.[219-221] In contact with water, poly(NIPAAm) swells at temperatures below approximately 27-30°C, the swelling determined by a balance between mixing osmotic pressure arising from contacts between segments and the entropic of chain stretching. As temperature is increased, hydrophobic interactions between isopropyl groups contract the network, expelling water in the process. [33-37, 223]

The swelling of the cross-linked layers were characterized with both neutron reflectivity and ATIR-FTIR. Neutron reflectivity provides an angstrom-scale measure of the average water distribution within the network perpendicular to the confining substrate and ATR-FTIR provides important clues into the chemical interactions of the network. Neutron reflectivity data revealed that water is expelled discontinuously at low crosslink densities and continuously at high crosslink densities. It is shown that the demarcation between the two behaviors occurs roughly at the critical point as measured by cloud point experiments. Interestingly, neutron reflection also revealed the presence of 2-3 water molecules per segment that remained after the collapse of the network, independent of crosslink density. This finding suggests that water is not completely expunged from the network but may remain in confined regions between the amide groups forming perhaps water bridges.

Parallel measurements with ATR-FTIR show that the characteristic bands connected to the vibrations of the amide II group and the stretching vibrations of the isopropyl aliphatic groups correlate approximately to the amount of water in the network. Peak positions were monitored for demixing as induced by either temperature changes or through water evaporation at constant temperature. While the FTIR spectra depend on water content in the layer, they do not depend on the method by which water is removed (*i.e.*, either by increasing the temperature above the LCST or through evaporation below the LCST). This shift in peak positions to lower wavenumbers has been attributed to changes between inter and intra-molecular hydrogen bonding [224-226]; however, the data herein suggest that the red shift to lower wavenumbers may be due to weaker hydrogen bonding interactions with confined water. Water in these spaces is strongly bound, remaining even at temperatures well above demixing. The internal water, however, is readily exchanged with deuterium oxide, suggesting heterogeneous domains through

which water can diffuse, also emphasizing the absence of a hydrophobic skin layer which allows water to diffuse in and out of the collapsed networks.

4.2 Results and Discussion

Previous results[1] have shown that neutron reflection is well-suited to measure the water distribution in thin, swollen films of poly(NIPAAm-co-MaBP) films. In this study, the water content of crosslinked poly(NIPAAm-co-MaBP) coatings was monitored both as a function of MaBP content (1-10 mole %) and temperature. Figures 4.1 and 4.2 show neutron reflection profiles for the two extremes in cross-linking, 1% and the 10%, respectively, at 23°C and 33°C in contact with D_2O. The dry thickness of each film was approximately 300 Å.

The most pronounced differences between the two crosslink densities occur at 23 °C. The reflectivity curve associated with the 1% MaBP sample shows only 1 Kiesseg fringe with a spacing of Δq = 0.004, corresponding to an overall thickness of roughly 1600 Å. In contrast, the 10% MaBP sample has 2 Keissig fringes with a spacing Δq = .02, corresponding to a thickness of approximately 350 Å. As the temperature is increased above approximately 30°C, the reflectivity curve of the 1% MABP sample undergoes an abrupt change, whereas the reflectivity curve of the 10% MaBP sample undergoes only a slight change in the shape and intensities of the interference fringes. All reflection profiles were fit with a profile consisting of 2-3 SLD slabs, with interfaces between the slabs smeared by error functions. At low temperatures, the interface between the coating and D_2O was difficult to fit, being non-Gaussian in nature.[1] This interface most likely arises due to a surface instability akin to a surface Rayleigh wave that results in surface-confined geometries.[227] The inset in both Figures 4.1 and 4.2 shows the best-fit SLD profiles.

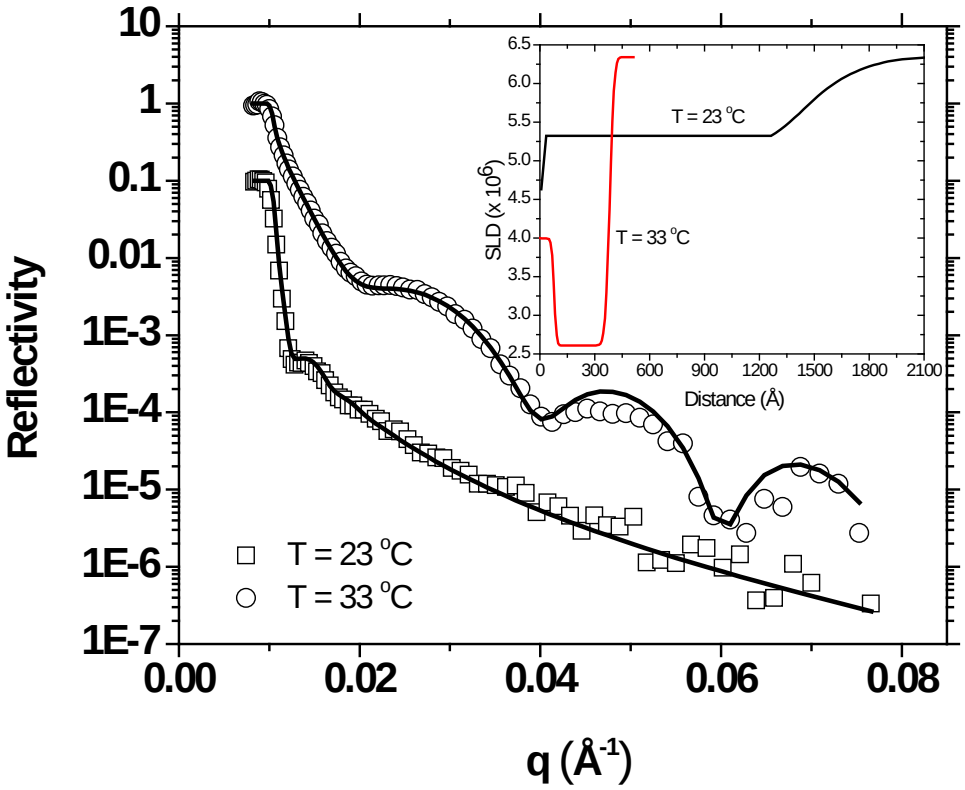

Figure 4.1 Neutron reflectivity data for surface-tethered poly(NIPAAm-co-MaBP(1%)) in a D_2O environment at 23°C and 33°C. The solid line though the data corresponds to the best fit and the inset shows the SLD distribution obtained from the best fit.

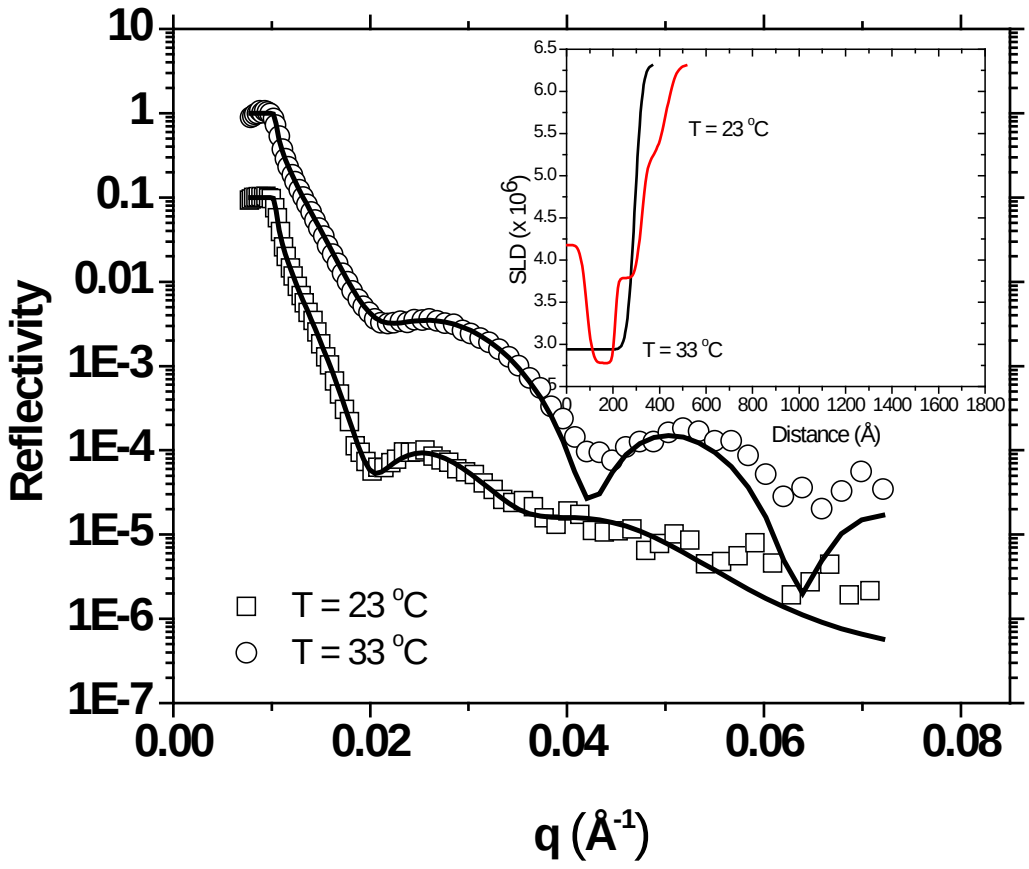

Figure 4.2 Neutron reflectivity data for surface-tethered poly(NIPAAm-co-MaBP(10%)) in a D_2O environment at 23°C and 33°C. The solid line though the data corresponds to the best fit and the inset shows the SLD distribution obtained from the best fit.

Neutron reflection experiments were performed for all 4 crosslink densities between 20°C-40°C. The average thicknesses <z> as a function of temperature are plotted in Figure 4.3 where <z> is defined as $2\int z\phi(z)dz \Big/ \int \phi(z)dz$ and ϕ is the volume fraction of the polymer. All samples show a small dependence on temperature below 28°C, expelling water as temperature is increased. At approximately 28°C, the 1% MaBP coating collapses from 1200 Å to 400 Å and the 3% MaBP coating collapses from 900 Å

to 400 Å. Interestingly, the collapse of the 3% MaBP network appears to be 1-2°C less than the 1% MaBP network. In the networks with 5% and 10% MaBP, the change in thickness is less pronounced and no abrupt changes in thickness were observed; both networks showed a smooth continuous transition from a more swollen to less swollen state.

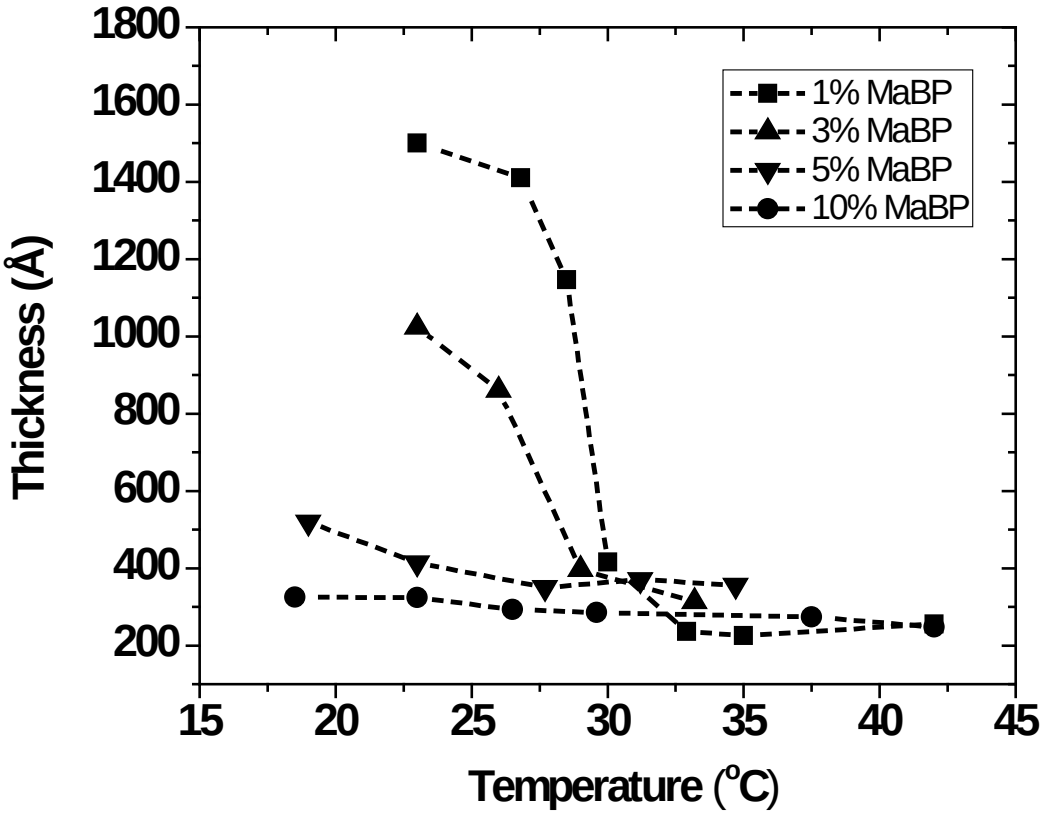

Figure 4.3 Variation of average thickness <z> of the surface-tethered poly(NIPAAm-co-MaBP) networks as a function of temperature.

In figure 4.4, the average volume fraction φ of the poly(NIPAAm-co-MaBP) coatings is plotted against temperature for each of the crosslink densities. The experimentally determined cloud point curve for poly(NIPAAm-MaBP(3%)) based on turbidity measurements is also shown. In the temperature regime below ~27°C, all the coatings lay entirely in the single phase region of the phase diagram. At approximately 27°C, the swelling of the 1% MaBP coating crosses the cloud point curve and the coating experiences a jump in concentration to approximately 65-70 volume % of polymer. The 3% MaBP coating intersects the cloud point curve at a slightly lower temperature and experiences a smaller increase in concentration.

The coatings with both 5% and 10% MaBP remain in the single phase region and thus experience no abrupt changes in concentration. All coatings, independent of the crosslink density, collapse to approximately the same concentration (~65 %) at temperatures above 30°C and follow a similar trajectory with increasing temperature. Above 30°C, the networks continue to expel water, but with a very weak dependence on temperature. The dashed line suggests the spinodal envelope for the networks, which closely follows the cloud point curve.[1, 228]

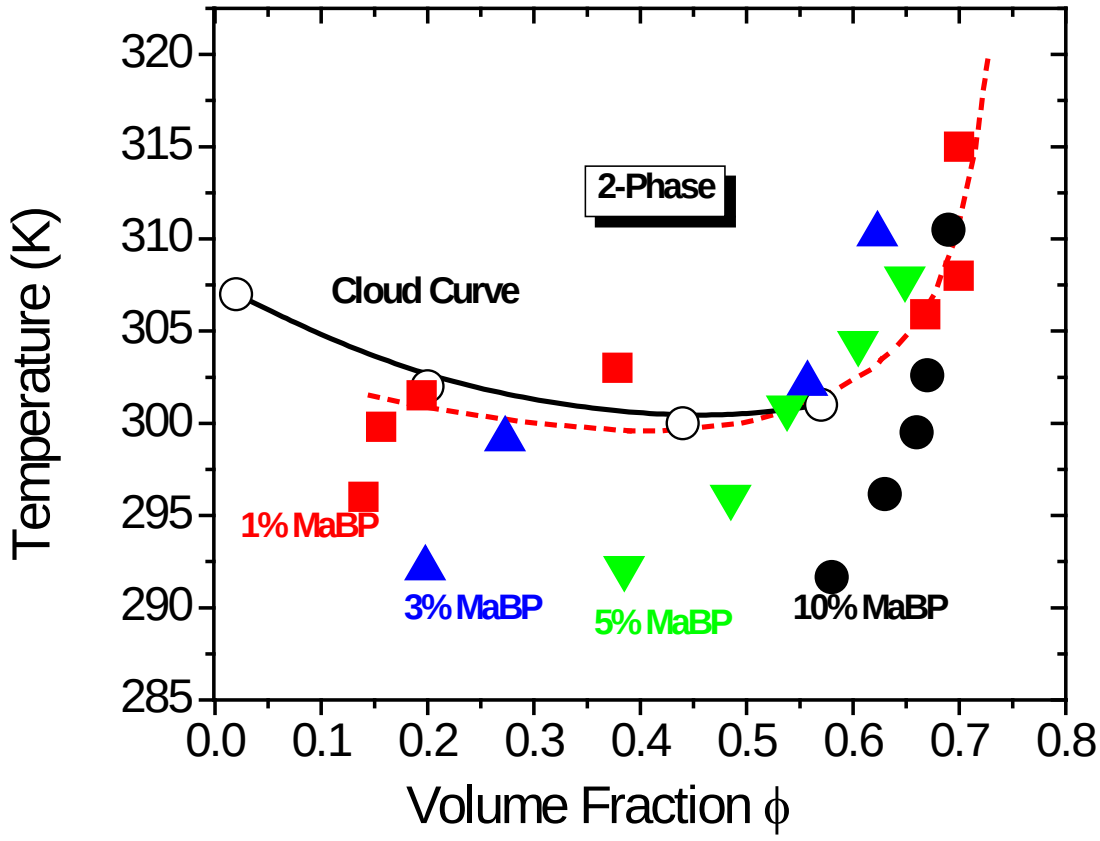

Figure 4.4 Experimental cloud point curve of linear poly(NIPAAm-co-MaBP(3%)) (open circles) and experimental swelling curves of surface-tethered poly(NIPAAm-co-MaBP(x%)) networks. The dotted line is the suggested spinodal for the network, which coincides closely with cloud point curve.

The experimental phase diagram raises some interesting questions. From a theoretical perspective, the concentration jump observed in the 1% and 3% MaBP samples must result from some form of cooperative dehydration.[229] Several experimental

techniques, including dielectric relaxation, differential scanning calorimetry and FTIR, suggest that hydrogen bonds between amide groups and water molecules are broken in the volume-phase transition, generating polymer domains that may form intermolecular hydrogen bonds.[79, 80, 104, 230-232] An important question is whether the residual water that remains after the volume-phase transition is physically trapped in cavities between hydrophobic domains. [233-235]

To gain further insight into the role of water during the collapse of the coatings, the coatings were monitored with FTIR in an ATR configuration. In each case, the poly(NIPAAm-co-MaBP) coating was much thicker than the penetration depth of the evanescent field, thus only the inside of the films were probed. This was done using the ATR correction mode using the Nicolet 6700 FTIR software. To remove all residual water, the samples were first annealed at 102^{o}C for two hours in a dry, humidity free environment. The FTIR spectrum of an annealed sample is shown in Figure 4.5. Generally, there are four resolvable bands that are indicative of hydration: The amide I, the amide II, and the symmetric and antisymmetric stretches of C-H groups.[35, 102] The amide I band consisted of a major peak at 1640 cm^{-1}, the amide II band consisted of a major peak at approximately 1516 cm^{-1}, and the antisymmetric C-H stretching band of the –C(CH$_3$)$_2$ consisted of a major group at 2971 cm^{-1}.

A prominent band was also found at 3320 cm^{-1}, which corresponds to the N-H stretch of the amide group and perhaps water still bound to the network. After this annealing process, contact of the coating with water at 25°C produced 3 general trends in all samples. First, the relative spectral intensities of the amide I and amide II bands decreased. Second, the appearance of a water band between 3000-3700 cm^{-1} occurred. Finally, the amide II peak and C-H stretching peaks blue-shifted, while the amide I peak

red-shifted. All three events are approximately related to the amount of water in the networks.

For instance, as distinguished in Figure 4.5, the amide II peak of the 1% MaBP coating blue-shifted by 42 cm^{-1} and the antisymmetric C-H peak by 15 cm^{-1} upon adding water at 25°C. The amide II peak of the 10% MaBP coating (not shown), on the other hand, blue-shifted by only 37 cm^{-1} and the C-H peak by 12 cm^{-1} as a consequence of a lower degree of swelling.

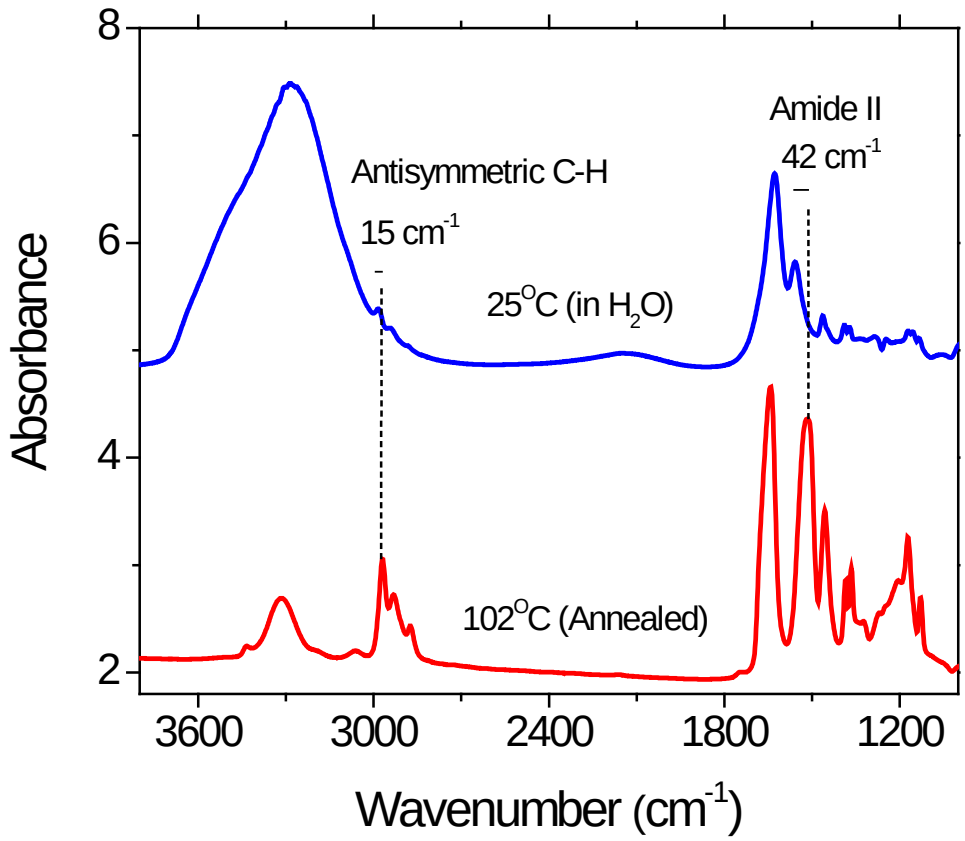

Figure 4.5 ATR-FTIR spectra of poly(NIPAAm-co-MaBP (1%)) solvated in water at 25°C and annealed to the ZnSe crystal at 102°C indicating peak positions in the isopropyl and amide II groups.

Following addition of water at 25°C, the temperature was increased. Figure 4.6 shows the resultant red-shifts in the amide II group and the antisymmetric C-H stretching of the $–C(CH_3)_2$ group as temperature is increased for the first 10 °C between 25°C and 35°C. Analogous to the neutron reflection results, a sharp change is seen starting at 28°C for both the 1% and 3% MaBP samples, whereas the change is much subtler for the 5% and 10% MaBP samples.

At 35°C, all the major peaks collapse to approximately the same values independent of crosslink density. At this temperature, however, the peak positions do not return to their annealed values, indicating that demixing does not completely expel water, which again is consistent with the neutron reflection results.

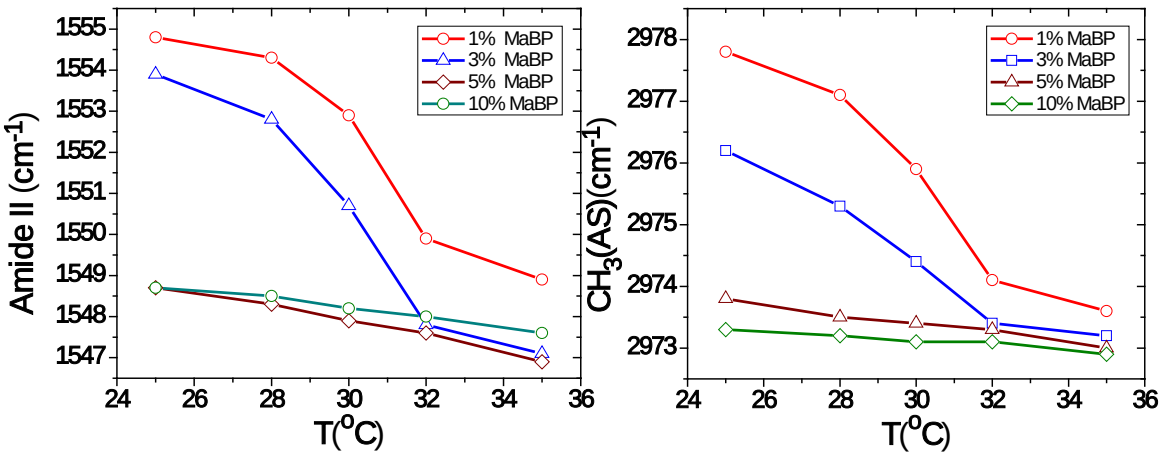

Figure 4.6 Change in the amide II and in the antisymmetric(AS) C-H stretching of -$C(CH_3)_2$ for poly(NIPAAm-MaBP) with MaBP 1-10% over a temperature range of 25°C - 35°C.

If water is not added directly to the coatings after annealing, but rather the coatings are allowed to remain under ambient conditions, the amide II band slowly blue-shifted from its annealed value of 1516 cm^{-1} to 1528 cm^{-1}, independent of crosslink density. On the other hand, the bands associated with the aliphatic stretching peaks did not change. This suggests that the natural humidity in the air is sufficient to hydrate the amide groups, but that the aliphatic groups remain in a hydrophobic environment.

Exposure of the sample to saturated water vapor at 25°C continued to shift the amide II peak to 1545 cm^{-1} indicative of further hydration; however, 100 % humidity was still not sufficient to affect the stretching band of the aliphatic groups. If the temperature is increased to 102 °C under 100 % humidity, the amide II peak red-shifted to 1530 cm^{-1} as shown in Figure 4.7, indicative of demixing, yet the amide II peak still did not completely return to its annealed value of 1516 cm^{-1}. Also in this case, there is still the presence of a sizable water band near 3500 cm^{-1}, which explains why perhaps the amide II does not return to its annealed value. Only if the heating chamber is evacuated of humidity does the amide II peak slowly shift back to 1516 cm^{-1} and the water band disappears.

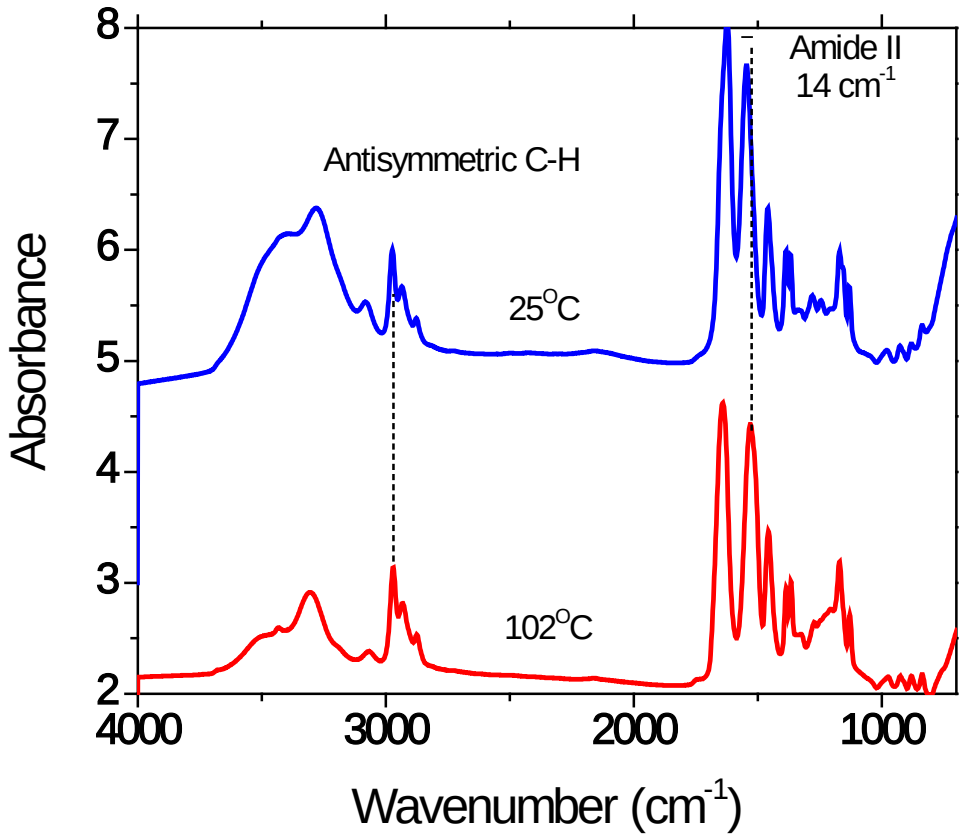

Figure 4.7 ATR-FTIR spectra of poly(NIPAAm-MaBP (1%)) exposed to water vapor at 25 °C and to water vapor at 102 °C indicating peak positions in the isopropyl and amide II groups.

Previously, it has been reported that the red-shift of the amide II region during the phase transition is due to the breakage of polymer-water N-H…O-H_2 hydrogen bonds in favor of polymer-polymer N-H…O=C hydrogen bonds or non-hydrogen bonded N-H groups.[236] The FTIR results herein coupled to the neutron reflection results suggest a more complicated scenario. To summarize, the experimental FTIR data show a substantial shift in the amide II band between an annealed and vapor-contacted coating (1516–1545 cm^{-1}), whereas the bands associated with the aliphatic stretching groups are largely

unaffected by water vapor. Fully exposing the coating to liquid water further shifts the amide II band (depending on crosslink density) as the layer swells, but this change is small (up to 10 cm^{-1}) compared to the first hydration step. Swelling in water also blue-shifts the position of the stretching bands associated with the aliphatic groups. Finally, as the temperature is increased above the cloud point in water, the stretching bands associated with the aliphatic peaks return to their position in the annealed state, but the amide II returns to its hydrated value in the weakly swollen state. Such findings suggest that during the polymer collapse, the isopropyl groups completely dehydrate but that the amide groups remain hydrated. This finding is consistent with recent dielectric relaxation experiments that show that the number of water molecules surrounding the amide groups of NIPAAm monomer did not change during the phase transition.[103]

Taken together, these experiments imply that the network is collapsed as driven by hydrophobic interactions and that water is destabilized around the amide groups as the structure collapses, but does not break free of the structure, perhaps leading to a heterogeneous structure with amide-rich hydrophilic domains and hydrophobic domains. Water is still free to diffuse through the layer, as evidenced by the fact that D_2O can be readily exchanged for H_2O in the collapsed poly(NIPAAm-co-MaBP) layer at both 50°C and at 102°C under a saturated vapor environment. Exposing the poly(NIPAAm-co-MaBP) coating to liquid D_2O at 25°C results in the amide II peak position near 1467 cm^{-1} as a result of isotopic substitution of deuterium for hydrogen in the N-H group. Figure 4.8 shows the collapsed layer in pure H_2O exposed to an equimolar H_2O/D_2O mixture at 50°C and 102°C. The layers were allowed to equilibrate for 25 minutes, after which time the presence of OH and OD stretching bands of nearly equal intensity appeared. Moreover, the amide II bands associated with both N-H group and N-D groups appear in

the spectrum, further suggestive of isotopic substitution of the amide groups with deuterium and access of D_2O to the amide groups.

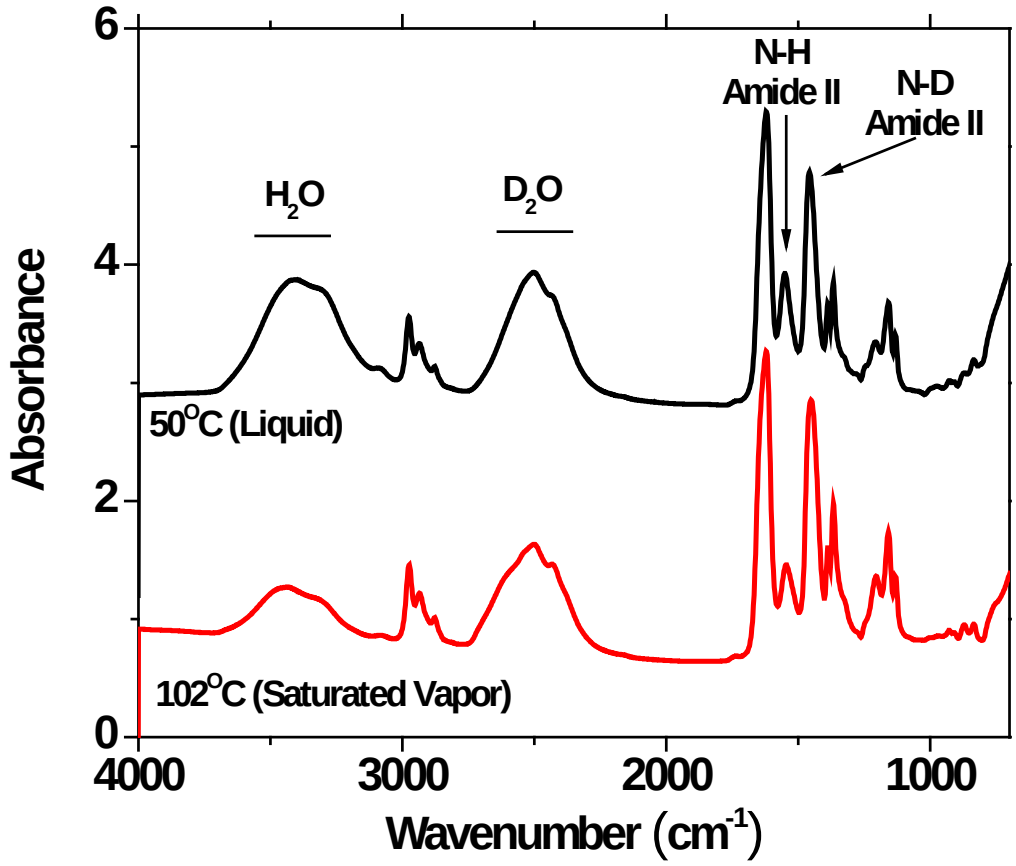

Figure 4.8 ATR-FTIR spectra of poly(NIPAAm-MaBP (1%)) upon equimolar water – deuterium substitution (1:1) at 50°C and at 102°C in the liquid and saturated vapor states, respectively.

4.2.1 Demixing Behavior of Poly(diethylacrylamide-co-MaBP(3%)) (Poly(DEA-co-MaBP))

The presence of confined water even in the collapsed state of poly(NIPAAm-MaBP) coatings have been reported.[1] Neutron reflection and FT-IR are excellent tools to investigate phase transition and the presence of confined water. In this study, we investigated the presence of water trapped in poly(DEA-MaBP) coatings and characterized their phase transition. We have also tried to draw comparisons between poly(DEA-MaBP) coatings with Poly(NIPAAm-MaBP) coatings with respect to their phase change and the presence of water. Figure 4.9 shows the neutron reflectivity profiles for poly(DEA-MaBP(3%)) coatings at temperature 8 ^{o}C through 43^{o}C.

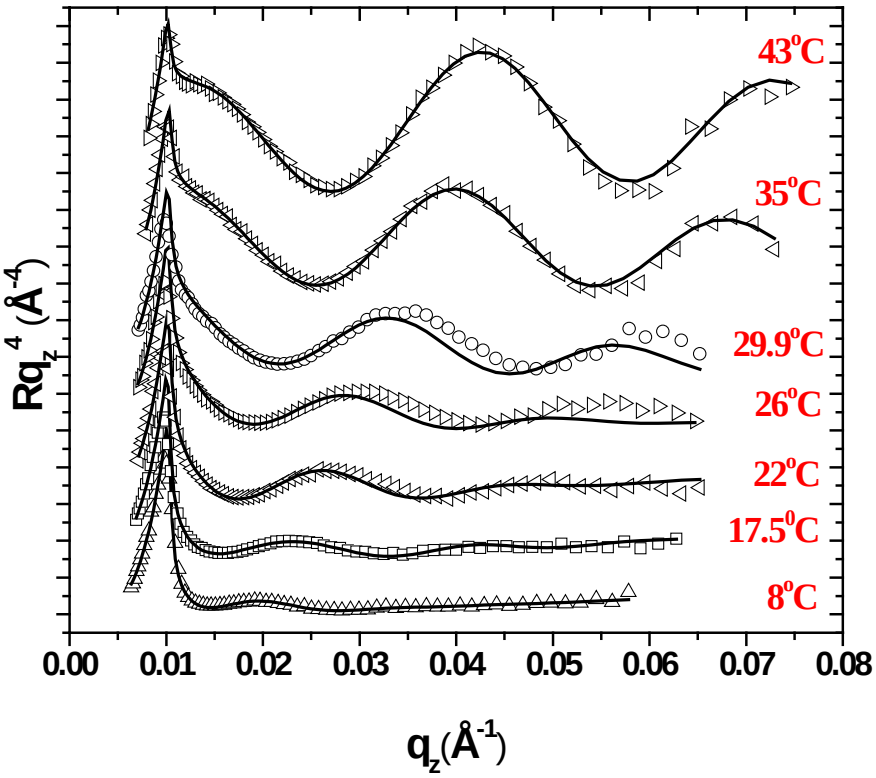

Figure 4.9 Neutron reflectivity data for surface-tethered poly(NIPAAm-co-MaBP(1%)) in D_2O environment at 23°C, 35^{0}C and 45°C. The solid line though the data corresponds to the best fit for the profiles.

The reflectivity profiles as shown in figure 4.9 for poly(DEA-MaBP(3%)) indicate a gradual continuous transition from 8^{o}C to 43^{o}C contrary poly(NIPAAm-MaBP(3%)) which shows a more discontinuous phase change.[1] We see the formation of the first kiesseg fringe at 8 ^{o}C with Δq=0.01 corresponding approximately to a thickness of 628 Å gradually broadening to more well defined fringe pattern at 42^{o}C with Δq=0.03 corresponding approximately to a thickness of 209 Å.

The change in fringe pattern directly corresponding to change film thickness is gradual with the transition clearly evident from 26^{o}C onwards. Figure 4.10 shows the volume fraction profiles for best fits reflection profiles shown in figure 4.9. For every temperature, the integral of the volume fraction profile over the extension of the layer was within 10-15% of each other thus ensuring that the total polymer mass remains relatively constant. SLD profiles for poly(DEA-MaBP(3%)) coatings consisting of 1-3 SLD slabs with interfaces between the slabs smeared by error functions.

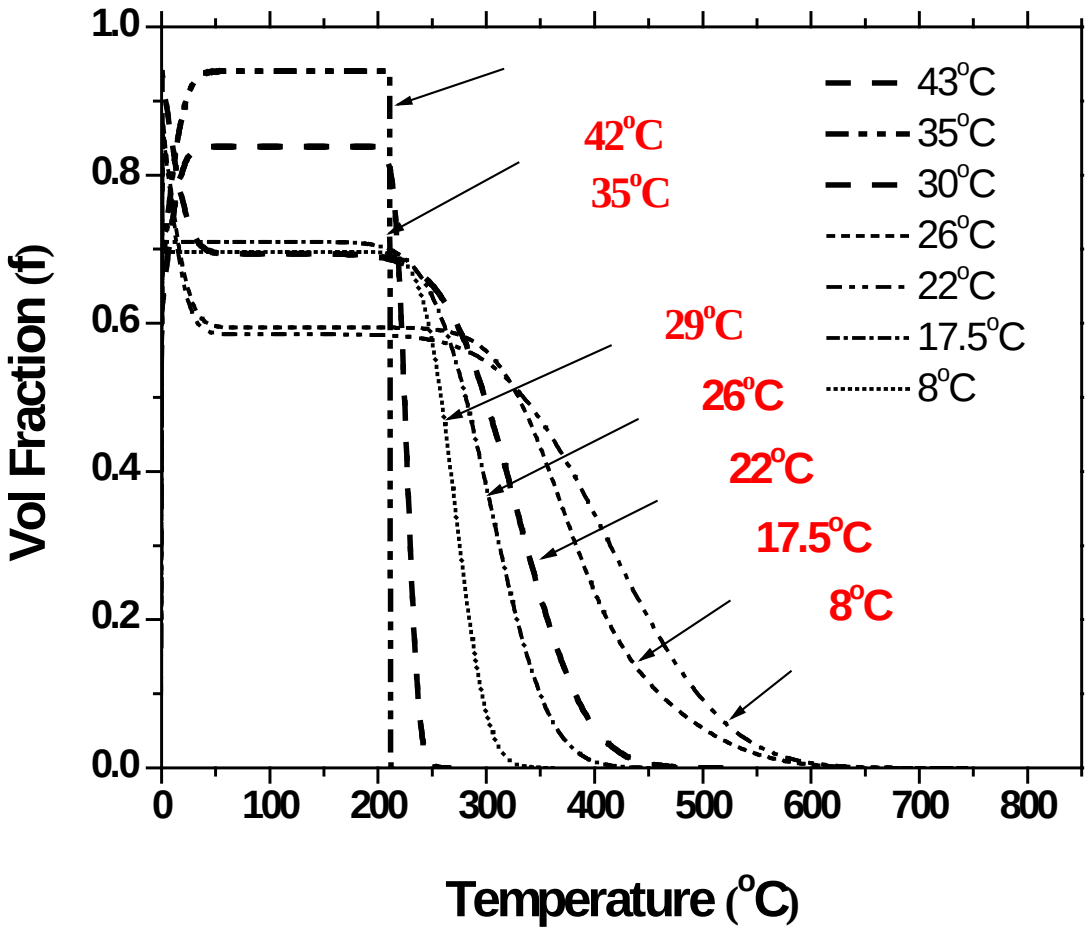

Figure 4.10 Volume fraction profiles for poly(DEA-MaBP(3%) coatings for temperatures 25^0C, 35^0C and 42^0C

Interestingly, the volume fraction profiles show that around 10%-15% of D_2O still trapped inside the coatings even after phase separation. Our previous results[1] show that around 30%-35% D_2O trapped in poly(NIPAAm-MaBP) coatings. This huge difference in the amount of water trapped might be because, poly(DEA-MaBP) is more hydrophobic and also due to subtle differences in their chemical structure. The formation of C=O…H-N bonds by cooperative hydration seem important in regulating phase transition. Water

tends to hydrogen bond with C=O and N-H moieties of the amide I and amide II peaks forming water bridges. In addition, the side chains of poly(DEA-MaBP) coatings contain an additional carbon in its side chains than poly(NIPAAm-MaBP) coatings thus increasing its hydrophobic surface area. This can reduce the amount of water uptake by poly(DEA-MaBP) coatings making these coatings swell to a lower degree compared to poly(NIPAAm-MaBP) coatings. Also, the presence of the donor hydrogen in the amide groups might be responsible for the sharp transition seen in poly(NIPAAm-MaBP(3%)) coatings. The absence of amide proton in poly(DEA-MaBP(3%)) coatings might hinder in forming less compact polymer segments at higher temperatures resulting in a smooth and more continuous transition. Recent reports have shown that greater compactness in poly(NIPAAm) structures in the collapsed phase compared to poly(DEA) due to intramolecular hydrogen bonding might lead to greater discontinuity in phase transition.[237]

The average thickness <z> for all measurements, defined as $2\int z\phi(z)dz \Big/ \int \phi(z)dz$, where $\phi(z)$ is the segment density profile, is shown for in figure 4.11. The average thickness of poly(DEA-MaBP(3%)) falls from 426 Å at 8°C to 217Å at 43°C Though similar to poly(NIPAAm-MaBP) structurally, poly(DEA-MaBP(3%)) exhibits a very continuous volume phase change compared to poly(NIPAAm-MaBP(3%)) where the average thickness changes from 1024 Å at 23°C to 313 Å at 33°C exhibiting a volume change very discontinuous in nature.

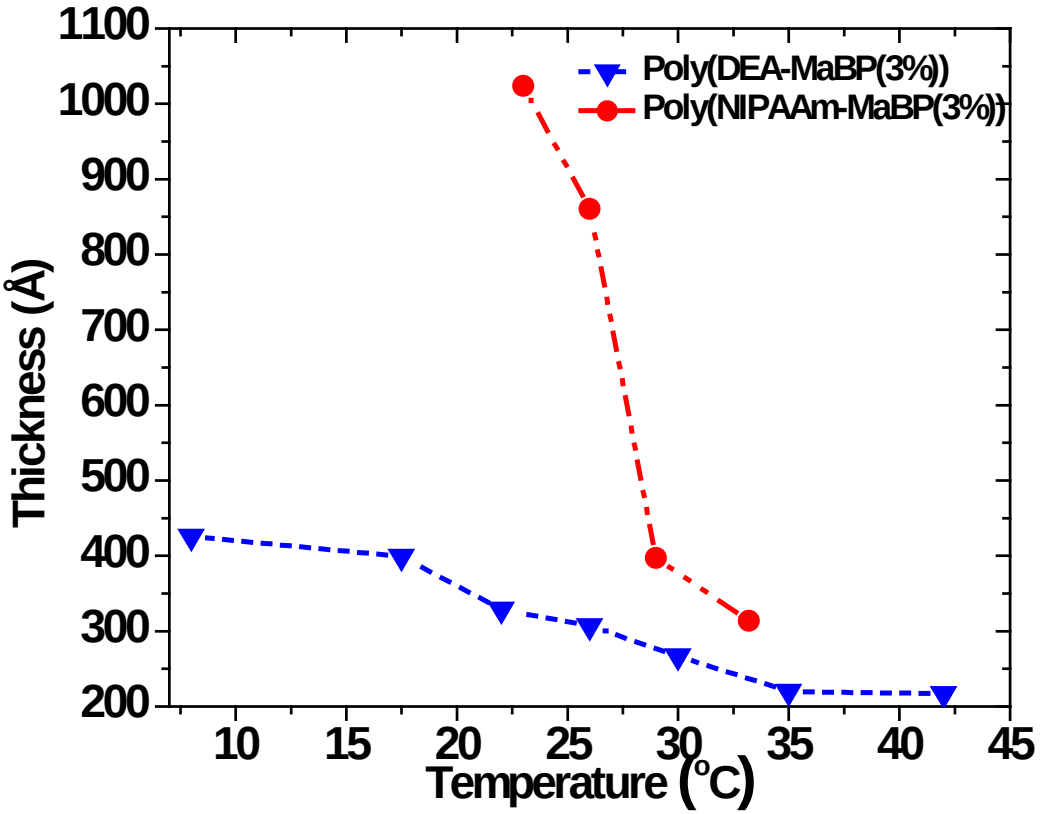

Figure 4.11 Variation of average thickness <z> as a function of temperature for surface-tethered poly(DEA-MaBP) AND poly(NIPAAm-co-MaBP) networks.

4.2.2 ATR-FTIR Results

FT-IR in ATR mode was used to investigate water confined inside poly(DEA-MaBP) coatings. The relatively small penetration depth of the evanescent field ensures that the water confined inside the poly coatings alone was measured. The films were cast directly on to the ZnSe crystal and heated to 102°C to remove any residual water. Unlike poly(NIPAAm-MaBP), poly(DEA-MaBP) has no dissociable proton in the amide II region. This limits interest mainly to the amide I and C-H stretch regions of the ethyl regions of the polymer.

Figure 4.12 shows the change peak positions in the ethyl groups in the annealed and solvated states. The annealed poly(DEA-MaBP) coatings show no change in any of the ethyl groups from 25°C TO 102°C. Solvating the polymer coating with water brings about a small red shift of around 10 cm^{-1} increase in (AS) C-H stretch of $–C(CH_3)_2$, 5cm^{-1} increase in both (S) C-H stretch of $–C(CH_3)_2$ and (AS) C-H stretch of $–C(CH_2)$ groups. All the aliphatic groups exhibit a red shift as the polymer coatings go through their phase transition. All the ethyl groups return to the peak positions in the annealed state as the water evaporates and anyways do not deviate much from their annealed state. This suggests that the ethyl groups remain dehydrated as the polymer goes through its transition and hence do not play a major role in promoting phase transition. The amide II peaks are more sensitive to solvent changes and in the case of poly(NIPAAm-MaBP), the peak positions of the amide II groups do not completely return to their annealed state. There still seems to be sufficient hydrogen bonding between water molecules and N-H and C=O trapping water even after the collapse of the polymer coatings. As a result, a large portion of water is still retained in the coatings. However, poly(DEA-MaBP) does not have a dissociable proton in the amide groups. As a result, the N-H bands in the amide II region and around the O-H stretch region are absent in these coatings. This implies that water does not form bonds in the amide II region as well as with water around the N-H stretch and 0-H stretch region. This could explain why there is relatively less water in poly(DEA-MaBP) coatings compared to poly(NIPAAm-MaBP) coatings.

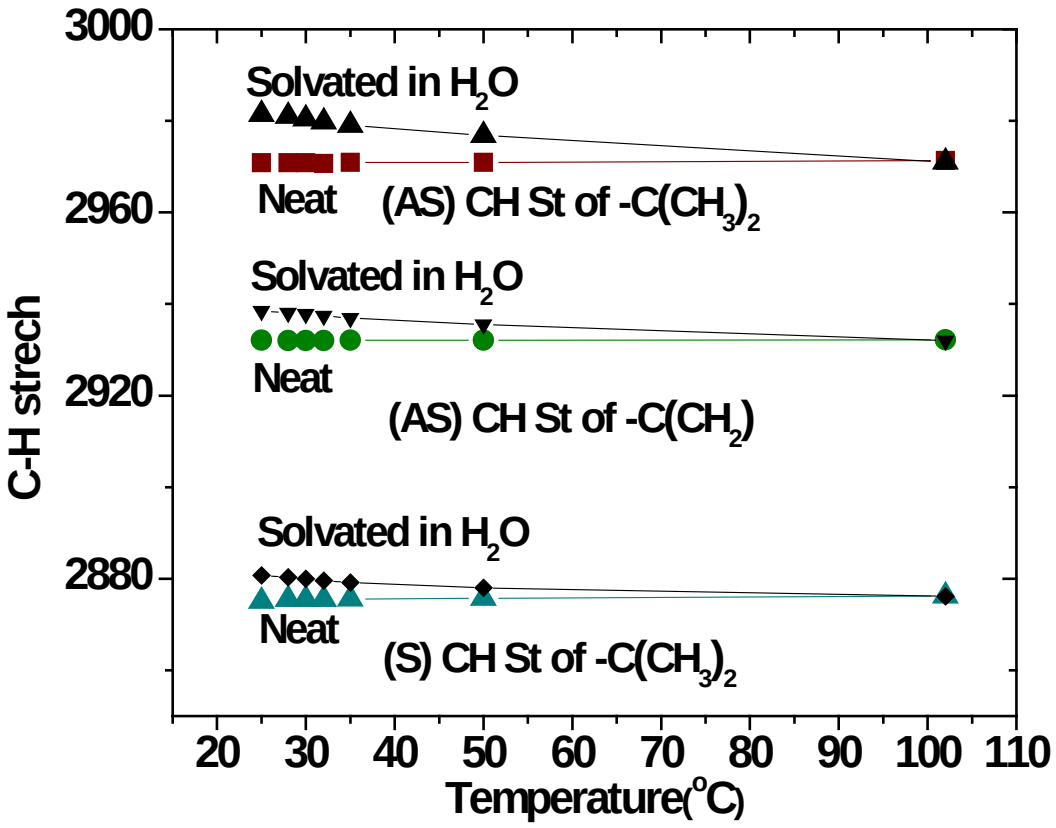

Figure 4.12 Change in the antisymmetric (AS) C-H stretching of $-C(CH_3)_2$, (AS) C-H stretch of $-C(CH_2)$ and symmetric C-H stretch of $-C(CH_3)_2$ for poly(DEA-MaBP(3%))

Figure 4.13 and 4.14 show poly(DEA-MaBP(3%)) in the neat and solvated states. The amide peaks are more sensitive to local environmental changes. In both cases, the amide II and the N-H stretch region around 3200cm^{-1} is missing due to the absence of the dissociable proton in poly(DEA-MaBP) coatings. The O-H stretch of water tends to overlap with the N-H region of poly(NIPAAm-MaBP) coatings and forms hydrogen bonds. Neat poly(DEA-MaBP) coatings hardly show any presence of O-H peaks due to water.

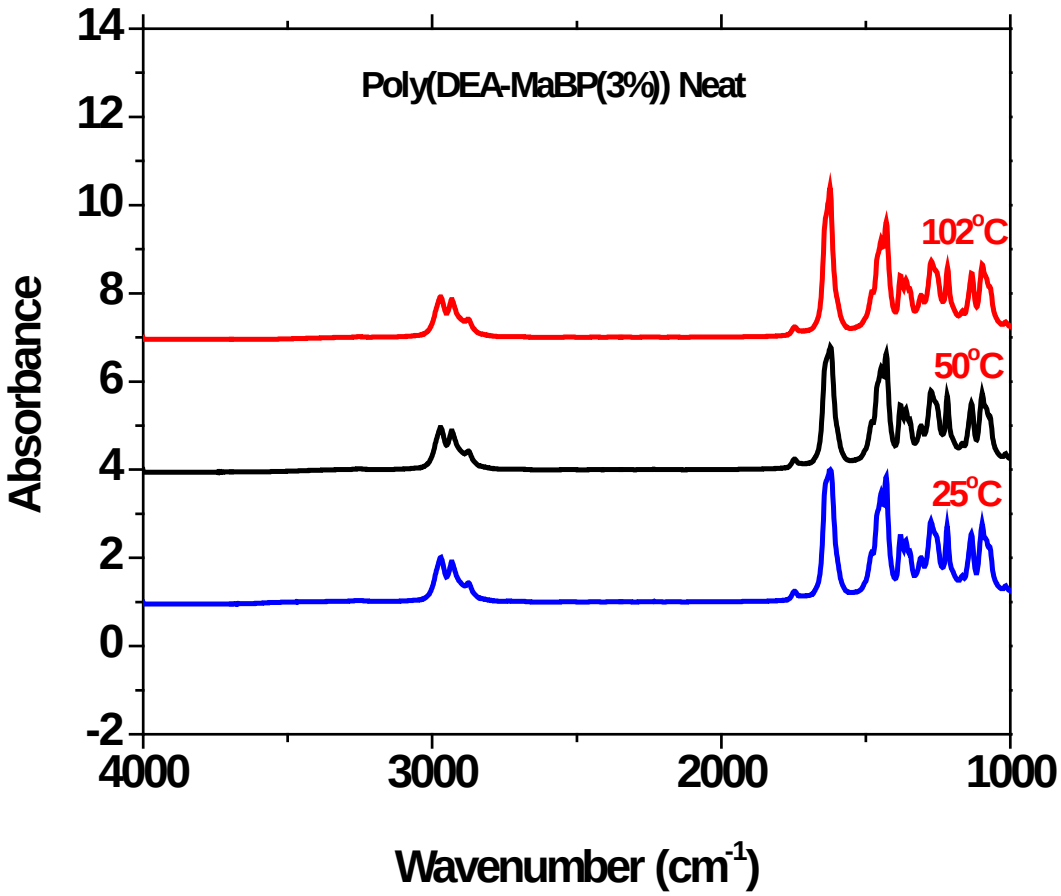

Figure 4.13 FT-IR spectrums of neat poly(DEA-MaBP (3%)) at 25°C, 50°C and annealed to the ZnSe crystal at 102°C

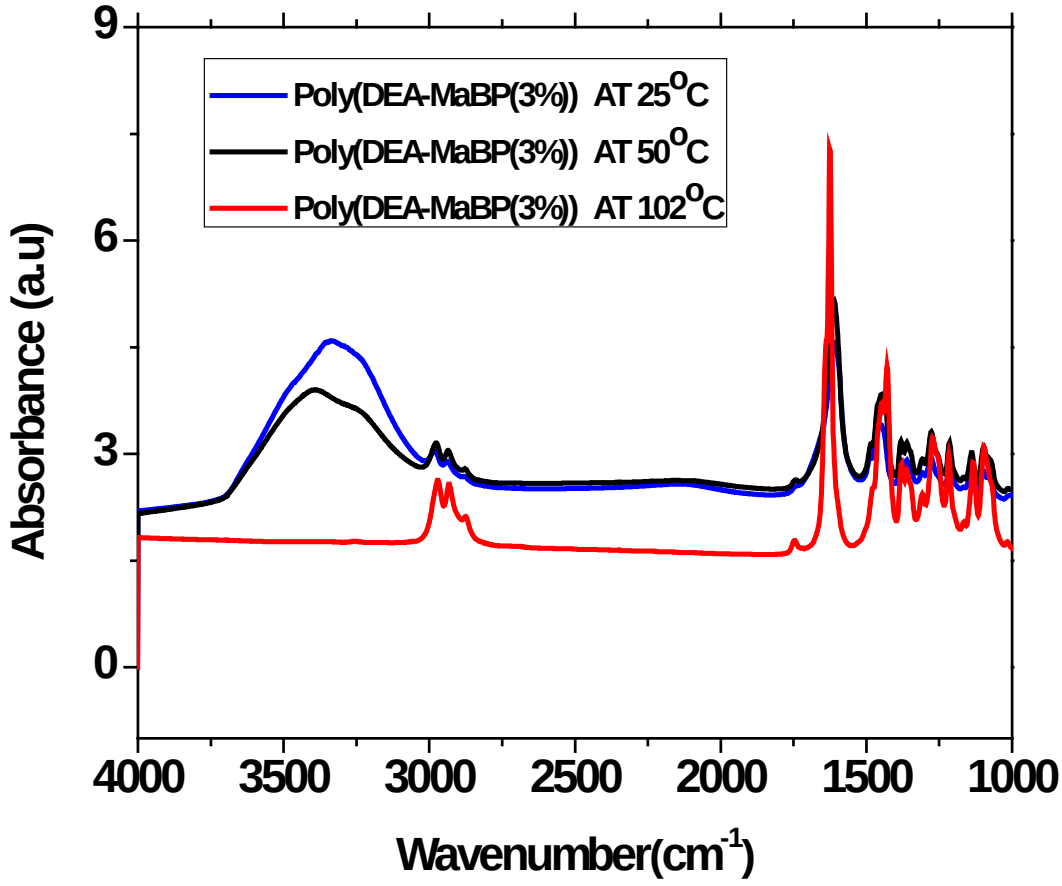

Figure 4.14 FT-IR spectrums of poly(DEA-MaBP (3%)) at solvated 25°C and 50°C and annealed to the ZnSe crystal at 102°C

The absence of N-H stretch prevents any hydrogen bonds from forming with the O-H stretch of water. In addition, the absence of the N-H bend region of the amide II peak considerably reduces the amount of water in the polymer coatings. Poly(DEA-MaBP) coatings solvated with water show the presence of water at the O-H stretch region at temperatures as high as 50°C. The presence of water above the cloud point indicates to

heterogeneous domains that may be present within polymer coatings even in the collapsed state. It is only at temperatures as high as 102°C, all residual water is expunged from the polymer coatings. These results are analogous to our previous neutron reflection results where we show that confined water is present in poly(NIPAAm-MaBP) even in the collapsed state.[1]

However, the presence of the dissociable proton in the amide II peaks and the presence of the N-H stretch region tend to significantly hold more water (30%-35%) by hydrogen bonding with the water molecules. The change in peak positions does not seem to depend on temperature per say, but more on the amount of water that's confined inside the networks. This finding is consistent with recent dielectric relaxation experiments that show that the number of water molecules surrounding the amide groups of NIPAAm monomer did not change during the phase transition.[103, 230]

Figure 4.15 shows the second derivative of poly(DEA-MaBP) in solvated in water. The regions around 1595(+/-5) cm^{-1}, peak positions around 1619(+/-5) cm^{-1} represent and peak positions around 1638(+/-8) cm^{-1}.[238] As poly(DEA-MaBP) coatings are devoid of the amide II proton which acts as a hydrogen donor, there is no C=O…H-N bond and also no N-H…0-H bonds at the N-H and O-H stretch region at around 3200 cm^{-1}.

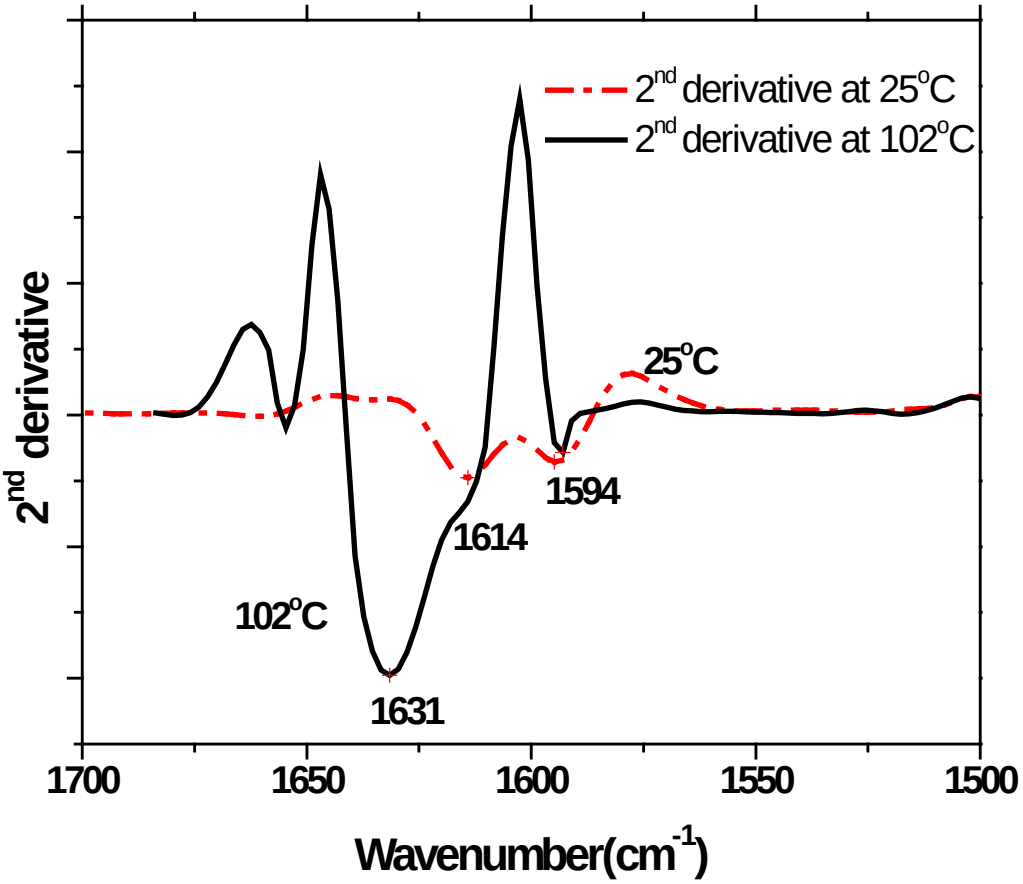

Figure 4.15 Second derivative of solvated poly(DEA-MaBP(3%)) coatings at temperature 25°C and 102°C.

The weak C-H…H-O-H at 1619cm^{-1} rapidly decrease in intensity as the temperature is increased from 25°C TO 102°C whereas the strong C=O…H-O-H interactions at 1595cm^{-1} decrease only marginally as water evaporates from the poly(DEA-MaBP) coatings. It is only at temperatures as high as 102°C, water is completely evaporated from the polymer coatings which results in a huge peak at 1631cm^{-1} representing free C=O groups.

All these results together suggest that the poly(DEA-MaBP(3%)) coatings like poly(NIPAAm-MaBP(3%)) coatings retain water even in the collapsed state. There seems to be heterogeneous domains inside the collapsed polymer coatings which still hold considerable amounts of water molecules. This water is tenaciously held inside hydrophilic and hydrophobic domains. The absence of a dissociable proton in poly(DEA-MaBP) coatings may play a role in why there is significantly less water (10%-15%) compared to poly(NIPAAm-MaBP) coatings which hold as much as 30%-35% water molecules as confirmed by our neutron reflection experiments. The aliphatic groups generally remain dehydrated even when the polymer coatings are completely saturated and do not play a major role in the collapse of the networks. The amide 1 and mainly amide II peaks are responsible in confining water molecules and are responsible in determining the nature of the transition by their interaction with water trapped inside them. There also seems to be pockets of water inside the collapsed poly(DEA-MaBP) coatings which are removed only at temperatures as high as 102^{o}C.

4.3 Conclusions

Surface-tethered poly(NIPAAm-co-MaBP) networks with varying crosslink density were characterized with both neutron reflection and ATR-FTIR and compared to the demixing behavior of linear poly(NIPAAm-co-MaBP) in solution. Neutron reflection revealed that the discontinuity in the volume transition of the surface-tethered networks coincided with the miscibility gap of non-cross-linked linear poly(NIPAAm-co-MaBP). This finding signifies that confinement does not alter the interactions that govern the coil-globule transition in single poly(NIPAAm) chains. Both neutron reflection and FTIR results showed that a discontinuous transition takes place only when the surface-tethered network is prepared in a state that is able to traverse the cloud point curve upon demixing. If, on the other hand, the network is prepared in a state that does not traverse

the cloud point curve, the network follows a continuous decrease in swelling upon demixing. FTIR results seem to indicate water molecules trapped between amide groups through hydrogen bonding can undergo substitution with D_2O even in the collapsed state. Comparative studies with poly(DEA-co-MaBP(3%)) show that the dissociable proton to be important in retaining more water in poly(NIPAAm) coatings than in poly(DEA-co-MaBP) coatings.

CHAPTER 5: ROLE OF HOFMEISTER SERIES OF SALTS ON THE DEMIXING BEHAVIOR OF POLY(NIPAAm) NETWORKS

5.1 Introduction

Poly(N-isopropylacrylamide) (poly(NIPAAm), is a well studied thermoresponsive polymer undergoes roughly a hydrophilic-hydrophobic transition at its demixing temperature finding applications in drug delivery,[239, 240] separations,[239, 240] tissue cultures,[241, 242] and chromatography.[243, 244]. The exact mechanism of the demixing behavior in poly(NIPAAm) remains debatable. The swelling below the demixing temperature is determined by a balance between mixing osmotic pressure arising from contacts between segments giving rise to greater intramolecular interaction between polymer segments and the entropic of chain stretching. As temperature approaches the critical value, hydrophobic interactions between isopropyl groups contract the network, expelling water in the process. [33-37, 223]

The demixing behavior of Poly(NIPAAm) is known to perturbed by the addition of cosolutes like salt.[3] The change in demixing temperature due to the salts is not purely concentration dependent. The change in magnitude of the demixing temperature is greatly affected by the nature of cosolute added and usually follows the Hofmeister series of salts.[3-5] ATR-FTIR, neutron reflection and ellipsometry was used to characterize the surface tethered poly(N-isopropylacrylamide) copolymerized with x mol % methacroyloxybenzophenone (MaBP) (where x= 3% and 5%) acting as the cross-linker. Neutron reflection and ellipsometry was used to derive average water distribution

and swelling characteristics of the surface confined polymer coating. ATR-FTIR was used to study the intermolecular and intramolecular interaction between the polymer coating, salts and water molecules.

Neutron reflection data suggests the presence of 2-3 water molecules per polymer segment corresponding to 30-35% of water that seems to be trapped even in the collapsed state.[1] We have investigated the role of Hofmeister salts on the demixing behavior of poly(NIPAAm-co-MaBP(3%)) coatings. The addition of salts seem to interact mainly with the amide groups suppressing the amide II group in the order SO_4^{-2}>Cl^->Br^- >I^-. In addition, the presence of strong salting out Na_2SO_4 seems to help in driving out most of the water. However, water that is bound strongly to amide moieties of the polymer is not completely expelled even in the presence of high Na_2SO_4 concentration (1M). FTIR experiments have shown the presence of 2 distinct populations of water present around 3400$cm^{-1}$and 3280cm^{-1} wavenumbers.[245] While the addition of Na_2SO_4 brings about a shift in the peak position of the band at 3400cm^{-1} representing of water bound to each other significantly, there is little change in the peak position of the band at 3280cm^{-1} representing water bound to the amide groups of the polymer coating perhaps forming water bridges and also seem to be independent of cross-link density.

FTIR experiments on poly(NIPAAm) coatings have shown that the peak positions of the isopropyl and amide groups shift due to changes in the intermolecular and intramolecular hydrogen bonding between the polymer and water molecules with water bound to amide groups even at temperatures well above the demixing temperature.[79, 80, 104] We present FTIR 2nd derivative spectra of poly(NIPAAm-MaBP) coatings solvated Na_2SO_4, NaCl, NaBr and NaI in order to better understand the finer nuances in the molecular interactions between salt and polymer groups below and above the

demixing temperature. We have for the first time shown the molecular interactions of the amide groups of surface-tethered photo-cross-linked poly(NIPAAm-MaBP(3%) coatings with the Hofmeister series of salts (SO_4^{-2}> Cl^-> Br^-> I^-) using ATR-FTIR.

5.2 Results and Discussion

We investigated the demixing behavior of photo cross-linked poly(NIPAAm-MaBP(3%)) coatings solvated in 0.1-1.0M Na_2SO_4 with neutron reflection. Neutron reflection profiles and their corresponding volume fraction profiles from figure 5.1 and 5.2 follow the conformational change in the polymer coatings across the demixing temperature. The NR profiles indicate a discontinuous phase transition in poly(NIPAAm-MaBP).There seems to be large dependence on Na_2SO_4 concentration between 0.1-0.3M where the coatings are swollen. The coatings collapse almost to their dry thickness (200 Å) at 1.0M Na_2SO_4, with change in thickness from 0.3-1.0M Na_2SO_4 being very minimal. The neutron profiles show 1 well defined kiesseg fringe at a concentration of 0.125M Na_2SO_4 with Δq = .008 which corresponds to an overall thickness of 785 Å. As the concentration of Na_2SO_4 increases to 1.0M, 2 well defined kiesseg fringes are formed with Δq = .03 corresponding to a thickness of 209 Å. All reflection profiles were fit with a profile consisting of 2-3 SLD slabs, with interfaces between the slabs smeared by error functions. At low temperatures, the interface between the coating and D_2O was difficult to fit, being non-Gaussian in nature.[1]

.

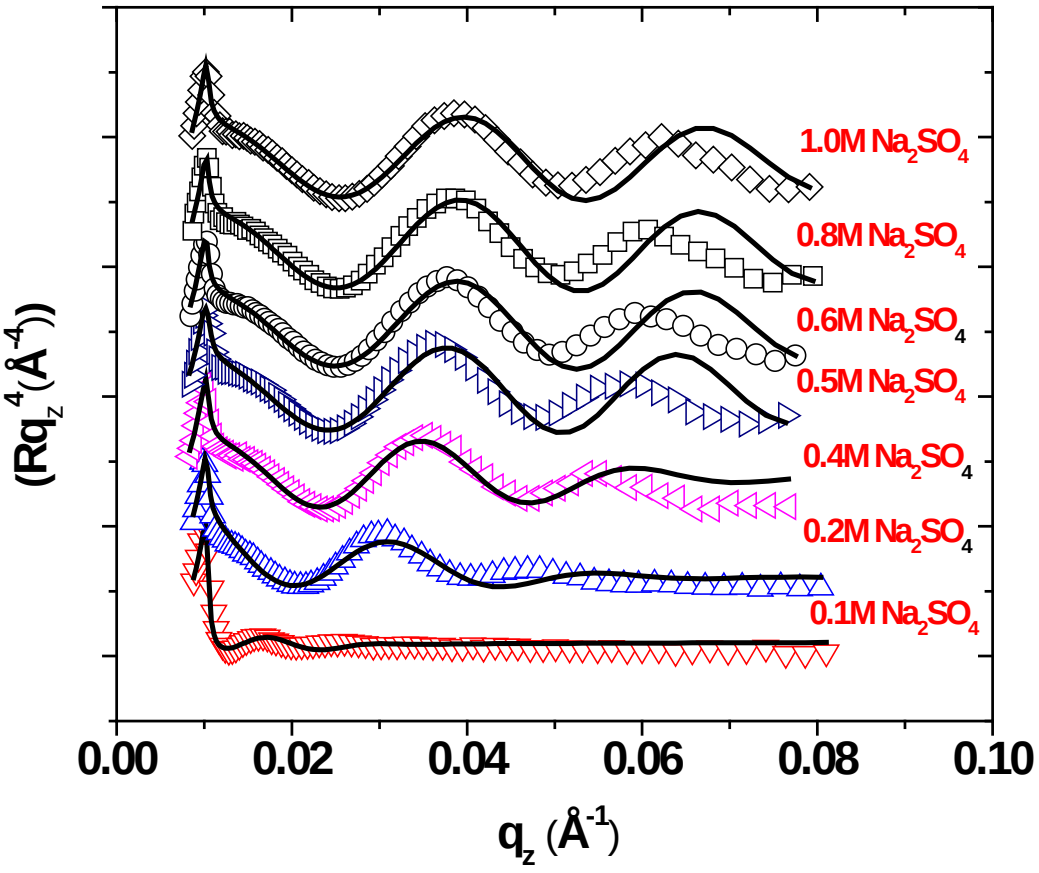

Figure 5.1 Reflectivity profiles for poly(NIPAAm-MaBP) from 0.1M -1.0M Na_2SO_4

The volume fraction profiles in figure 5.2 show that the coating collapse from an extended conformation at 0.1M NA_2SO_4 to a collapsed state at 1.0M NA_2SO_4. However, the polymer coatings swell to a lesser extent compared to coatings that have been solvated in water.[1] The change in volume phase transition seems to be continuous due to the water-salt interaction caused by the salting out effect of NA_2SO_4.

It is also evident from the volume fraction profiles that the amount of water confined in poly(NIPAAm) coatings solvated in Na_2SO_4 retain considerably less water (18-20%) compared to poly(NIPAAm) coatings solvated in D_2O (30-35%) in the collapsed state.[1].

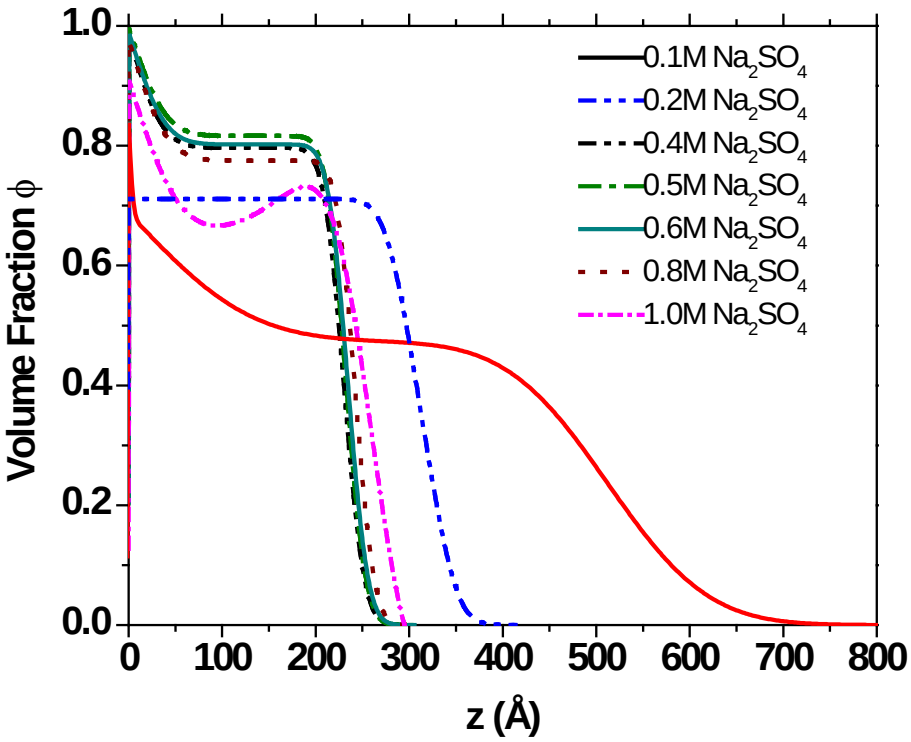

Figure 5.2 Volume fraction profiles for poly(NIPAAm-MaBP) from 0.1M-1.0M Na_2SO_4.

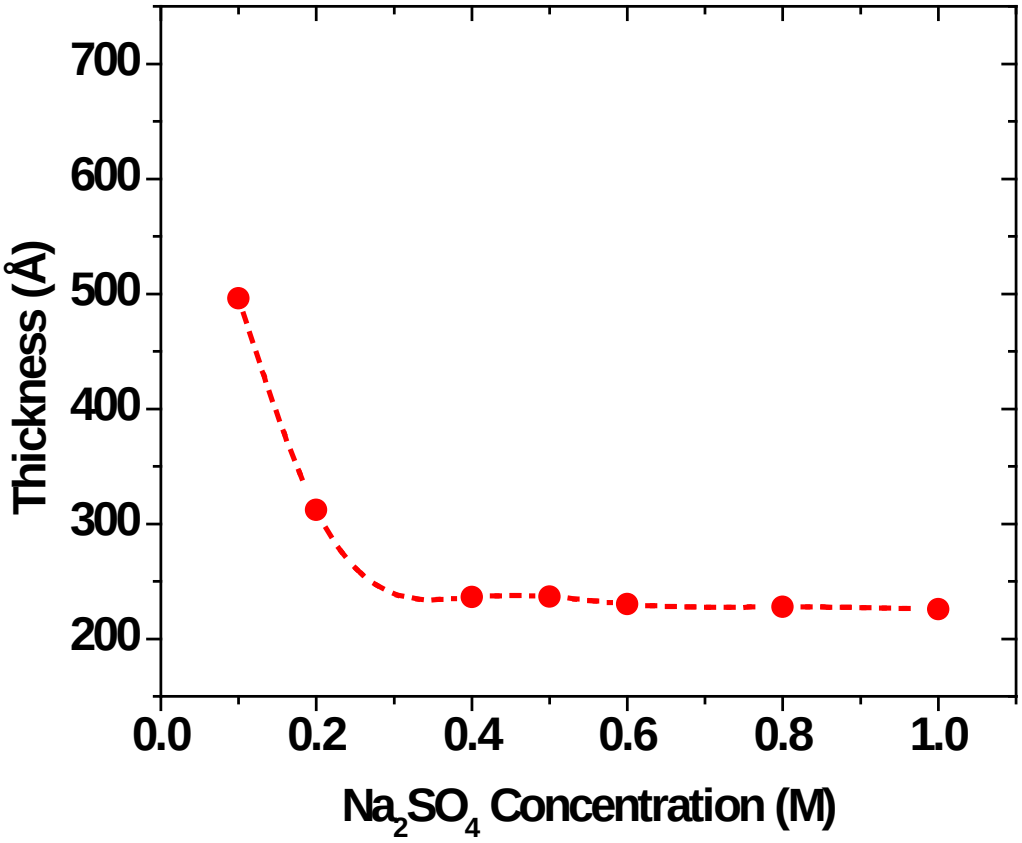

Figure 5.3 Variation of average thickness <z> of the surface-tethered poly(NIPAAm-co-MaBP) networks as a function of concentration.

The average thicknesses <z> as a function of temperature are plotted in Figure 5.3 where <z> is defined as $2\int z\phi(z)dz \Big/ \int \phi(z)dz$ and ϕ is the volume fraction of the polymer. The networks are swollen to a average thickness of 496 Å at 0.1 M Na_2SO_4 collapse to 236 Å at 0.4M Na_2SO_4.There is a weak dependence for film thickness with concentration above 0.4M and the coatings collapse to a average thickness of 226Å at 1.0M Na_2SO_4.

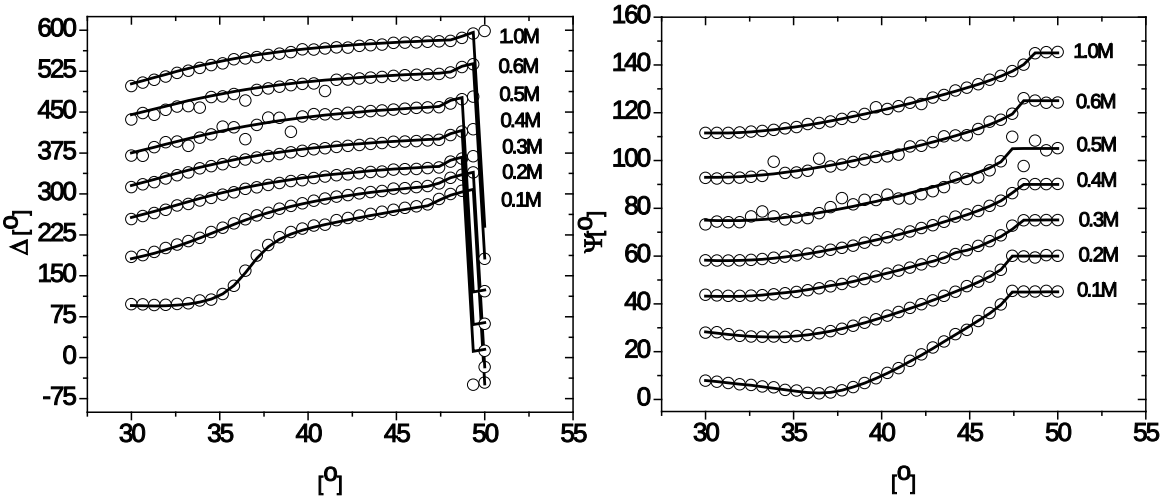

Figure 5.4 The ellipsometry Δ and ψ values and the simulated fits as a function of the angle of incidence for poly(NIPAAm-MaBP) coatings solvated in 0.1-1.0M Na_2SO_4. The data and the simulated fits have been shifted for clarity.

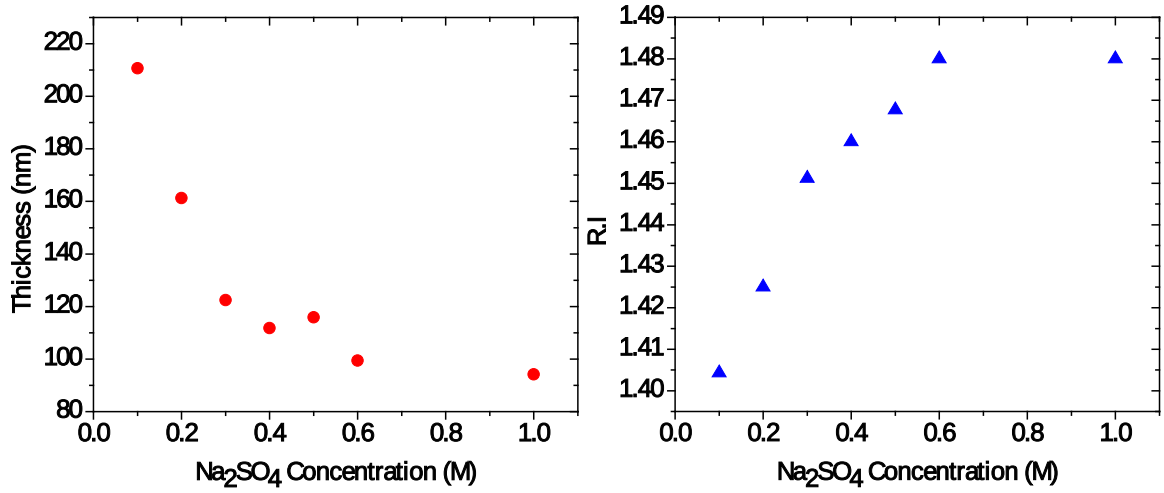

Figure 5.5 Thickness versus concentration and refractive index versus concentration for poly(NIPAAm-MaBP) solvated in 0.1-1.0M Na_2SO_4.

Ellipsometry data also shows a discontinuous trend in the collapse of the coatings solvated in Na_2SO_4. The best fit single box profiles for Δ and ψ values are as shown in figure 5.4. It can be seen that the Δ and ψ values change between 0.1-0.2M Na_2SO_4, with no significant changes for concentrations from 0.2-1.0M Na_2SO_4. The thickness and the corresponding refractive index determined using Δ and ψ values as a function of Na_2SO_4 concentration is shown in figure 5.5. There is a steep decrease in thickness of the polymer coating between 0.1-0.3M Na_2SO_4 followed by no significant change in thickness from 0.3-1.0M Na_2SO_4. The dry polymer coating has a refractive index of 1.445 falling to 1.396 when solvated in water. It can be seen that with the addition of 0.1M Na_2SO_4, the refractive index goes up to 1.404 indicating that some amount of water is expelled out of the polymer coating due to the salting out effect of Na_2SO_4. The thickness of the polymer coating swells up to 238 nm in water from a dry thickness of 78.7 nm corresponding to a swell ratio of 3.01. The thickness of the polymer coating goes down to 210.7 nm when solvated in 0.1M Na_2SO_4 corresponding to a swell ratio of 2.67 due to expulsion of water molecules from the polymer coating. The polymer coating collapses to a thickness of 94.2 nm at 1.0M Na_2SO_4 suggesting that water is still trapped in the collapsed polymer coating corresponding well with neutron reflection data in the same concentration regime.

We then extended our study to investigate the interaction of Hofmeister series of salts (SO_4^->Cl^->Br^->I^-) on the hydrophilic amide moieties and hydrophobic isopropyl moieties of poly(NIPAAm-co-MaBP(3%)).

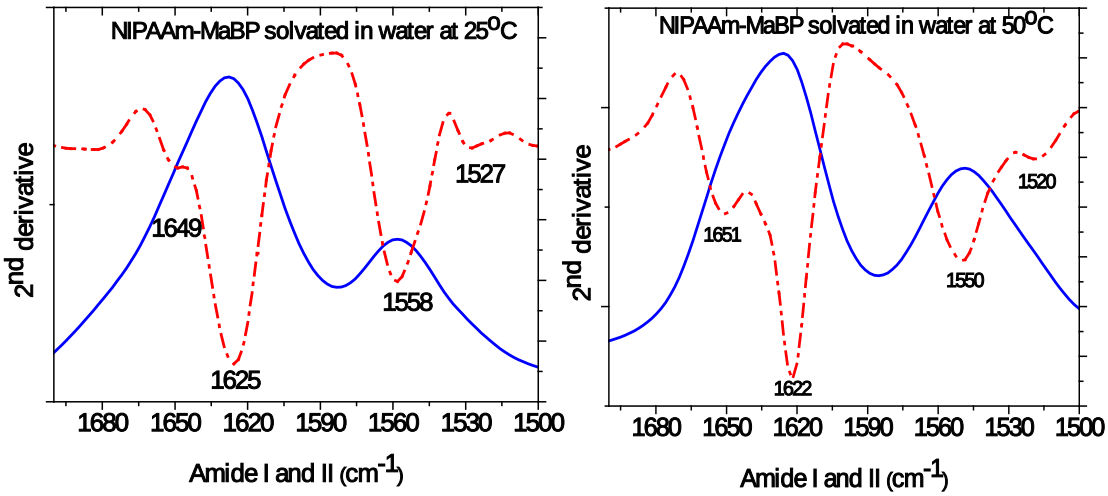

Figure 5.6 2nd derivative FTIR spectra of poly(NIPAAm-MaBP(3%)) solvated in water at 25°C and 50°C.

Figure 5.6 shows 2nd derivative FITR spectra OF poly(NIPAAm-MaBP(3%)) coating at 25°C where it is completely solvated in water and at 35°C,wherein most of the water is expelled from the collapsed coating. The 2nd derivative FTIR spectra show the presence of 2 subbands at 1625 cm^{-1} and a shoulder at 1649cm^{-1} in the amide I region and 1 subband at 1550 cm^{-1} in the amide II region at 25°C. The shoulder at 1649cm^{-1} at 25°C increases in intensity and is blue-shifted by 2cm^{-1} at 35°C. The subband at 1558cm^{-1} is red-shifted by 8cm^{-1} as the temperature increases from 25°C-50°C. This change is also accompanied by a drastic change in the peak intensity of the amide II moiety as the polymer coating collapses above its demixing temperature.

The addition of salts brings about a drastic change in the demixing behavior of poly(NIPAAm-MaBP(3%)). The salts tend to reorient water molecules and seem to enhance greater polymer-polymer interaction. The Hofmeister series lists salts on their

increasing ability to 'salt out' from solution (SO_4^-> Cl^-> Br^-> I^-) with the sulphate ion being a strong salting out agent and the iodide ion being a weak salting out or rather a strong 'salting in' agent.[4, 5]

We solvated poly(NIPAAm-MaBP) coatings in Na_2SO_4, NaCl, NaBr and NaI solutions with concentrations ranging from 0.125M-2.0M and the FITR 2nd derivative spectrum for various salts is shown in figure 5.7. The 2nd derivative FTIR spectra of poly(NIPAAm-MaBP(3%)) coatings solvated in Na_2SO_4 show the presence of 2 distinct subbands at 1620cm^{-1} and 1647cm^{-1} in the amide I region and prominent subband at 1548cm^{-1} in the amide II region at 0.125M. The subbands of poly(NIPAAm-MaBP(3%)) coating solvated in Na_2SO_4 appear similar to the coating solvated in water. However, due to the salting out nature of Na_2SO_4, the subband at 1647cm^{-1} in the amide I region is red shifted by 2cm^{-1} compared to the coating solvated in water and also increases in intensity. The amide II subbands seem to remain identical for poly(NIPAAm-MaBP(3%)) solvated in water and Na_2SO_4. Also noticeable is that the amide II region does not change a lot in peak intensity even as the concentration increases from 0.125-2.0M for Na_2SO_4.

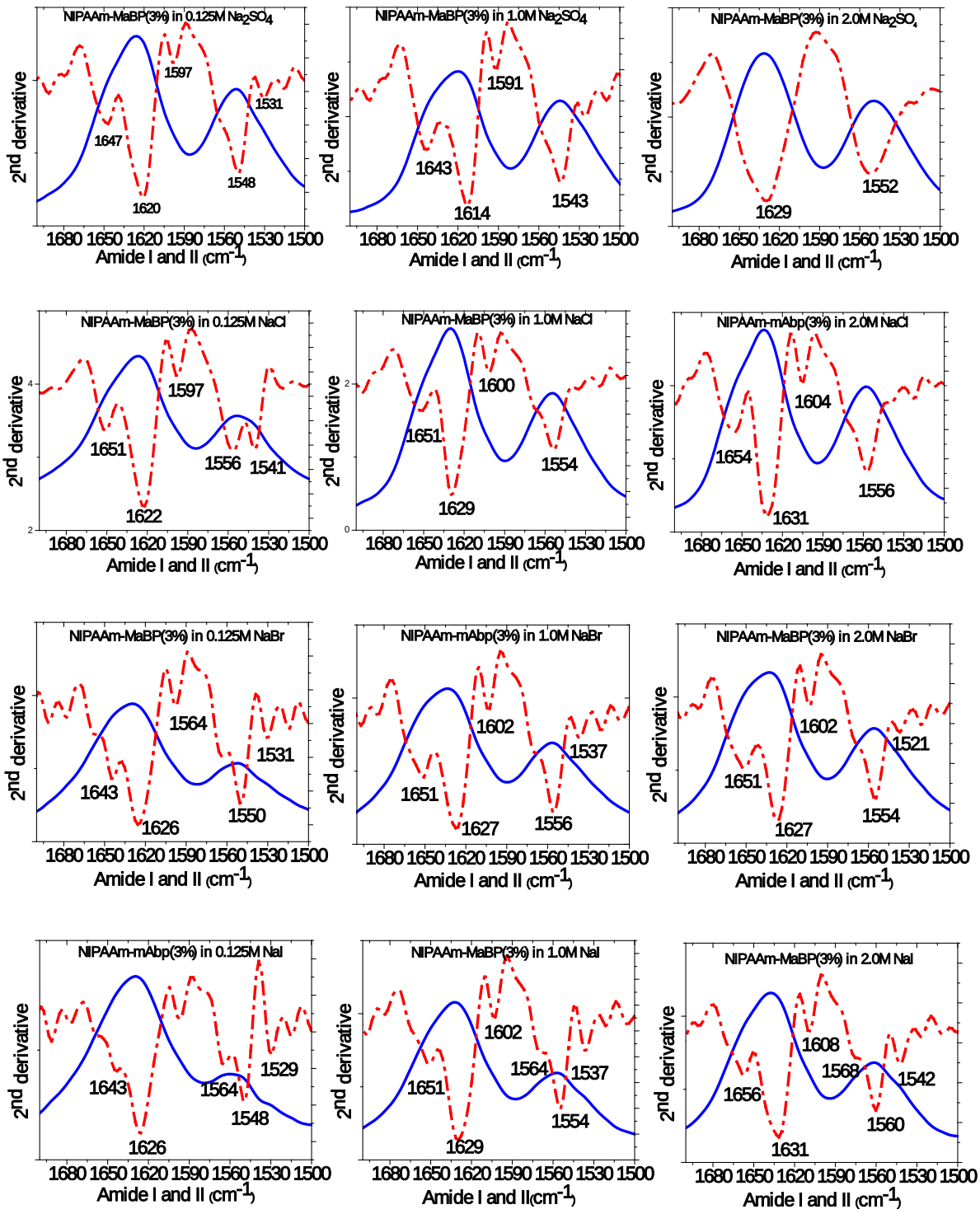

Figure 5.7 2nd derivative FTIR spectra of poly(NIPAAm-MaBP(3%)) coatings solvated in 0.125-2.0M Na_2SO_4, NaCl, NaBr and NaI.

Poly(NIPAAm-MaBP(3%)) coatings solvated in NaCl and NaBr also exhibit 2 sub bands in the amide I region similar to Na_2SO_4 and water. However, we see the emergence of a secondary sub band ($1564cm^{-1}$) in addition to a very prominent subband around $1550cm^{-1}$ in the amide II region at 0.125M. The subband decreases in intensity as the concentration increases to 2.0M in cases. The emergence of a secondary subband seems to suppress the amide II moiety as seen at lower concentrations (0.125M). At higher concentrations (2.0M), we see that the amide II region begins to increase in intensity corresponding to a simultaneous decrease in the intensity of the secondary subband in the amide II region.

Poly(NIPAAm-MaBP(3%)) coatings solvated in NaI also show 2 secondary subbands in the amide I region where in the subband at $1643cm^{-1}$ increases in intensity as the concentration changes from 0.125-2.0M. The addition of NaI seems to suppress the amide II moiety from increasing in intensity even as the concentration changes from 0.125-2.0M. The presence of a secondary peak in the amide II region at around $1564cm^{-1}$ might be responsible in suppressing the amide II moiety. The addition of even very low concentration (<0.05M) of NaI is enough to bring about the suppression of the amide II moiety (data not shown). These results clearly indicate the role of salting out and salting in salts on the demixing behavior of poly(NIPAAm-MaBP(3%)) coatings changes as in the order (SO_4^-> Cl^-> Br^-> I^-).

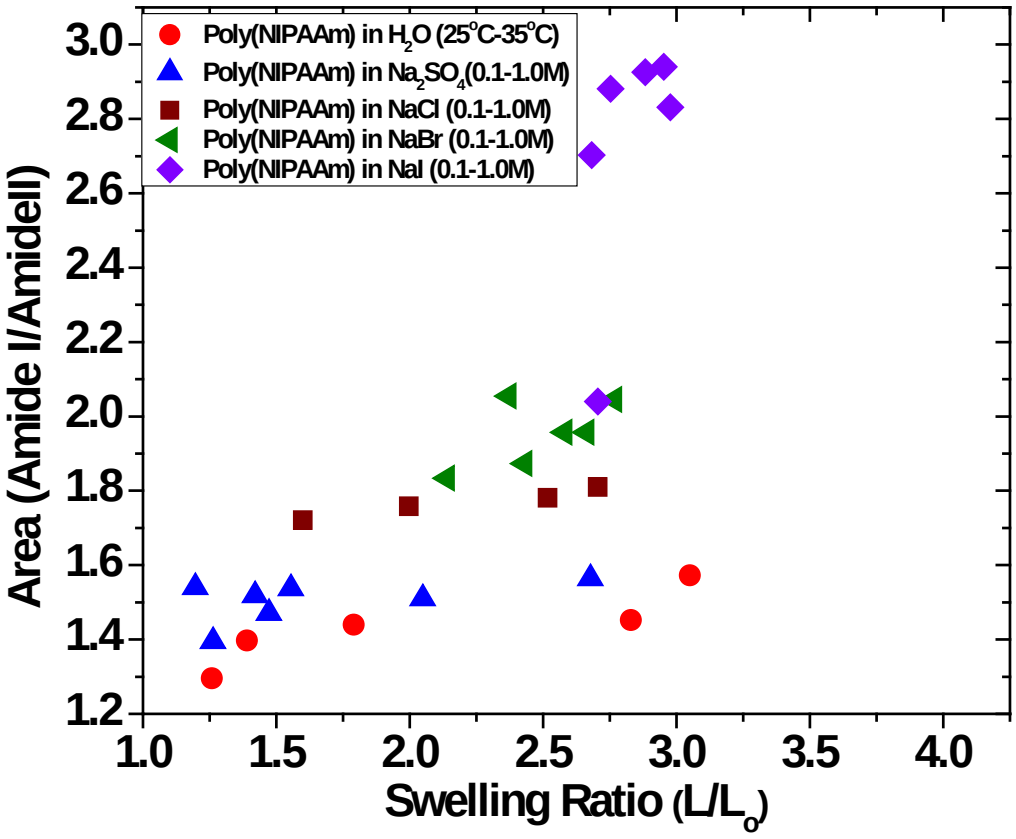

Figure 5.8 Change in the area of amide I/amide II of poly(NIPAAm-co-MaBP(3%)) solvated in water, Na_2SO_4, NaCl, NaBr and NaI as a function of swelling ratio.

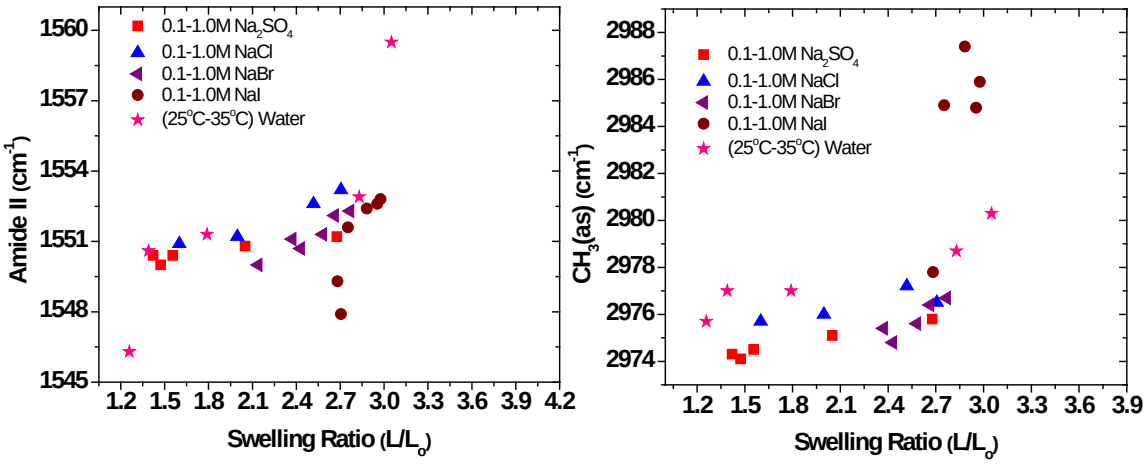

Figure 5.9 Change in amide II and CH_3(as) groups of poly(NIPAAm-co-MaBP(3%)) solvated in water, Na_2SO_4, NaCl, NaBr and NaI as a function of swelling ratio.

It has been suggested that that salt, poly(NIPAAm) and the first hydration layer interact in 3 different mechanisms.[4-6] Firstly, the anions can polarize the water molecules that are hydrogen bonded to poly(NIPAAm). Secondly, the anions can interact with the hydrophobic hydration increasing the surface tension at the polymer/aqueous interface. Thirdly, the anions can directly bind with the amide groups of poly(NIPAAm).[4-6]

Figure 5.8 shows the area of the ratio of amide I/amide II as a function of polymer swelling. The data represents change in the area of (amide I/amide II) over a concentration range of 0.1-1.0M for each of the Hofmeister salts. There is a strong correlation on the change in the area of the amide moieties with the introduction of Hofmeister salts. The swelling ratio of 3.0 seen in polymer coatings solvated in water and in the case of NaI, a strong salting in agent. We see a slight drop polymer swelling

ratio of approximately 2.67, 2.7, and 2.76 for Na_2SO_4, NaCl and NaBr respectively with a corresponding decrease in the area of amide I/amide II indicating a strong interaction between the polymer amide groups and salts. Figure 5.9 shows the change in wave number of the hydrophilic amide II (N-H) moiety and the hydrophobic CH_3(as) moiety of poly(NIPAAm-co-MaBP(3%)) coatings as a function of swelling for a concentration range of 0.125M-1.0M for Na_2SO_4, NaCl, NaBr and NaI. It can be seen that the change in wavenumbers amide II when the polymer coatings were solvated in water is 13cm^{-1} for a temperature range of 25°C-35°C. The addition of salts drastically brings down the change in the wavenumbers for all salt types for a concentration range of 0.125M-1.0M at 25°C. However, the change in the wavenumbers for the isopropyl groups (CH_3(as)) is only 3cm^{-1} even when solvated in water alone providing further evidence which support a strong polymer-salt interaction responsible for the demixing behavior

The addition of salts does not induce any significant changes in the wavenumbers of the CH_3(as) group for all salt types. This suggests that the interaction of Hofmeister salts on poly(NIPAAm) is through a direct binding effect of the salts with the amide groups displacing water molecules around the immediate vicinity of the amide moieties. Above the demixing temperature, the amide-salt interaction is weakened. This leads to a secondary driving force which contributes in the expulsion of water from the collapsed polymer coatings. This offers a plausible explanation for the presence of relatively lower amount of water present (15-20%) in the collapsed polymer coatings compared to polymer coatings solvated in water alone. It is noted that NaI exhibits slightly different behavior compared to other Hofmeister salts. This might be due to the fact that the highly salting in nature of NaI prevents the polymer coatings to undergo demixing completely.

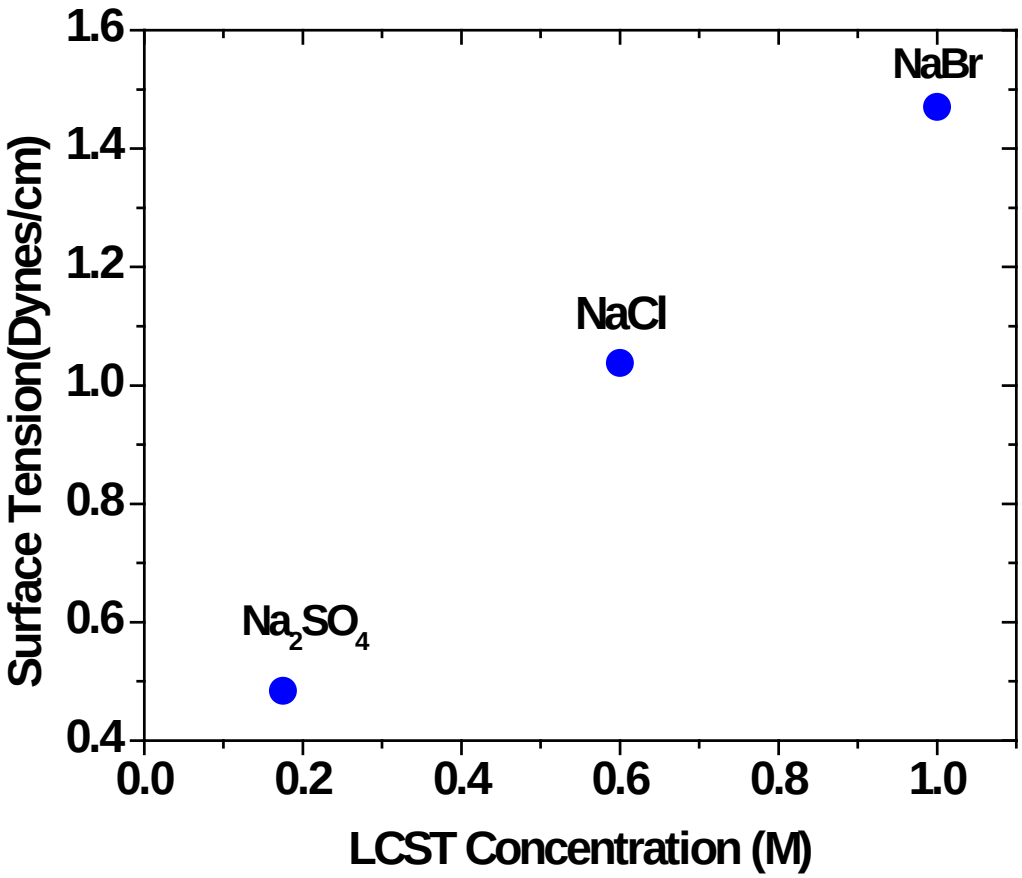

Figure 5.10 Surface tension calculated from surface tension increments as a function of demixing concentration for Na_2SO_4, NaCl and NaBr at 25°C.[246]

The dehydration of the hydrophobic groups during the demixing process seems to be independent of salt type and their concentration as indicated by FTIR data. The data shows that the change in the wave numbers of the isopropyl groups is minimal for all salts for 0.1-2.0M concentration as shown in figure 5.9. The surface tension change calculated from surface tension increments for Na_2SO_4, NaCl and NaBr at their demixing concentration of 0.175M, 0.6M and 1.0M at 25°C respectively is shown in figure

5.10.[246] We see that the demixing salt concentration follows the Hofmeister series with a corresponding increase in surface tension. This suggests that there is no correlation with salts affecting the hydrophobic hydration around the isopropyl groups as any interaction with the hydrophobic groups, the surface tension change for Na_2SO_4, NaCl and NaBr will be constant. This suggests that the hydrophobic groups remain more or less dehydrated with or without the addition of salts and the change in the surface tension needed to bring about dehydration is as a result of a direct interaction of the Hofmeister anions with the amide II moiety.

All these results together suggest that the amount of water in the polymer is strongly dependent on the concentration of the salt solution. Na_2SO_4 brings about a reduction in the amount of water bound to the polymer coatings in the collapsed state. The water that is driven out seems loosely hydrogen bound to other water molecules which readily come out on addition of Na_2SO_4. However there is still about 15% of water that is trapped inside the polymer coatings in the collapsed state which is much lower than when solvated in water.[1] This may be water that is strongly hydrogen bound to the amide groups of the polymer.

CHAPTER 6: PEPTIDE EMBEDDED SMART POLY(N-ISOPROPYLACRYLAMIDE) HYDROGELS

6.1 Introduction

The hydrophilic to hydrophobic phase transition of poly(N-isopropylacrylamide) or poly(NIPAAm) based polymers have been of considerable interest. These polymers are termed smart, which arises due to an entropic gain as water molecules surrounding hydrophobic isopropyl groups are expelled into the bulk as the temperature is increased beyond a certain critical value called the lower critical solution temperature (LCST)The responsive nature of poly(NIPAAm) based polymers have found applications in drug delivery,[239, 240] separations,[239, 240] tissue cultures,[241, 242] and chromatography.[243, 244]

To this effect, we have synthesized poly(NIPAAm) based hydrogels copolymerized with 3-aminopropylmehtaacrylamide which provides a free amine functional group. This provides us a starting point to couple bio-polymers like peptides to create peptide-based hybrid polymers with both thermo and pH responsiveness. Using a modified Merrifield solid phase peptide synthesis technique,[194, 195] the elastin family of pentapeptide, Gly- Glu- Gly-Val-Pro (GEGVP) with Glu being the guest residue was incorporated to provide pH responsiveness to the hydrogels.

Our results show that poly(NIPAAm) hydrogels can be made to go through their transition in a narrow pH range by only changing the peptide sequence to alter their isoelectric point. Hybrid polymers composed of synthetic polymer and protein-folding

motifs have been reported that collaspse at 40°C where the peptides was tagged using nickel and histidine to hydroxypropylmethaacrylamide (HEMA) copolymers.[9] It has been reported that Gly(G) and His (H) residues form complexes with heavy metal such as copper, nickel and zinc.[247, 248]

We have shown that poly(NIPAAm)-GGH constructs can be similarly fabricated which aggregate on chelating to heavy metal ions like Cu(II), Ni(II) and Zn(II), but do not aggregate in water. We have hence demonstrated a simple technique to effectively separate metal ions easily by conjugating the tripeptide GGH to poly(NIPAAm) hydrogels.

6.2 Results and Discussion

The overall goal of this study is to demonstrate a facile and simple synthesis strategy to bring about conformational changes in the structure of the peptides embedded in poly(NIPAAm) hydrogels by inducing volume phase change in response to very specific environmental cues and to also act as a sensing platform. To this effect, poly(NIPAAm) hydrogels was copolymerized with 3-aminopropylmethaacrylamide hydrochloride(3-APMA) which has a free amine end group. The amine functionalized hydrogels were then embedded with two different types of peptide sequences; GEGVP, a pentapeptide belonging to the elastin family of proteins and GGH, a tripeptide with an affinity towards heavy metals like Cu(II), Ni(II) and Zn were engineered by modifying the Merrifield solid phase peptide synthesis.

Figure 6.1 shows the change in volume phase transition in poly(NIPAAm) hydrogels embedded with GEGVP for pH 2.23-10.95. The hybrid polymer hydrogel has an

isoelectric point of~7.0. The hydrogel is completely protonated at lower pH (2.23-5.87) which cause the hydrogels to remain swollen. As the pH approaches the isoelectric point(pH 6.57), we see that the gels undergo a volume phase transition collapsing to their hydrophobic state. At higher pH (8.95-10.92), the gels become deprotonated and this causes them to reswell again. In essence, the protonation and deprotonation of the hydrogels on either side of the isoelectric point enables sufficient charge distribution which prevents the hydrogels from collapsing. The hydrogels thus exhibit a phase transition in a narrow pH range of 6.57-7.67 close to the physiological pH of 7.4.

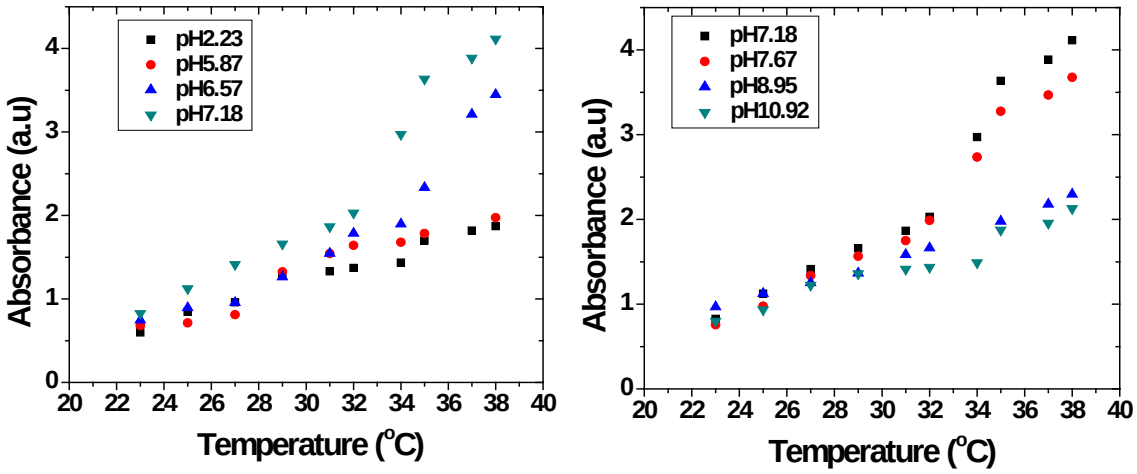

Figure 6.1 Volume phase change in poly(NIPAAm) hydrogels conjugated with GEGVP for a pH range of 2.23-10.95.

Another strategy was to engineer poly(NIPAAm) hydrogels with GGH, a tripeptide with an affinity towards heavy metals.[ref] We chose to study the binding properties of copper. Nickel and zinc to GGH modified poly(NIPAAm) hydrogels. It has been well documented that GGH has metal chelating abilities towards Cu(II, Ni(II) and Zn(II).[249]We have demonstrated that poly(NIPAAm)-GGH constructs can be used to chelate Cu(II), Ni(II) and Zn and also bring about unique phase transitions depending on the type of metal ion that has been chelated to the hydrogel.

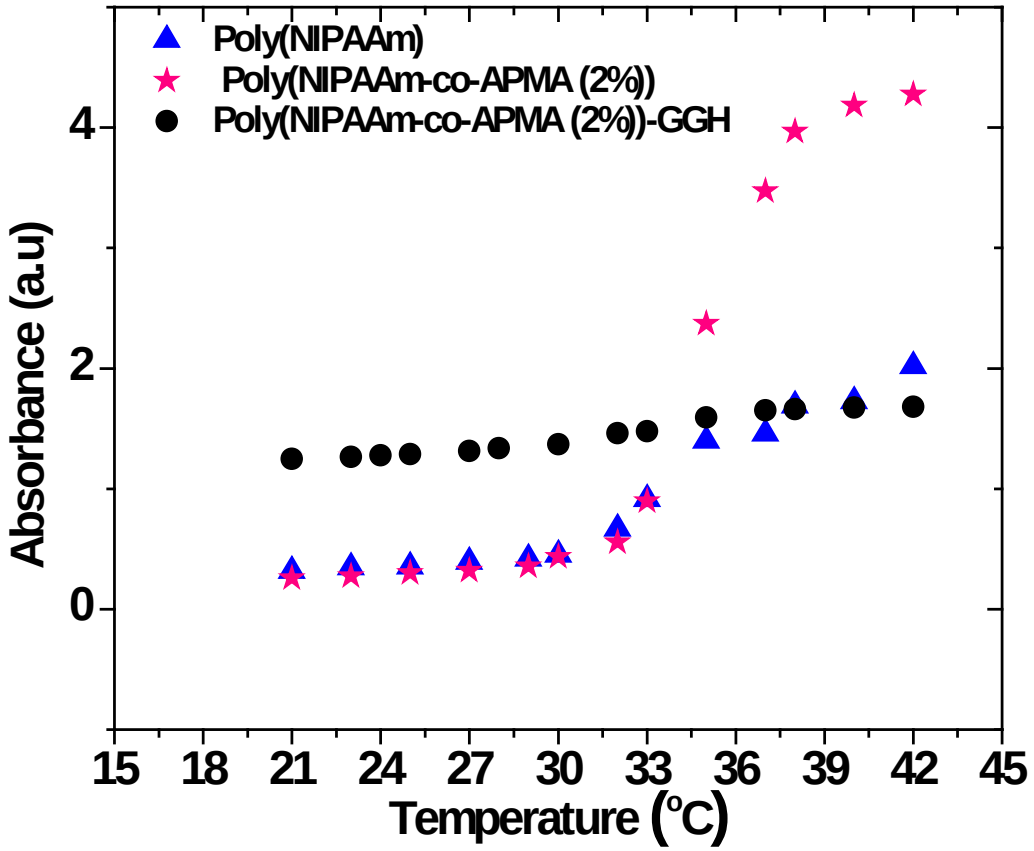

Figure 6.2 Change in swelling behavior as a function of temperature for poly(NIPAAm), poly(NIPAAm-co-APMA(2%)) and poly(NIPAAm-co-APMA(2%))-GGH hydrogels.

Figure 6.2 shows the change in swelling behavior for poly(NIPAAm), poly(NIPAAm) copolymerized with 3-APMA and poly(NIPAAm-co-APMA(2%)) conjugated with GGH. We see that both poly(NIPAAm) and poly(NIPAAm-co-APMA(2%)) exhibit a change in swelling behavior for temperature 21 ^{o}C-42 ^{o}C.

The addition of 2% of APMA makes poly(NIPAAm) much more hydrophilic and this causes the hydrogel to swell more and also shifts the transition temperature from 33°C for poly(NIPAAm) to 36°C for poly(NIPAAm-co-APMA(2%)) respectively. However, the addition of the tripeptide GGH prevents the collapse of the poly(NIPAAm-co-APMA(2%)) by changing the balance between the hydrophilic and hydrophobic moieties of the peptide embedded hydrogel.

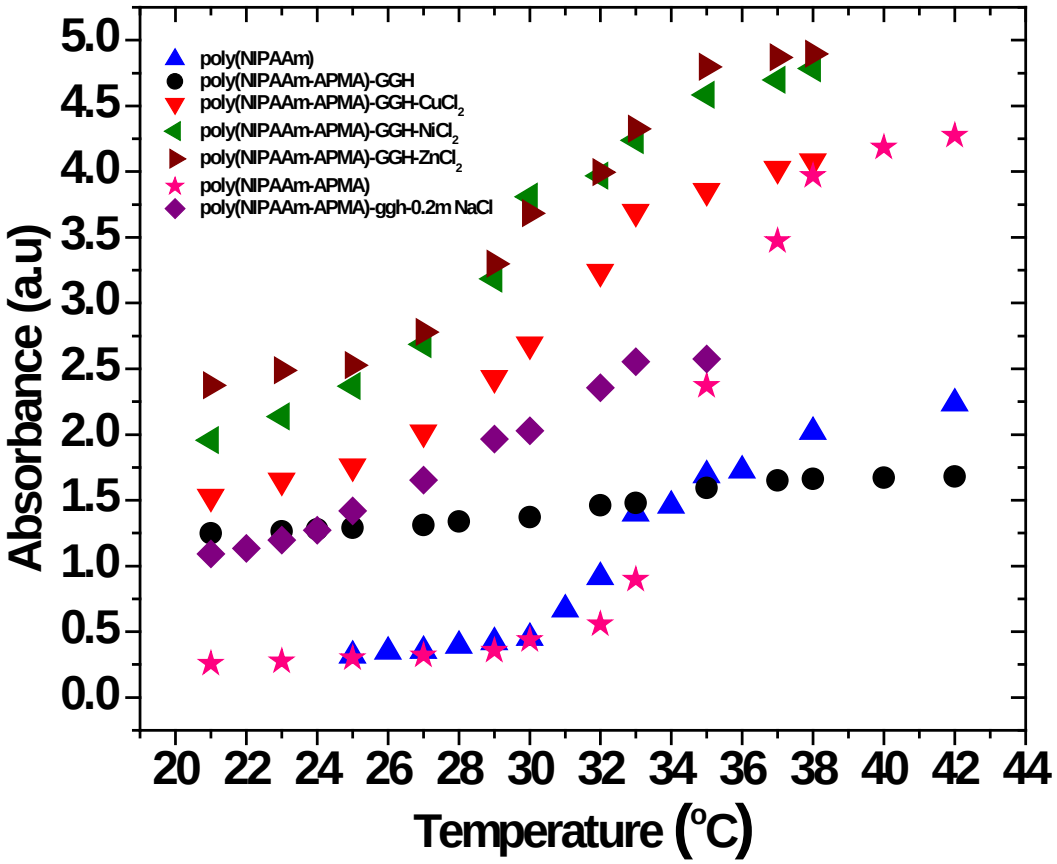

Figure 6.3 Swelling behavior of poly(NIPAAm-co-APMA(2%)) solvated in water and 0.1M solutions of $CuCl_2$, $NiCl_2$, $ZnCl_2$ and 0.2M NaCl.

Poly(NIPAAm-co-APMA(2%)-GGH hydrogels were then solvated water and in 0.1M solutions $Cu(II)Cl_2$, $Ni(II)Cl_2$,$ZnCl_2$ and NaCl as shown in figure 6.3. We see that the GGH conjugated poly(NIPAAm-co-APMA(2%)) hydrogels solvated in 0.1M $CuCl_2$ undergoes deswelling as is the case with 0.1M solutions of $NiCl_2$ and $ZnCl_2$. GGH conjugated poly(NIPAAm) can thus be used as a sensor to separate heavy metals from solutions by increasing the temperature above the transition temperature. As these hydrogels do not aggregate in water but tend to deswell and aggregate in solutions of copper, nickel and zinc, providing an easy route to detect and remove metal complexed hydrogels from sample solutions.

The addition of 0.2M NaCl to poly(NIPAAm-co-APMA(2%))-GGH constructs brings about only a partial deswelling of the hydrogels. This suggests that the metal cations are mainly responsible in the deswelling process of the poly(NIPAAm) hydrogel. However, higher concentrations of salts also form an efficient way to aggregate hydrogels complexed with metal ions providing an alternative route to aggregate the hydrogels.

6.3 Conclusions

Poly(NIPAAm-co-APMA(2%)) hydrogels were used to embed GEGVP and GGH to form hybrid polymer constructs that respond to specific cues such as pH and chelate to metal ions. By carefully fabricating poly(NIPAAm) hydrogels with GEGVP, we have an alternative route to make the polymers really smart by making the hydrogels to respond to a narrow range of pH. Poly(NIPAAm)-GGH constructs can be used to chelate heavy metal ions and offers an easy way to separate them from sample solutions. This synthesis method thus offers a simple yet robust route to fabricate an effective sensor that responds to multiple environmental cues.

SUMMARY

We present a simple photochemical technique for fabricating responsive polymer thin films using benzophenone chemistry. The method is simple and gives us control over cross-link density and film thickness. Poly(NIPAAm-MaBP) copolymer can be spin-casted and cross-linked with UV light (365 nm).

1. Permits opportunities for patterning.
2. Wide range of potential substrates.

Neutron reflection experiments have shown that poly(NIPAAm-MaBP) films undergo a reversible thickness-phase transition around 30°C.

1. Above the collapse temperature, approximately 35% of water (D_2O molecules) still trapped in the collapsed network with 3 D_2O molecules per polymer segment.
2. Varying only cross-link density, the volume transition can be discontinuous or exhibit a more continuous change.
3. The binodal envelope for two-phase region in solutions of linear poly(NIPAAm) serves as a potential guide for understanding volume-phase transitions in networks and other confined geometries.
4. Strong salting out salt like Na_2SO_4 induces a concentration dependent phase transition with around 15-20% D_2O still trapped in the network. The presence of salts might form a secondary driving force for the expulsion of water from the collapsed polymer coatings.

5. Comparative studies with poly(DEA-co-MaBP) have shown that due to their greater hydrophobic surface area and also the absence of a dissociable proton in the amide moieties, there is only 10-15% D_20 molecules in the collapsed poly(DEA-MaBP) coatings.

ATR-FT-IR of poly(NIPAAm-MaBP) indicate structural changes manifested by the demixing process.

1. The relative position of the amide peaks is determined by the amount of confined water trapped in the network and is largely independent of temperature.
2. D_2O –H_2O exchange takes place even at 50°C indicating the presence of heterogeneous domains in the collapsed poly(NIPAAm) coatings.
3. FTIR results indicate the presence of a direct interaction between the Hofmeister salts and the amide moieties of poly(NIPAAm-MaBP) polymers.

Peptide modified poly(NIPAAm) hydrogels exhibit unique phase transition behavior.

1. A simple and robust method to conjugate small peptide sequences using a modified Fmoc solid phase peptide synthesis technique into poly(NIPAAm) hydrogels is demonstrated.
2. pH controlled phase transition seen in poly(NIPAAm)-GEGVP conjugated gels which aggregate in a very narrow pH range.
3. Metal ion induced phase transition seen in poly(NIPAAm)-GGH conjugated gels which can be used to detect and separate heavy metal ions like copper, nickel and zinc from solution.

FUTURE DIRECTIONS

Chapter 3 and chapter 4 discuss results on characterizing the volume phase transition of poly(NIPAAm) based polymer networks. Our data as shown that the demixing behavior can be predicted by changing only the cross-link density of the polymer networks and can be mapped using phase diagram of linear poly(NIPAAm) solutions. Similar experiments can be conducted on a slew of other responsive polymers like poly(diethyleacrylamide), poly(cyclopropylacrylamide), poly(vinylcaprolactam) among others. The inclusion of other hydrophilic and hydrophobic copolymers which provide additional functionalities is also an option that can be explored. As poly(NIPAAm) is not biodegradable, it presents a limitation in certain biological scenarios where using a more biocompatible comonomer might help to expand their biomedical applications

In chapter 5, we have shown that certain additives like the Hofmeister series of salts have a profound effect on the demixing behavior of poly(NIPAAm) coatings. It is seen that salts have a direct interaction with the amide moieties of poly(NIPAAm) while very less interaction with the isopropyl groups. The addition of salts tend to form an additional driving force for water molecules to be driven out of the collapsed network Investigating the effect of salt on poly(NIPAAm) offers us a simple model to better understand the complex nature of protein denaturation We have mainly investigated the role of monovalent anions in this study. It would be an interesting experiment to look at the effect of divalent and trivalent anions on the demixing behavior of polymers.

In chapter 6, we have demonstrated a simple method of creating smart hydrogels based on poly(NIPAAm) conjugated with specific peptide sequences using the Merrifield solid phase peptide synthesis. We have shown that by conjugating GEGVP, an elastin family of pentapeptide, the hydrogel can be made to respond to specific pH close to the physiological pH of 7.4.

We have also shown that poly(NIPAAm) conjugated with GGH, a tripeptide can be used to chelates to heavy metal ions like copper, nickel and zinc bringing about their separation by aggregating the hydrogel. We can expand this study by looking at other peptide sequences having different functionalities and also conjugating different combinations of the same peptides to fine tune their responsiveness. Another possibility is to fabricate peptide embedded polymer surfaces which would have huge potential in microfluidics and separation of specific bio-molecules both in vitro and in vivo. Peptide embedded polymer coatings can also be used to study cell adhesion as demonstrated by Okano and coworkers.[53, 54]

REFERENCES

1. Vidyasagar, A., J. Majewski, and R. Toomey, Temperature Induced Volume-Phase Transitions in Surface-Tethered Poly(N-isopropylacrylamide) Networks. Macromolecules, 2008. 41(3): p. 919-924.

2. Vidyasagar, A., et al., Continuous and discontinuous volume-phase transitions in surface-tethered, photo-crosslinked poly(N-isopropylacrylamide) networks. Soft Matter, 2009. 5(23): p. 4733-4738.

3. Freitag, R. and F. Garret-Flaudy, Salt Effects on the Thermoprecipitation of Poly-(N-isopropylacrylamide) Oligomers from Aqueous Solution. Langmuir, 2002. 18(9): p. 3434-3440.

4. Zhang, Y., et al., Specific Ion Effects on the Water Solubility of Macromolecules: PNIPAM and the Hofmeister Series. Journal of the American Chemical Society, 2005. 127(41): p. 14505-14510.

5. Zhang, Y., et al., Effects of Hofmeister Anions on the LCST of PNIPAM as a Function of Molecular Weight The Journal of Physical Chemistry C, 2007. 111(25): p. 8916-8924.

6. Zhang, Y. and P.S. Cremer, Chemistry of Hofmeister Anions and Osmolytes. Annual Review of Physical Chemistry. 61(1).

7. Jeong, B. and A. Gutowska, Lessons from nature: stimuli-responsive polymers and their biomedical applications. Trends in Biotechnology, 2002. 20(7): p. 305-311.

8. Ehrick, J.D., et al., Genetically engineered protein in hydrogels tailors stimuli-responsive characteristics. Nat Mater, 2005. 4(4): p. 298-302.

9. Wang, C., R.J. Stewart, and J. KopeCek, Hybrid hydrogels assembled from synthetic polymers and coiled-coil protein domains. Nature, 1999. 397(6718): p. 417-420.

10. Kopecek, J., Hydrogel biomaterials: A smart future? Biomaterials, 2007. 28(34): p. 5185-5192.

11. Zhang, J.-T., S.-W. Huang, and R.-X. Zhuo, A novel sol–gel strategy to prepare temperature-sensitive hydrogel for encapsulation of protein. Colloid & Polymer Science, 2005. 284(2): p. 209-213.

12. Hassan, C.M., J.E. Stewart, and N.A. Peppas, Diffusional characteristics of freeze/thawed poly(vinyl alcohol) hydrogels: Applications to protein controlled release from multilaminate devices. European Journal of Pharmaceutics and Biopharmaceutics, 2000. 49(2): p. 161-165.

13. Wells, L.A. and H. Sheardown, Extended release of high pI proteins from alginate microspheres via a novel encapsulation technique. European Journal of Pharmaceutics and Biopharmaceutics, 2007. 65(3): p. 329-335.

14. Gombotz, W.R. and S. Wee, Protein release from alginate matrices. Advanced Drug Delivery Reviews, 1998. 31(3): p. 267-285.

15. Kim, Y.J., et al., Controlled Release of Insulin from Injectable Biodegradable Triblock Copolymer. Pharmaceutical Research, 2001. 18(4): p. 548-550.

16. Peppas, N.A. and R.E. Berner Jr, Proposed method of intracopdal injection and gelation of poly (vinyl alcohol) solution in vocal cords: polymer considerations. Biomaterials, 1980. 1(3): p. 158-162.

17. Dai, W.S. and T.A. Barbari, Hydrogel membranes with mesh size asymmetry based on the gradient crosslinking of poly(vinyl alcohol). Journal of Membrane Science, 1999. 156(1): p. 67-79.

18. Edman, P., B. Ekman, and I. Sjöholm, Immobilization of proteins in microspheres of biodegradable polyacryldextran. Journal of Pharmaceutical Sciences, 1980. 69(7): p. 838-842.

19. Hennink, W.E. and C.F. van Nostrum, Novel crosslinking methods to design hydrogels. Advanced Drug Delivery Reviews, 2002. 54(1): p. 13-36.

20. Kuijpers, A.J., et al., In vivo and in vitro release of lysozyme from cross-linked gelatin hydrogels: a model system for the delivery of antibacterial proteins from prosthetic heart valves. Journal of Controlled Release, 2000. 67(2-3): p. 323-336.

21. Sperinde, J.J. and L.G. Griffith, Control and Prediction of Gelation Kinetics in Enzymatically Cross-Linked Poly(ethylene glycol) Hydrogels. Macromolecules, 2000. 33(15): p. 5476-5480.

22. Sperinde, J.J. and L.G. Griffith, Synthesis and Characterization of Enzymatically-Cross-Linked Poly(ethylene glycol) Hydrogels. Macromolecules, 1997. 30(18): p. 5255-5264.

23. Nakayama, M., et al., Molecular design of biodegradable polymeric micelles for temperature-responsive drug release. Journal of Controlled Release, 2006. 115(1): p. 46-56.

24. Gil, E.S. and S.M. Hudson, Stimuli-reponsive polymers and their bioconjugates. Progress in Polymer Science, 2004. 29(12): p. 1173-1222.

25. Gupta, P., K. Vermani, and S. Garg, Hydrogels: from controlled release to pH-responsive drug delivery. Drug Discovery Today, 2002. 7(10): p. 569-579.

26. Schmaljohann, D., Thermo- and pH-responsive polymers in drug delivery. Advanced Drug Delivery Reviews, 2006. 58(15): p. 1655-1670.

27. Szczubiałka, K., M. Jankowska, and M. Nowakowska, “Smart” polymeric nanospheres as new materials for possible biomedical applications. Journal of Materials Science: Materials in Medicine, 2003. 14(8): p. 699-703.

28. Kathmann, E.E.L., L.A. White, and C.L. McCormick, Water-Soluble Polymers. 73. Electrolyte- and pH-Responsive Zwitterionic Copolymers of 4-[(2-Acrylamido-2-methylpropyl)- dimethylammonio]butanoate with 3-[(2-Acrylamido-2-methyl-propyl)dimethylammonio]propanesulfonate. Macromolecules, 1997. 30(18): p. 5297-5304.

29. Anal, A.K., Stimuli-induced Pulsatile or Triggered Release Delivery Systems for Bioactive Compounds. Recent Patents on Endocrine, Metabolic &; Immune Drug Discovery, 2007. 1: p. 83-90.

30. Pankhurst, Q.A., et al., Applications of magnetic nanoparticles in biomedicine. Journal of Physics D: Applied Physics, 2003(13): p. R167.

31. Qiu, Y. and K. Park, Environment-sensitive hydrogels for drug delivery. Advanced Drug Delivery Reviews, 2001. 53(3): p. 321-339.

32. Bawa, P., et al., Stimuli-responsive polymers and their applications in drug delivery. Biomedical Materials, 2009(2): p. 022001.

33. Heskins, M., J.E. Guillet, and E. James, Solution properties of poly(N-isopropylacrylamide). Journal of Macromolecular Science, Chemistry, 1968. 2(8): p. 1441-55.

34. Hirokawa, Y. and T. Tanaka, Volume phase transition in a nonionic gel. The Journal of Chemical Physics, 1984. 81(12): p. 6379-6380.

35. Maeda, Y., T. Nakamura, and I. Ikeda, Changes in the hydration states of poly(N-alkylacrylamide)s during their phase transitions in water observed by FTIR spectroscopy. Macromolecules, 2001. 34(5): p. 1391.

36. Schild, H.G., Poly (N-Isopropylacrylamide) - Experiment, Theory and Application. Progress in Polymer Science, 1992. 17(2): p. 163-249.

37. Tanaka, T., Phase-Transitions In Gels And A Single Polymer. Polymer, 1979. 20(11): p. 1404.

38. Hoffman, A.S., et al., Really smart bioconjugates of smart polymers and receptor proteins. Journal of Biomedical Materials Research, 2000. 52(4): p. 577-586.

39. Díez-Peña, E., I. Quijada-Garrido, and J.M. Barrales-Rienda, On the water swelling behaviour of poly(N-isopropylacrylamide) [P(N-iPAAm)], poly(methacrylic acid) [P(MAA)], their random copolymers and sequential interpenetrating polymer networks (IPNs). Polymer, 2002. 43(16): p. 4341-4348.

40. Ju, H.K., S.Y. Kim, and Y.M. Lee, pH/temperature-responsive behaviors of semi-IPN and comb-type graft hydrogels composed of alginate and poly(N-isopropylacrylamide). Polymer, 2001. 42(16): p. 6851-6857.

41. Tonge, S.R. and B.J. Tighe, Responsive hydrophobically associating polymers: a review of structure and properties. Advanced Drug Delivery Reviews, 2001. 53(1): p. 109-122.

42. Benns, J.M., et al., pH-Sensitive Cationic Polymer Gene Delivery Vehicle: N-Ac-poly(l-histidine)-graft-poly(l-lysine) Comb Shaped Polymer. Bioconjugate Chemistry, 2000. 11(5): p. 637-645.

43. Mori, T., D. Umeno, and M. Maeda, Sequence-specific affinity precipitation of oligonucleotide using poly(N-isopropylacrylamide)-oligonucleotide conjugate. Biotechnology and Bioengineering, 2001. 72(3): p. 261-268.

44. Baughman, R.H., Conducting polymer artificial muscles. Synthetic Metals, 1996. 78(3): p. 339-353.

45. Lehmann, W., et al., Giant lateral electrostriction in ferroelectric liquid-crystalline elastomers. Nature, 2001. 410(6827): p. 447-450.

46. Fukushima, T., et al., Fully Plastic Actuator through Layer-by-Layer Casting with Ionic-Liquid-Based Bucky Gel. Angewandte Chemie International Edition, 2005. 44(16): p. 2410-2413.

47. Akle, B.J., M.D. Bennett, and D.J. Leo, High-strain ionomeric-ionic liquid electroactive actuators. Sensors and Actuators A: Physical, 2006. 126(1): p. 173-181.

48. Ahn, S.-k., et al., Stimuli-responsive polymer gels. Soft Matter, 2008. 4(6): p. 1151-1157.

49. Shankar, R., T.K. Ghosh, and R.J. Spontak, Dielectric elastomers as next-generation polymeric actuators. Soft Matter, 2007. 3(9): p. 1116-1129.

50. Zrínyi, M., Intelligent polymer gels controlled by magnetic fields. Colloid & Polymer Science, 2000. 278(2): p. 98-103.

51. Canavan, H.E., et al., Cell sheet detachment affects the extracellular matrix: A surface science study comparing thermal liftoff, enzymatic, and mechanical methods. Journal of Biomedical Materials Research Part A, 2005. 75A(1): p. 1-13.

52. Nandkumar, M.A., et al., Two-dimensional cell sheet manipulation of heterotypically co-cultured lung cells utilizing temperature-responsive culture dishes results in long-term maintenance of differentiated epithelial cell functions. Biomaterials, 2002. 23(4): p. 1121-1130.

53. Okano, T., et al., Mechanism of cell detachment from temperature-modulated, hydrophilic-hydrophobic polymer surfaces. Biomaterials, 1995. 16(4): p. 297-303.

54. Okano, T., et al., A novel recovery system for cultured cells using plasma-treated polystyrene dishes grafted with poly(N-isopropylacrylamide). Journal of Biomedical Materials Research, 1993. 27(10): p. 1243-1251.

55. Yamato, M., et al., Thermally responsive polymer-grafted surfaces facilitate patterned cell seeding and co-culture. Biomaterials, 2002. 23(2): p. 561-567.

56. Hirose, M., et al., Creation of Designed Shape Cell Sheets That Are Noninvasively Harvested and Moved onto Another Surface. Biomacromolecules, 2000. 1(3): p. 377-381.

57. Kalb, E., S. Frey, and L.K. Tamm, Formation of supported planar bilayers by fusion of vesicles to supported phospholipid monolayers. Biochimica et Biophysica Acta (BBA) - Biomembranes, 1992. 1103(2): p. 307-316.

58. Hubbard, J.B., V. Silin, and A.L. Plant, Self assembly driven by hydrophobic interactions at alkanethiol monolayers: mechanism of formation of hybrid bilayer membranes. Biophysical Chemistry, 1998. 75(3): p. 163-176.

59. Koenig, B.W., et al., Neutron Reflectivity and Atomic Force Microscopy Studies of a Lipid Bilayer in Water Adsorbed to the Surface of a Silicon Single Crystal. Langmuir, 1996. 12(5): p. 1343-1350.

60. Thomson, N.L., K.H. Pearce, and H.V. Hsieh, Total internal reflection fluorescence microscopy: application to substrate-supported planar membranes. European Biophysics Journal, 1993. 22(5): p. 367-378.

61. Cornell, B.A., et al., A biosensor that uses ion-channel switches. Nature, 1997. 387(6633): p. 580-583.

62. Johnson, J.M., et al., Early Steps of Supported Bilayer Formation Probed by Single Vesicle Fluorescence Assays. Biophysical Journal, 2002. 83(6): p. 3371-3379.

63. Diaz, A.J., et al., Double Cushions Preserve Transmembrane Protein Mobility in Supported Bilayer Systems. Langmuir, 2008. 24(13): p. 6820-6826.

64. Bayerl, T.M. and M. Bloom, Physical properties of single phospholipid bilayers adsorbed to micro glass beads. A new vesicular model system studied by 2H-nuclear magnetic resonance. Biophysical Journal, 1990. 58(2): p. 357-362.

65. Johnson, S.J., et al., Structure of an adsorbed dimyristoylphosphatidylcholine bilayer measured with specular reflection of neutrons. Biophysical Journal, 1991. 59(2): p. 289-294.

66. Kiessling, V. and L.K. Tamm, Measuring Distances in Supported Bilayers by Fluorescence Interference-Contrast Microscopy: Polymer Supports and SNARE Proteins. Biophysical Journal, 2003. 84(1): p. 408-418.

67. Smith, H.L., et al., Model Lipid Membranes on a Tunable Polymer Cushion. Physical Review Letters, 2009. 102(22): p. 228102.

68. Bohringer K.F., Surface modification and modulation in microstructures: controlling protein adsorption, monolayer desorption and micro-self-assembly. Journal of Micromechanics and Microengineering, 2003. 13: p. S1-S10.

69. Ravaine, V., C. Ancla, and B. Catargi, Chemically controlled closed-loop insulin delivery. Journal of Controlled Release, 2008. 132(1): p. 2-11.

70. Cao, X., S. Lai, and L. James Lee, Design of a Self-Regulated Drug Delivery Device. Biomedical Microdevices, 2001. 3(2): p. 109-118.

71. Parker, R.S., F.J. Doyle, III, and N.A. Peppas, A model-based algorithm for blood glucose control in Type I diabetic patients. Biomedical Engineering, IEEE Transactions on, 1999. 46(2): p. 148-157.

72. Li, H. and R. Luo, Modeling and characterization of glucose-sensitive hydrogel: Effect of Young's modulus. Biosensors and Bioelectronics, 2009. 24(12): p. 3630-3636.

73. Kang, S.I. and Y.H. Bae, A sulfonamide based glucose-responsive hydrogel with covalently immobilized glucose oxidase and catalase. Journal of Controlled Release, 2003. 86(1): p. 115-121.

74. Tanaka, T., Dynamics of critical concentration fluctuations in gels. Physical Review A, 1978. 17(2): p. 763.

75. Tanaka, T., et al., Phase Transitions in Ionic Gels. Physical Review Letters, 1980. 45(20): p. 1636.

76. Dusek, k., Responsive Gels: Volume Transitions I. Advances in Polymer Science, ed. k. Dusek. 1993: Springer-Verlag.

77. Otake, K., et al., Thermal analysis of the volume phase transition with N-isopropylacrylamide gels. Macromolecules, 2002. 23(1): p. 283-289.

78. Inomata, H., S. Goto, and S. Saito, Phase transition of N-substituted acrylamide gels. Macromolecules, 1990. 23(22): p. 4887-4888.

79. Aline Percot, X.X.Z., Michel Lafleur,, A simple FTIR spectroscopic method for the determination of the lower critical solution temperature of <I>N</I>-isopropylacrylamide copolymers and related hydrogels. Journal of Polymer Science Part B: Polymer Physics, 2000. 38(7): p. 907-915.

80. Ory Ramon, E.K., Ronen Berkovici, Yachin Cohen, Yaron Paz,, Attenuated total reflectance/fourier transform infrared studies on the phase-separation process of aqueous solutions of poly(N-isopropylacrylamide). Journal of Polymer Science Part B: Polymer Physics, 2001. 39(14): p. 1665-1677.

81. Katayama, S. and A. Ohata, Phase transition of a cationic gel. Macromolecules, 1985. 18(12): p. 2781-2782.

82. Shibayama, M. and T. Tanaka, Volume Phase-Transition and Related Phenomena of Polymer Gels. Advances in Polymer Science, 1993. 109: p. 1-62.

83. Otake, K., et al., Thermal analysis of the volume phase transition with N-isopropylacrylamide gels. Macromolecules, 1990. 23(1): p. 283-289.

84. Lin, S.-Y., K.-S. Chen, and R.-C. Liang, Thermal micro ATR/FT-IR spectroscopic system for quantitative study of the molecular structure of poly(N-isopropylacrylamide) in water. Polymer, 1999. 40(10): p. 2619-2624.

85. Volpert, E., J. Selb, and F. Candau, Associating behaviour of polyacrylamides hydrophobically modified with dihexylacrylamide. Polymer, 1998. 39(5): p. 1025-1033.

86. Horne, R.A., et al., Macromolecule hydration and the effect of solutes on the cloud point of aqueous solutions of polyvinyl methyl ether: A possible model for protein denaturation and temperature control in homeothermic animals. Journal of Colloid and Interface Science, 1971. 35(1): p. 77-84.

87. Nemethy, G. and H.A. Scheraga, Structure of Water and Hydrophobic Bonding in Proteins. I. A Model for the Thermodynamic Properties of Liquid Water. The Journal of Chemical Physics, 1962. 36(12): p. 3382-3400.

88. Flory, P.J., Thermodynamics of High Polymer Solutions. The Journal of Chemical Physics, 1941. 9(8): p. 660.

89. Huggins, M.L., Solutions of Long Chain Compounds. The Journal of Chemical Physics, 1941. 9(5): p. 440.

90. Flory, P.J., Thermodynamics of High Polymer Solutions. The Journal of Chemical Physics, 1942. 10(1): p. 51-61.

91. Huggins, M.L., Thermodynamic properties of solutions of high polymers: the empirical constant in the activity equation. Ann. N. Y. Acad. Sci, 1942a. 43: p. 431−443.

92. Hirotsu, S., Coexistence of phases and the nature of first-order phase transition in poly-N-isopropylacrylamide gels, in Responsive Gels: Volume Transitions II. 1993. p. 1-26.

93. Hirotsu, S., Critical points of the volume phase transition in N-isopropylacrylamide gels. The Journal of Chemical Physics, 1988. 88(1): p. 427-431.

94. Erman, B. and P.J. Flory, Critical Phenomena and Transitions in Swollen Polymer Networks and in Linear Macromolecules. Macromolecules, 1986. 19(9): p. 2342-2353.

95. Beltran, S., et al., Swelling equilibria for ionized temperature-sensitive gels in water and in aqueous salt solutions. Journal of Chemical Physics, 1990. 92(3): p. 2061.

96. Murase, N., K. Gonda, and T. Watanabe, Unfrozen compartmentalized water in gels and its anomalous crystallization during warming. The Journal of Physical Chemistry, 1986. 90(21): p. 5420-5426.

97. Ohno, H., M. Shibayama, and E. Tsuchida, DSC analyses of bound water in the microdomains of interpolymer complexes. Die Makromolekulare Chemie, 1983. 184(5): p. 1017-1024.

98. Maeda, Y., M. Ide, and H. Kitano, Vibrational spectroscopic study on the structure of water in polymer systems. Journal of Molecular Liquids, 1999. 80(2-3): p. 149-163.

99. Terada, T., Y. Maeda, and H. Kitano, Raman spectroscopic study on water in polymer gels. The Journal of Physical Chemistry, 1993. 97(14): p. 3619-3622.

100. Maeda, Y., et al., Raman spectroscopic study of water in aqueous polymer solutions. The Journal of Physical Chemistry, 1993. 97(51): p. 13903-13906.

101. Cho, E.C., J. Lee, and K. Cho, Role of Bound Water and Hydrophobic Interaction in Phase Transition of Poly(N-isopropylacrylamide) Aqueous Solution. Macromolecules, 2003. 36(26): p. 9929-9934.

102. Maeda, Y., T. Higuchi, and I. Ikeda, Change in Hydration State during the Coil-Globule Transition of Aqueous Solutions of Poly(N-isopropylacrylamide) as Evidenced by FTIR Spectroscopy. Langmuir, 2000. 16(19): p. 7503-7509.

103. Ono, Y. and T. Shikata, Contrary Hydration Behavior of N-Isopropylacrylamide to its Polymer, P(NIPAm), with a Lower Critical Solution Temperature. The Journal of Physical Chemistry B, 2007. 111(7): p. 1511-1513.

104. Ellina Kesselman, O.R., Ronen Berkovici, Yaron Paz,, ATR-FTIR studies on the effect of strong salting-out salts on the phase separation scenario in aqueous solutions of poly(N-isopropylacrylamide) Polymers for Advanced Technologies, 2002. 13(10-12): p. 982-991.

105. Hirose, H. and M. Shibayama, Kinetics of Volume Phase Transition in Poly(N-isopropylacrylamide-co-acrylic acid) Gels. Macromolecules, 1998. 31(16): p. 5336-5342.

106. Li, Y. and T. Tanaka, Kinetics of swelling and shrinking of gels. Journal of Chemical Physics, 1990. 92(2): p. 1365.

107. Dhara, D. and P.R. Chatterji, Swelling and deswelling pathways in non-ionic poly(N-isopropylacrylamide) hydrogels in presence of additives. Polymer, 2000. 41(16): p. 6133-6143.

108. Park, T.G. and A.S. Hoffman, Estimation of Temperature-Dependent Pore Size in Poly(N-isopropylacrylamide) Hydrogel Beads. Biotechnology Progress, 1994. 10(1): p. 82-86.

109. Murray, M.J. and M.J. Snowden, The preparation, characterisation and applications of colloidal microgels. Advances in Colloid and Interface Science, 1995. 54: p. 73-91.

110. LaVan, D.A., D.M. Lynn, and R. Langer, Moving smaller in drug discovery and delivery. Nat Rev Drug Discov, 2002. 1(1): p. 77-84.

111. Budhlall, B.M., M. Marquez, and O.D. Velev, Microwave, Photo- and Thermally Responsive PNIPAMâˆ'Gold Nanoparticle Microgels. Langmuir, 2008. 24(20): p. 11959-11966.

112. Zhang, D., et al., Multilayer Assembly of Prussian Blue Nanoclusters and Enzyme-Immobilized Poly(toluidine blue) Films and Its Application in Glucose Biosensor Construction. Langmuir, 2004. 20(17): p. 7303-7307.

113. Beebe, D.J., et al., Functional hydrogel structures for autonomous flow control inside microfluidic channels. Nature, 2000. 404(6778): p. 588-590.

114. Harmon, M.E., et al., A surface plasmon resonance study of volume phase transitions in N-isopropylacrylamide gel films. Macromolecules, 2002. 35(15): p. 5999.

115. Harmon, M.E., D. Kuckling, and C.W. Frank, Photo-cross-linkable PNIPAAm copolymers. 2. Effects of constraint on temperature and pH-responsive hydrogel layers. Macromolecules, 2003. 36(1): p. 162-172.

116. Flory, P.J., Statistical Mechanics of Swelling of Network Structures. Journal of Chemical Physics, 1950. 18(1): p. 108-111.

117. Flory, P.J. and J. Rehner, Statistical mechanics of cross-linked polymer networks II Swelling. Journal of Chemical Physics, 1943. 11(11): p. 521-526.

118. Toomey, R., D. Freidank, and J. Ruhe, Swelling behavior of thin, surface-attached polymer networks. Macromolecules, 2004. 37(3): p. 882-887.

119. Flory, P.J., Principles of Polymer Chemistry. 1953: Cornell University Press: Ithaca, NY.

120. Harmon, M.E., et al., Photo-Cross-Linkable PNIPAAm Copolymers. 4. Effects of Copolymerization and Cross-Linking on the Volume-Phase Transition in Constrained Hydrogel Layers. Langmuir, 2003. 19(26): p. 10947-10956.

121. Kuckling, D., M.E. Harmon, and C.W. Frank, Photo-Cross-Linkable PNIPAAm Copolymers. 1. Synthesis and Characterization of Constrained Temperature-Responsive Hydrogel Layers. Macromolecules, 2002. 35(16): p. 6377-6383.

122. Tokarev, I. and S. Minko, Stimuli-responsive hydrogel thin films. Soft Matter, 2009. 5(3): p. 511-524.

123. Sharp, J.S. and R.A.L. Jones, Micro-buckling as a Route Towards Surface Patterning. Advanced Materials, 2002. 14(11): p. 799-802.

124. Bashir, R., et al., Micromechanical cantilever as an ultrasensitive pH microsensor. Applied Physics Letters, 2002. 81(16): p. 3091-3093.

125. Liang, L., et al., Temperature-sensitive membranes prepared by UV photopolymerization of N-isopropylacrylamide on a surface of porous hydrophilic polypropylene membranes. Journal of Membrane Science, 1999. 162(1-2): p. 235-246.

126. Roffey, C.G., Photopolymerization of Surface Coating. 1981: Wiley, New York.

127. Reuber, J., H. Reinhardt, and D. Johannsmann, Formation of Surface-Attached Responsive Gel Layers via Electrochemically Induced Free-Radical Polymerization. Langmuir, 2006. 22(7): p. 3362-3367.

128. Pan, Y.V., et al., Plasma Polymerized N-Isopropylacrylamide: Synthesis and Characterization of a Smart Thermally Responsive Coating. Biomacromolecules, 2001. 2(1): p. 32-36.

129. Tamirisa, P.A., J. Koskinen, and D.W. Hess, Plasma polymerized hydrogel thin films. Thin Solid Films, 2006. 515(4): p. 2618-2624.

130. Bullett, N.A., et al., Chemical and thermo-responsive characterisation of surfaces formed by plasma polymerisation of N-isopropyl acrylamide. Surface and Interface Analysis, 2006. 38(7): p. 1109-1116.

131. Lesho, M.J. and N.F. Sheppard, Adhesion of polymer films to oxidized silicon and its effect on performance of a conductometric pH sensor. Sensors and Actuators B: Chemical, 1996. 37(1-2): p. 61-66.

132. Cunliffe, D., et al., Thermoresponsive Surface-Grafted Poly(Nâ'isopropylacrylamide) Copolymers: Effect of Phase Transitions on Protein and Bacterial Attachment. Langmuir, 2003. 19(7): p. 2888-2899.

133. Liang, et al., Surfaces with Reversible Hydrophilic/Hydrophobic Characteristics on Cross-linked Poly(N-isopropylacrylamide) Hydrogels. Langmuir, 2000. 16(21): p. 8016-8023.

134. Liang, et al., Temperature-Sensitive Surfaces Prepared by UV Photografting Reaction of Photosensitizer and N-Isopropylacrylamide. The Journal of Physical Chemistry B, 2000. 104(49): p. 11667-11673.

135. Guenther, M., et al., Chemical sensors based on multiresponsive block copolymer hydrogels. Sensors and Actuators B: Chemical, 2007. 126(1): p. 97-106.

136. Gupta, S., et al., Synthesis and characterization of stimuli-sensitive micro- and nanohydrogels based on photocrosslinkable poly(dimethylaminoethyl methacrylate). Journal of Polymer Science Part A: Polymer Chemistry, 2007. 45(4): p. 669-679.

137. Matsukuma, D., K. Yamamoto, and T. Aoyagi, Stimuli-Responsive Properties of N-Isopropylacrylamide-Based Ultrathin Hydrogel Films Prepared by Photo-Cross-Linking. Langmuir, 2006. 22(13): p. 5911-5915.

138. Recum, H.A.v., et al., Novel thermally reversible hydrogel as detachable cell culture substrate. Journal of Biomedical Materials Research, 1998. 40(4): p. 631-639.

139. Hegewald, J., et al., Electron Beam Irradiation of Poly(Vinyl Methyl Ether) Films: 1. Synthesis and Film Topography. Langmuir, 2005. 21(13): p. 6073-6080.

140. Tirumala, V.R., et al. Direct-write e-beam patterning of stimuli-responsive hydrogel nanostructures. 2005: AVS.

141. Harnish, B., et al., UV-Cross-Linked Poly(vinylpyridine) Thin Films as Reversibly Responsive Surfaces. Chemistry of Materials, 2005. 17(16): p. 4092-4096.

142. Zhang, X. and J. Shen, Self-Assembled Ultrathin Films: From Layered Nanoarchitectures to Functional Assemblies. Advanced Materials, 1999. 11(13): p. 1139-1143.

143. Serizawa, T., et al., Thermoresponsive Ultrathin Hydrogels Prepared by Sequential Chemical Reactions. Macromolecules, 2002. 35(6): p. 2184-2189.

144. Dormán G, P.G., Benzophenone photophores in biochemistry. Biochemistry, 1994. 33(19): p. 5661-73.

145. Prestwich, G.D., et al., Benzophenone Photoprobes for Phosphoinositides, Peptides and Drugs. Photochemistry and Photobiology, 1997. 65(2): p. 222-234.

146. Dhara, D. and P.R. Chatterji, Phase Transition in Linear and Cross-Linked Poly(N-Isopropylacrylamide) in Water: Effect of Various Types of Additives. Polymer Reviews, 2000. 40(1): p. 51-68.

147. Ishidao, T., et al., Swelling equilibria of poly(N-isopropylacrylamide) gel in glucose and starch aqueous solution. Fluid Phase Equilibria, 1997. 136(1-2): p. 163-171.

148. Winnik, F.M., H. Ringsdorf, and J. Venzmer, Methanol-water as a co-nonsolvent system for poly(N-isopropylacrylamide). Macromolecules, 2002. 23(8): p. 2415-2416.

149. Asano, M., et al., Fluorescence Studies of Dansyl-Labeled Poly(N-isopropylacrylamide) Gels and Polymers in Mixed Water/Methanol Solutions. Macromolecules, 2002. 28(17): p. 5861-5866.

150. Schild, H.G., M. Muthukumar, and D.A. Tirrell, Cononsolvency in mixed aqueous solutions of poly(N-isopropylacrylamide). Macromolecules, 2002. 24(4): p. 948-952.

151. Zhu, P.W. and D.H. Napper, Volume phase transitions of poly(N-isopropylacrylamide) latex particles in mixed water-N,N-dimethylformamide solutions. Chemical Physics Letters, 1996. 256(1-2): p. 51-56.

152. Liu, M., F. Bian, and F. Sheng, FTIR study on molecular structure of poly(N-isopropylacrylamide) in mixed solvent of methanol and water. European Polymer Journal, 2005. 41(2): p. 283-291.

153. Kiritoshi, Y. and K. Ishihara, Molecular recognition of alcohol by volume phase transition of cross-linked poly(2-methacryloyloxyethyl phosphorylcholine) gel. Science and Technology of Advanced Materials, 2003. 4(2): p. 93-98.

154. Eliassaf, J., Aqueous solutions of poly(N-isopropylacrylamide). Journal of Applied Polymer Science, 1978. 22(3): p. 873-874.

155. Lee, J.L., E.M. Pearce, and T.K. Kwei, Morphological Development in Alkyl-Substituted Semiflexible Polymers. Macromolecules, 1997. 30(26): p. 8233-8244.

156. Meewes, M., et al., Coil-globule transition of poly(N-isopropylacrylamide): a study of surfactant effects by light scattering. Macromolecules, 2002. 24(21): p. 5811-5816.

157. Inomata, H., et al., Effect of additives on phase transition of N-isopropylacrylamide gels. Langmuir, 2002. 8(2): p. 687-690.

158. Schild, H.G. and D.A. Tirrell, Microheterogeneous solutions of amphiphilic copolymers of N-isopropylacrylamide. An investigation via fluorescence methods. Langmuir, 2002. 7(7): p. 1319-1324.

159. Sakai, M., et al., Effects of Surfactants on the Phase Transition of a Hydrophobic Polymer Gel. Langmuir, 2002. 11(7): p. 2493-2495.

160. Schild, H.G., PhD dissertation. 1990, University of Massachusetts at Amherst

161. Wu, C. and S. Zhou, Effects of surfactants on the phase transition of poly(N-isopropylacrylamide) in water. Journal of Polymer Science Part B: Polymer Physics, 1996. 34(9): p. 1597-1604.

162. Von Hippel, P.H. and T. Schleich, Ion effects on the solution structure of biological macromolecules. Accounts of Chemical Research, 2002. 2(9): p. 257-265.

163. Von Hippel, P.H. and K.-Y. Wong, Neutral Salts: The Generality of Their Effects on the Stability of Macromolecular Conformations. Science, 1964. 145(3632): p. 577-580.

164. Hofmeister, F., Zur Lehre von der Wirkung der Salze. Naunyn-Schmiedeberg's Archives of Pharmacology, 1888. 24(4): p. 247-260.

165. Voet, A., Quantative Lyotropy. Chemical Reviews, 2002. 20(2): p. 169-179.

166. Suzuki, A., Phase transition in gels of sub-millimeter size induced by interaction with stimuli, in Responsive Gels: Volume Transitions II. 1993. p. 199-240.

167. Saito, S.K., M.; Inomata, H., Volume phase transition of N-alkylacrylamide gels. Adv. Polym. Sci, 1993. 109: p. 207-32.

168. Inomata, H., S. Goto, and S. Saito, Effect of sodium dodecyl sulfate on the volume phase transition of N-isopropylacrylamide gel. Langmuir, 1992. 8(3): p. 1030-1031.

169. Pegram, L.M. and M.T. Record, Partitioning of atmospherically relevant ions between bulk water and the water/vapor interface. Proceedings of the National Academy of Sciences, 2006. 103(39): p. 14278-14281.

170. Pegram, L.M. and M.T. Record, Thermodynamic Origin of Hofmeister Ion Effects. The Journal of Physical Chemistry B, 2008. 112(31): p. 9428-9436.

171. Long, F.A. and W.F. McDevit, Activity Coefficients of Nonelectrolyte Solutes in Aqueous Salt Solutions. Chemical Reviews, 1952. 51(1): p. 119-169.

172. Frank, F.C., Dislocations and point defects. Discuss. Faraday Soc.,, 1957. 23: p. 122-127.

173. Stokes, R.H. and R. and Mills, Viscosity of Electrolyte and Related Properties 1965, Chapter 4, Pergamon , Oxford, U.K.

174. Breslau, B.R. and I.F. Miller, Viscosity of concentrated aqueous electrolyte solutions. The Journal of Physical Chemistry, 1970. 74(5): p. 1056-1061.

175. Park, S., H. Yu, and T. Chang, A new analysis scheme for complex forced Rayleigh scattering profiles. Macromolecules, 1993. 26(12): p. 3086-3091.

176. Cantor, C.R. and P.R. and Schimmel, The Conformation of Biological Macromolecules , chap. 5 in Biophysical Chemistry Part I. 1980, W. H. Freeman and Co. , San Francisco

177. Von Hippel, P.H., et al., Model studies on the effects of neutral salts on the conformational stability of biological macromolecules. I. Ion binding to polyacrylamide and polystyrene columns. Biochemistry, 1973. 12(7): p. 1256-1264.

178. Hamabata, A., S. Chang, and P.H. Von Hippel, Model studies on the effects of neutral salts on the conformational stability of biological macromolecules. IV. Properties of fatty acid amide micelles. Biochemistry, 1973. 12(7): p. 1278-1282.

179. Meyer, D.E. and A. Chilkoti, Quantification of the Effects of Chain Length and Concentration on the Thermal Behavior of Elastin-like Polypeptides. Biomacromolecules, 2004. 5(3): p. 846-851.

180. Chockalingam, K., M. Blenner, and S. Banta, Design and application of stimulus-responsive peptide systems. Protein Engineering, Design and Selection, 2007. 20(4): p. 155-161.

181. Urry, D.W., et al., Hydrophobicity scale for proteins based on inverse temperature transitions. Biopolymers, 1992. 32(9): p. 1243-1250.

182. Urry, D.W., B. Haynes, and R.D. Harris, Temperature dependence of length of elastin and its polypentapeptide. Biochemical and Biophysical Research Communications, 1986. 141(2): p. 749-755.

183. Urry, D.W., et al., Temperature of polypeptide inverse temperature transition depends on mean residue hydrophobicity. Journal of the American Chemical Society, 1991. 113(11): p. 4346-4348.

184. Urry, D.W., T.L. Trapane, and K.U. Prasad, Phase-structure transitions of the elastin polypentapeptide-water system within the framework of composition-temperature studies. Biopolymers, 1985. 24(12): p. 2345-2356.

185. McHale, M.K., L.A. Setton, and A. Chilkoti, Synthesis and in Vitro Evaluation of Enzymatically Cross-Linked Elastin-Like Polypeptide Gels for Cartilaginous Tissue Repair. Tissue Engineering, 2005. 11(11-12): p. 1768-1779.

186. Hyun, J., et al., Capture and Release of Proteins on the Nanoscale by Stimuli-Responsive Elastin-Like Polypeptide. Journal of the American Chemical Society, 2004. 126(23): p. 7330-7335.

187. Chilkoti, A., et al., Targeted drug delivery by thermally responsive polymers. Advanced Drug Delivery Reviews, 2002. 54(5): p. 613-630.

188. Meyer, D.E. and A. Chilkoti, Purification of recombinant proteins by fusion with thermally-responsive polypeptides. Nat Biotech, 1999. 17(11): p. 1112-1115.

189. Prabhukumar, G., et al., Cadmium Removal from Contaminated Soil by Tunable Biopolymers. Environmental Science & Technology, 2004. 38(11): p. 3148-3152.

190. Massodi, I., G.L. Bidwell Iii, and D. Raucher, Evaluation of cell penetrating peptides fused to elastin-like polypeptide for drug delivery. Journal of Controlled Release, 2005. 108(2-3): p. 396-408.

191. Bidwell, G.L. and D. Raucher, Application of thermally responsive polypeptides directed against c-Myc transcriptional function for cancer therapy. Molecular Cancer Therapeutics, 2005. 4(7): p. 1076-1085.

192. Raucher, D. and A. Chilkoti, Enhanced Uptake of a Thermally Responsive Polypeptide by Tumor Cells in Response to Its Hyperthermia-mediated Phase Transition. Cancer Res, 2001. 61(19): p. 7163-7170.

193. Meyer, D.E., et al., Targeting a Genetically Engineered Elastin-like Polypeptide to Solid Tumors by Local Hyperthermia. Cancer Res, 2001. 61(4): p. 1548-1554.

194. Merrifield, R.B., Solid Phase Peptide Synthesis. I. The Synthesis of a Tetrapeptide. J. Am. Chem. Soc, 1963. 85(14): p. 2149-2154.

195. J.D. Wade, J.B., R.C. Sheppard and G.W. Tregaer, DBU as an N alpha-deprotecting reagent for the fluorenylmethoxycarbonyl group in continuous flow solid-phase peptide synthesis. Peptide Research, 1991. 4: p. 194-199.

196. Kates SA, S.N., Beyermann M, Barany G, Albericio F., Optimized preparation of deca(L-alanyl)-L-valinamide by 9-fluorenylmethyloxycarbonyl (Fmoc) solid-phase synthesis on polyethylene glycol-polystyrene (PEG-PS) graft supports, with 1,8-diazobicyclo [5.4.0]-undec-7-ene (DBU) deprotection. Peptide research, 1996. 9(3): p. 106-113.

197. P.D.White, W.C.C.a., Fmoc Solid Phase Peptide Synthesis. A Pratical Approach, ed. B.D.Hames. 2004.

198. Russell, T.P., The Characterization of Polymer Interfaces. Annual Review of Materials Science, 1991. 21: p. 249-268.

199. Lu, J.R. and R.K. Thomas, Neutron reflection from wet interfaces. Journal of the Chemical Society-Faraday Transactions, 1998. 94(8): p. 995-1018.

200. Parratt, L.G., Phys. Rev., 1954. 95: p. 359-369.

201. Vigano, C., et al., Attenuated total reflection IR spectroscopy as a tool to investigate the structure, orientation and tertiary structure changes in peptides and membrane proteins. Peptide Science, 2000. 55(5): p. 373-380.

202. Born, M.W., E. , Principles of Optics; University Press: Amsterdam,. Principles of Optics; University Press: Amsterdam, 1997.

203. Meersman, F., et al., Pressure effect on the hydration properties of poly(N-isopropylacrylamide) in aqueous solution studied by FTIR spectroscopy. Macromolecules, 2005. 38(21): p. 8923.

204. Cheng, H., L. Shen, and C. Wu, LLS and FTIR studies on the hysteresis in association and dissociation of poly(N-isopropylacrylamide) chains in water. Macromolecules, 2006. 39(6): p. 2325.

205. Katsumoto, Y., et al., Conformational change of poly(N-isopropylacrylamide) during the coil-globule transition investigated by attenuated total reflection/infrared spectroscopy and density functional theory calculation. Journal of Physical Chemistry A, 2002. 106(14): p. 3429-3435.

206. Okada, Y. and F. Tanaka, Cooperative hydration, chain collapse, and flat LCST behavior in aqueous poly(N-isopropylacrylamide) solutions. Macromolecules, 2005. 38(10): p. 4465.

207. Afroze, F., E. Nies, and H. Berghmans, Phase transitions in the system poly(N-isopropylacrylamide)/water and swelling behaviour of the corresponding networks. Journal Of Molecular Structure, 2000. 554(1): p. 55.

208. Moerkerke, R., et al., Phase-Transitions In Swollen Networks. Macromolecules, 1995. 28(4): p. 1103.

209. Solc, K., et al., "Zero" and "off-zero" critical concentrations in solutions of polydisperse polymers with very high molar masses. Collection Of Czechoslovak Chemical Communications, 1995. 60(10): p. 1661.

210. Baulin, V.A., E.B. Zhulina, and A. Halperin, Self-consistent field theory of brushes of neutral water-soluble polymers. Journal of Chemical Physics, 2003. 119(20): p. 10977-10988.

211. Yim, H., et al., Evidence for vertical phase separation in densely grafted, high-molecular-weight poly(N-isopropylacrylamide) brushes in water. Physical Review E, 2005. 72(5).

212. Mendez, S., et al., Computational modeling of the temperature-induced structural changes of tethered poly(N-isopropylacrylamide) with self-consistent field theory. Macromolecules, 2005. 38(1): p. 174-181.

213. Balamurugan, S., et al., Thermal response of poly(N-isopropylacrylamide) brushes probed by surface plasmon resonance. Langmuir, 2003. 19(7): p. 2545-2549.

214. Yim, H., et al., Effects of grafting density and molecular weight on the temperature-dependent conformational change of poly(N-isopropylacrylamide) grafted chains in water. Macromolecules, 2006. 39(9): p. 3420.

215. Yim, H., et al., Study of the conformational change of poly(N-isopropylacrylamide)-grafted chains in water with neutron reflection: Molecular weight dependence at high grafting density. Journal of Polymer Science Part B-Polymer Physics, 2004. 42(17): p. 3302-3310.

216. Prucker, O., et al., Photochemical attachment of polymer films to solid surfaces via monolayers of benzophenone derivatives. Journal Of The American Chemical Society, 1999. 121(38): p. 8766.

217. Yim, H., et al., Adsorption of sodium poly(styrenesulfonate) to the air surface of water by neutron and X-ray reflectivity and surface tension measurements: Polymer concentration dependence. Macromolecules, 2002. 35(26): p. 9737-9747.

218. Yim, H., et al., Adsorption of poly(styrenesulfonate) to the air surface of water by neutron reflectivity. Macromolecules, 2000. 33(16): p. 6126-6133.

219. Schild, H.G. and D.A. Tirrell, Microcalorimetric Detection of Lower Critical Solution Temperatures in Aqueous Polymer-Solutions. Journal of Physical Chemistry, 1990. 94(10): p. 4352-4356.

220. Marchetti, M., S. Prager, and E.L. Cussler, Thermodynamic Predictions of Volume Changes in Temperature-Sensitive Gels .1. Theory. Macromolecules, 1990. 23(6): p. 1760-1765.

221. Fujishige, S., K. Kubota, and I. Ando, Phase-Transition of Aqueous-Solutions of Poly(N-Isopropylacrylamide) and Poly(N-Isopropylmethacrylamide). Journal of Physical Chemistry, 1989. 93(8): p. 3311-3313.

222. Suzuki, A. and S. Kojima, Phase-Transition in Constrained Polymer Gels. Journal of Chemical Physics, 1994. 101(11): p. 10003-10007.

223. Ptitsyn, O.B.K., A. K.; Eizner, Yu. E., The models of the denaturation of globular proteins. I. Theory of globula-coil transitions in macromolecules. Journal of Polymer Science, Polymer Symposia 1968. 16(6).

224. Aline Percot, X.X.Z., Michel Lafleur,, A simple FTIR spectroscopic method for the determination of the lower critical solution temperature of N-isopropylacrylamide copolymers and related hydrogels. Journal of Polymer Science Part B: Polymer Physics, 2000. 38(7): p. 907-915.

225. Ellina Kesselman, O.R., Ronen Berkovici, Yaron Paz,, ATR-FTIR studies on the effect of strong salting-out salts on the phase separation scenario in aqueous solutions of poly(N-isopropylacrylamide) [PNIPA]. Polymers for Advanced Technologies, 2002. 13(10-12): p. 982-991.

226. Ory Ramon, E.K., Ronen Berkovici, Yachin Cohen, Yaron Paz,, Attenuated total reflectance/fourier transform infrared studies on the phase-separation process of aqueous solutions of poly(n-isopropylacrylamide). Journal of Polymer Science Part B: Polymer Physics, 2001. 39(14): p. 1665-1677.

227. Tanaka, T., et al., Mechanical instability of gels at the phase transition. Nature, 1987. 325(6107): p. 796-798.

228. Afroze, F., E. Nies, and H. Berghmans, Phase transitions in the system poly(N-isopropylacrylamide)/water and swelling behaviour of the corresponding networks. Journal of Molecular Structure, 2000. 554(1): p. 55-68.

229. Okada, Y. and F. Tanaka, Cooperative Hydration, Chain Collapse, and Flat LCST Behavior in Aqueous Poly(N-isopropylacrylamide) Solutions. Macromolecules, 2005. 38(10): p. 4465-4471.

230. Ono, Y. and T. Shikata, Hydration and Dynamic Behavior of Poly(N-isopropylacrylamide)s in Aqueous Solution: A Sharp Phase Transition at the Lower Critical Solution Temperature. Journal of the American Chemical Society, 2006. 128(31): p. 10030-10031.

231. Salmerón Sánchez, M., et al., Thermal transitions of poly(N-isopropylmethacrylamide) in aqueous solutions. Polymer, 2004. 45(12): p. 4087-4094.

232. Tiktopulo, E.I., et al., Cooperativity of the Coil-Globule Transition in a Homopolymer: Microcalorimetric Study of Poly(N-isopropylacrylamide). Macromolecules, 1994. 27(10): p. 2879-2882.

233. Beines, P.W., et al., Responsive Thin Hydrogel Layers from Photo-Cross-Linkable Poly(N-isopropylacrylamide) Terpolymersâ€ Langmuir, 2007. 23(4): p. 2231-2238.

234. Makino, K., J. Hiyoshi, and H. Ohshima, Kinetics of swelling and shrinking of poly (N-isopropylacrylamide) hydrogels at different temperatures. Colloids and Surfaces B: Biointerfaces, 2000. 19(2): p. 197-204.

235. Tae Gwan Park and Allan S. Hoffman, Deswelling characteristics of poly(N-isopropylacrylamide) hydrogel. Journal of Applied Polymer Science, 1994. 52(1): p. 85-89.

236. Schmidt, P., et al., Role of Water in Structural Changes of Poly(AVGVP) and Poly(GVGVP) Studied by FTIR and Raman Spectroscopy and ab Initio Calculations. Biomacromolecules, 2005. 6(2): p. 697-706.

237. Zhou, K., et al., The Coil-to-Globule-to-Coil Transition of Linear Polymer Chains in Dilute Aqueous Solutions: Effect of Intrachain Hydrogen Bonding. Macromolecules, 2008. 41(22): p. 8927-8931.

238. Maeda, Y., T. Nakamura, and I. Ikeda, Change in Solvation of Poly(N,N-diethylacrylamide) during Phase Transition in Aqueous Solutions As Observed by IR Spectroscopy. Macromolecules, 2002. 35(27): p. 10172-10177.

239. Cunliffe, D., et al., Thermoresponsive surface-grafted poly(N-isopropylacrylamide) copolymers: Effect of phase transitions on protein and bacterial attachment. Langmuir, 2003. 19(7): p. 2888-2899.

240. Huber, D.L., et al., Programmed adsorption and release of proteins in a microfluidic device. Science, 2003. 301(5631): p. 352-354.

241. Kushida, A., et al., Decrease in culture temperature releases monolayer endothelial cell sheets together with deposited fibronectin matrix from temperature-responsive culture surfaces. Journal Of Biomedical Materials Research, 1999. 45(4): p. 355.

242. Kwon, O.H., et al., Rapid cell sheet detachment from poly(N-isopropylacrylamide)-grafted porous cell culture membranes. Journal Of Biomedical Materials Research, 2000. 50(1): p. 82.

243. Kikuchi, A. and T. Okano, Intelligent thermoresponsive polymeric stationary phases for aqueous chromatography of biological compounds. Progress In Polymer Science, 2002. 27(6): p. 1165.

244. Kobayashi, J., et al., Aqueous chromatography utilizing pH-/temperature responsive polymer stationary phases to separate ionic bioactive compounds. Analytical Chemistry, 2001. 73(9): p. 2027.

245. Ping, Z.H., et al., States of water in different hydrophilic polymers-DSC and FTIR studies. Polymer, 2001. 42(20): p. 8461-8467.

246. Pegram, L.M. and M.T. Record, Hofmeister Salt Effects on Surface Tension Arise from Partitioning of Anions and Cations between Bulk Water and the Airâˆ’Water Interface. The Journal of Physical Chemistry B, 2007. 111(19): p. 5411-5417.

247. Conato, C., et al., Copper and nickel complex-formation equilibria with Lys-Gly-His-Lys, a fragment of the matricellular protein SPARC. Polyhedron, 2002. 21(14-15): p. 1469-1474.

248. Truffert, J.-C., et al., Synthesis, purification and characterization of two peptide-oligonucleotide conjugates as potential artificial nucleases. Tetrahedron, 1996. 52(8): p. 3005-3016.

249. Anwar, Z.M. and H.A. Azab, Ternary Complexes in Solution. Comparison of the Coordination Tendency of Some Biologically Important Zwitterionic Buffers toward the Binary Complexes of Some Transition Metal Ions and Some Amino Acids. Journal of Chemical & Engineering Data, 1999. 44(6): p. 1151-1157.

ABOUT THE AUTHOR

Ajay K Vidyasagar was born in Secunderabad, India. He obtained his Bachelors degree in Chemical Engineering from Bangalore University with honors. He has a Masters degree in Biophysics from the National Institute of Mental Health and Neurosciences (NIMHANS). He then proceeded to get his PhD in Chemical Engineering from the University of South Florida in 2010 specilizing in polymer science and engineering. He has published several peer reviewed journal articles in high impact journals and has also presented at several national conferences including AIChE, ACS and APS.